NUREG/CR–4744
Vol. 5, No. 2
ANL–91/10

Long-Term Embrittlement of Cast Duplex Stainless Steels in LWR Systems

Semiannual Report
April–September 1990

Prepared by O. K. Chopra

Argonne National Laboratory

Prepared for
U.S. Nuclear Regulatory Commission

AVAILABILITY NOTICE

Availability of Reference Materials Cited in NRC Publications

Most documents cited in NRC publications will be available from one of the following sources:

1. The NRC Public Document Room, 2120 L Street, NW, Lower Level, Washington, DC 20555

2. The Superintendent of Documents, U.S. Government Printing Office, P.O. Box 37082, Washington, DC 20013-7082

3. The National Technical Information Service, Springfield, VA 22161

Although the listing that follows represents the majority of documents cited in NRC publications, it is not intended to be exhaustive.

Referenced documents available for inspection and copying for a fee from the NRC Public Document Room include NRC correspondence and internal NRC memoranda; NRC Office of Inspection and Enforcement bulletins, circulars, information notices, inspection and investigation notices; Licensee Event Reports; vendor reports and correspondence; Commission papers; and applicant and licensee documents and correspondence.

The following documents in the NUREG series are available for purchase from the GPO Sales Program: formal NRC staff and contractor reports, NRC-sponsored conference proceedings, and NRC booklets and brochures. Also available are Regulatory Guides, NRC regulations in the *Code of Federal Regulations*, and *Nuclear Regulatory Commission Issuances*.

Documents available from the National Technical Information Service include NUREG series reports and technical reports prepared by other federal agencies and reports prepared by the Atomic Energy Commission, forerunner agency to the Nuclear Regulatory Commission.

Documents available from public and special technical libraries include all open literature items, such as books, journal and periodical articles, and transactions. *Federal Register* notices, federal and state legislation, and congressional reports can usually be obtained from these libraries.

Documents such as theses, dissertations, foreign reports and translations, and non-NRC conference proceedings are available for purchase from the organization sponsoring the publication cited.

Single copies of NRC draft reports are available free, to the extent of supply, upon written request to the Office of Information Resources Management, Distribution Section, U.S. Nuclear Regulatory Commission, Washington, DC 20555.

Copies of industry codes and standards used in a substantive manner in the NRC regulatory process are maintained at the NRC Library, 7920 Norfolk Avenue, Bethesda, Maryland, and are available there for reference use by the public. Codes and standards are usually copyrighted and may be purchased from the originating organization or, if they are American National Standards, from the American National Standards Institute, 1430 Broadway, New York, NY 10018.

DISCLAIMER NOTICE

NUREG/CR--4744-Vol.5-No.2

TI91 015983

Long-Term Embrittlement of Cast Duplex Stainless Steels in LWR Systems

Semiannual Report
April–September 1990

Manuscript Completed: March 1991
Date Published: July 1991

Prepared by
O. K. Chopra

Argonne National Laboratory
9700 South Cass Avenue
Argonne, IL 60439

Prepared for
Division of Engineering
Office of Nuclear Regulatory Research
U.S. Nuclear Regulatory Commission
Washington, DC 20555
NRC FINs A2243, A2256

Previous Documents in Series

Long-Term Embrittlement of Cast Duplex Stainless Steels in LWR Systems: Annual Report, October 1982–September 1983, NUREG/CR-3857, ANL-84-44 (August 1984).

Long-Term Embrittlement of Cast Duplex Stainless Steels in LWR Systems: Annual Report, October 1983–September 1984, NUREG/CR-4204, ANL-85-20 (March 1985).

Long-Term Embrittlement of Cast Duplex Stainless Steels in LWR Systems: Annual Report, October 1984–September 1985, NUREG/CR-4503, ANL-86-3 (January 1986).

Long-Term Embrittlement of Cast Duplex Stainless Steels in LWR Systems: Semiannual Report, October 1985–March 1986, NUREG/CR-4744 Vol. I, No. 1, ANL-86-54 (January 1987).

Long-Term Embrittlement of Cast Duplex Stainless Steels in LWR Systems: Semiannual Report, April–September 1986, NUREG/CR-4744 Vol. I, No. 2, ANL-87-16 (March 1987).

Long-Term Embrittlement of Cast Duplex Stainless Steels in LWR Systems: Semiannual Report, October 1986–March 1987, NUREG/CR-4744, Vol. 2, No. 1, ANL-87-45 (July 1987).

Long-Term Embrittlement of Cast Duplex Stainless Steels in LWR Systems: Semiannual Report, April–September 1987, NUREG/CR-4744, Vol. 2, No. 2, ANL-89/6 (August 1989).

Long-Term Embrittlement of Cast Duplex Stainless Steels in LWR Systems: Semiannual Report, October 1987–March 1988, NUREG/CR-4744, Vol. 3, No. 1, ANL-89/22 (February 1990).

Long-Term Embrittlement of Cast Duplex Stainless Steels in LWR Systems: Semiannual Report, April–September 1988, NUREG/CR-4744, Vol. 3, No. 2, ANL-90/5 (August 1990).

Long-Term Embrittlement of Cast Duplex Stainless Steels in LWR Systems: Semiannual Report, October 1988–March 1989, NUREG/CR-4744, Vol. 4, No. 1, ANL-90/44 (May 1991).

Long-Term Embrittlement of Cast Duplex Stainless Steels in LWR Systems: Semiannual Report, April–September 1989, NUREG/CR-4744, Vol. 4, No. 2, ANL-90/49 (June 1991).

Long-Term Embrittlement of Cast Duplex Stainless Steels in LWR Systems: Semiannual Report, October 1989–March 1990, NUREG/CR-4744, Vol. 5, No. 1, ANL-91/7 (July 1991).

Long–Term Embrittlement of Cast Duplex Stainless Steels in LWR Systems

by

O. K. Chopra

Abstract

This progress report summarizes work performed by Argonne National Laboratory on long–term embrittlement of cast duplex stainless steels in LWR systems during the six months from April 1990 to September 1990. A procedure and correlations are presented for predicting fracture toughness J–R curves and impact strength of aged cast stainless steels from known material information. Fracture toughness of a specific cast stainless steel is estimated from the extent and kinetics of thermal embrittlement. The extent of thermal embrittlement is characterized by the room–temperature "normalized" Charpy–impact energy. A correlation for the extent of embrittlement at "saturation," i.e., the minimum impact energy that would be achieved by the material after long–term aging, is given in terms of a material parameter, Φ, which is determined from the chemical composition. The fracture toughness J–R curve for the material is then obtained from correlations between room–temperature Charpy–impact energy and fracture toughness parameters. Fracture toughness as a function of time and temperature of reactor service is estimated from the kinetics of thermal embrittlement, which are determined from chemical composition. A common "lower–bound" J–R curve for cast stainless steels with unknown chemical composition is also defined for a given material specification, ferrite content, and temperature. Examples for estimating impact strength and fracture toughness of cast stainless steel components during reactor service are described. Mechanical–property degradation suffered by cast stainless steel components from the decommissioned Shippingport reactor has been characterized. The results are used to validate the correlations and benchmark the laboratory studies. Charpy–impact, tensile, and fracture toughness data for materials from the hot–leg shutoff valve and cold–leg check valves and pump volute are presented. The results indicate a relatively modest degree of thermal embrittlement.

Contents

List of Figures

List of Tables

Nomenclature

α	Shape factor for the curve for the change in room-temperature Charpy-impact energy with time and temperature of aging.
β	Half the maximum change in room-temperature Charpy-impact energy.
δ	Ferrite content of the material (%).
δ_c	Ferrite content calculated from the chemical composition of the material (%).
δ_m	Measured ferrite content of the material (%).
Δa	Crack extension (mm).
Φ	Material parameter.
λ	Mean ferrite spacing of the material (μm).
θ	Represents the aging behavior at 400°C. It is the log of the time to achieve β reduction in impact energy at 400°C.
Cr_{eq}	Chromium equivalent for the material (wt.%).
C_V	Room-temperature "normalized" Charpy-impact energy, i.e., Charpy-impact energy per unit area, at any given service or aging time (J/cm^2). The fracture area for a standard Charpy V-notch specimen (ASTM Specification E 23) is 0.8 cm^2. Divide by 0.8 to obtain "normalized" impact energy.
C_{Vint}	Initial room-temperature "normalized" Charpy-impact energy of the material, i.e., unaged material (J/cm^2).
C_{Vsat}	Room-temperature "normalized" Charpy-impact energy of the material at saturation, i.e., the minimum impact energy that would ever be achieved for the material after long-term service (J/cm^2).
J_d	Deformation J per ASTM Specification E 813-85 or E 1152 (kJ/m^2).
Ni_{eq}	Nickel equivalent for the material (wt.%).
P	Aging parameter that is the log of the time of aging at 400°C.
Q	Activation energy for the process of embrittlement (kJ/mole).
t	Service or aging time (h).
T_s	Service or aging temperature (°C).

SI units of measurements have been used in this report. Conversion factors for measurements in British units are as follows:

To convert from	to	multiply by
mm	in.	0.0394
J*	ft·lb	0.7376
kJ/m^2	in.-lb/$in.^2$	5.71015
kJ/mole	kcal/mole	0.239

*When impact energy is expressed in J/cm^2, first multiply by 0.8 to obtain impact energy of a standard Charpy V-notch specimen in J.

Executive Summary

Cast stainless steels used in pump casings, valve bodies, piping, and other components in coolant systems of light-water nuclear reactors (LWRs) suffer loss of toughness after many years of service at 280–320°C (536–608°F). A program is being conducted to investigate the low-temperature thermal embrittlement of cast duplex stainless steels under LWR operating conditions and to evaluate possible remedies for thermal embrittlement problems in existing and future plants. The scope of the investigation includes the following goals: (1) characterize and correlate the microstructure of in-service reactor components and laboratory-aged material with loss of fracture toughness to establish the mechanism of aging and validate the simulation of in-reactor degradation by accelerated aging, (2) establish the effects of key compositional and metallurgical variables on the kinetics and extent of thermal embrittlement, and (3) develop the methodology and correlations for predicting the toughness loss suffered by cast stainless steel components during normal and extended life of LWRs.

Microstructural and mechanical property data are being obtained on 25 experimental heats (19 in the form of static-cast keel blocks and 6 in the form of slabs) and 6 commercial heats (centrifugally cast pipes and a static-cast pump impeller and pump casing ring), as well as on reactor-aged material of grades CF-3, CF-8, and CF-8M cast stainless steel. The ferrite content of the cast materials ranges from 3 to 30%. Ferrite morphology for the castings containing >5% ferrite is either lacy or acicular.

Charpy-impact, tensile, and J-R curve tests have been conducted on several experimental and commercial heats of cast stainless steel that were aged up to 30,000 h at 290–400°C (554–752°F). Results indicate that thermal aging at these temperatures increases the tensile strength and decreases the impact energy and fracture toughness of the steels. The Charpy transition curve shifts to higher temperatures. Different heats exhibit different degrees of thermal embrittlement. In general, the low-C CF-3 steels are the most resistant, and the Mo-bearing high-C CF-8M steels are the least resistant to thermal embrittlement. The increase in flow stress of fully aged cast stainless steels is ≈10% for CF-3 steels and ≈20% for CF-8 and CF-8M steels. The values of fracture toughness J_{IC} and average tearing modulus for heats that are sensitive to thermal aging (e.g., CF-8M steels) are as low as ≈90 kJ/m^2 and ≈60, respectively. Correlations have been developed for estimating the increase in flow stress of the steels from data on the kinetics of thermal embrittlement.

Embrittlement of cast stainless steels results in brittle fracture associated with either cleavage of the ferrite or separation of the ferrite/austenite phase boundary. Predominantly brittle failure occurs when either the ferrite phase is continuous, e.g., in cast material with a large ferrite content, or the ferrite/austenite phase boundary provides an easy path for crack propagation, e.g., in high-C grades of cast steel with large phase-boundary carbides. Consequently, the amount, size, and distribution of the ferrite phase in the duplex structure, and the presence of phase-boundary carbides are important parameters in controlling the degree or extent of thermal embrittlement.

Thermal aging of cast stainless steels at <500°C (<932°F) leads to precipitation of additional phases in the ferrite, e.g., formation of a Cr-rich α' phase by spinodal decomposition; nucleation and growth of α'; precipitation of a Ni- and Si-rich G phase, $M_{23}C_6$, and γ_2

(austenite); and additional precipitation and/or growth of existing carbides at the ferrite/austenite phase boundaries. Formation of α' phase provides the strengthening mechanisms that increase strain hardening and local tensile stress. Consequently, the critical stress level for brittle fracture is achieved at higher temperatures. The kinetics of thermal embrittlement of cast stainless steels is controlled primarily by the kinetics of strengthening of ferrite. The log of the time of aging at 400°C for a 50% reduction in Charpy-impact energy has been shown to be a useful parameter to characterize the kinetics of thermal embrittlement. Production heat treatment and possibly the casting process influence the aging behavior at 400°C and, therefore, the kinetics of thermal embrittlement. Activation energy for thermal embrittlement is high for those steels that show fast embrittlement at 400°C and is low for those that show slow embrittlement at 400°C. Precipitation of G phase in the ferrite has little or no effect on the kinetics of thermal embrittlement. Material parameters that influence the kinetics of thermal embrittlement also effect G-phase precipitation. However, activation energy for thermal embrittlement is generally low for cast stainless steels that contain G-phase.

This report presents a procedure and correlations for predicting fracture toughness of cast stainless steel components due to thermal aging during service in LWRs at 280–330°C (536–626°F). The fracture toughness J-R curve and Charpy-impact energy are estimated from material information that can be determined from the certified material test record. Fracture toughness of a specific cast stainless steel is estimated from the extent and kinetics of thermal embrittlement. The extent of thermal embrittlement is characterized by the room-temperature "normalized" Charpy-impact energy. Correlations for the extent of thermal embrittlement at "saturation," i.e., the minimum impact energy that can be achieved by the material after long-term aging, are given in terms of a material parameter that consists of the chemical composition and ferrite morphology. Different correlations are used for estimating the saturation impact energy of CF-3 or CF-8 steels and CF-8M steels. A common expression for the relationship between the material parameter and saturation impact energy is used when metallographic information, i.e., the measured values of ferrite content and mean ferrite spacing, is known. Extent of thermal embrittlement as a function of time and temperature of reactor service is then estimated from the extent of thermal embrittlement at saturation and from the correlations describing the kinetics of thermal embrittlement, which are also given in terms of chemical composition and the aging behavior at 400°C. The fracture toughness J-R curve for the material is then obtained from the correlation between fracture toughness parameters and room-temperature Charpy-impact energy used to characterize the extent of thermal embrittlement. A common lower-bound J-R curve for cast materials with unknown chemical composition is also defined as a function of material specification, ferrite content , and temperature. Examples for estimating impact strength and fracture toughness of cast stainless steel components during reactor service are presented.

Mechanical-property degradation suffered by cast stainless steel components from the decommissioned Shippingport reactor has been characterized. The results are used to validate the correlations and benchmark the laboratory studies. Charpy-impact, tensile, and fracture toughness data for materials from the hot-leg shutoff valve and cold-leg check valves and pump volute are presented. Baseline mechanical properties for unaged material were determined from tests on either recovery-annealed material, i.e., annealed 1 h at 550°C (1022°F) and then water quenched, or material from cooler regions of the components. The results indicate a relatively modest degree of thermal embrittlement.

1 Introduction

Cast duplex stainless steels used in LWR systems for primary pressure-boundary components such as valve bodies, pump casings, and primary coolant piping are susceptible to thermal embrittlement at reactor operating temperatures, i.e., 280–320°C (536–608°F). Aging of cast stainless steels at these temperatures causes an increase in hardness and tensile strength and a decrease in ductility, impact strength, and fracture toughness of the material. Most studies on thermal embrittlement of cast stainless steels involve simulation of end-of-life reactor conditions by accelerated aging at higher temperatures, viz., 400°C (752°F), because the time period for operation of power plants (≈40 y) is far longer than can generally be considered for laboratory studies. Thus, estimates of the loss of fracture toughness suffered by cast stainless steel components are based on an Arrhenius extrapolation of high-temperature data to reactor operating conditions.

A program is being conducted to investigate the significance of low-temperature embrittlement of cast duplex stainless steels under light water reactor (LWR) operating conditions and to evaluate possible remedies for thermal embrittlement problems in existing and future plants. The scope of the program includes the following goals: (1) characterize and correlate the microstructure of in-service reactor components and laboratory-aged material with loss of fracture toughness to establish the mechanism of aging and validate the simulation of in-reactor degradation by accelerated aging, (2) establish the effects of key compositional and metallurgical variables on the kinetics and extent of thermal embrittlement, and (3) develop the methodology and correlations for predicting the toughness loss suffered by cast stainless steel components during normal and extended life of LWRs.

Microstructural and mechanical-property data are being obtained on 25 experimental heats (19 in the form of static-cast keel blocks and 6 in the form of 76-mm slabs) and 6 commercial heats (centrifugally cast pipes and a static-cast pump impeller and pump casing ring) as well as reactor-aged material of grades CF-3, CF-8, and CF-8M cast stainless steel. Specimen blanks for Charpy-impact, tensile, and J-R curve tests have been aged at 290, 320, 350, 400, and 450°C (554, 608, 662, 752, and 842°F) for times up to 60,000 h. The reactor-aged material is from the recirculating-pump cover plate assembly of the KRB reactor, which was in service in Gundremmingen, West Germany, for ≈8 yr at 284°C (543°F). Fractured impact test bars from five heats of aged cast stainless steel were obtained from the Georg Fischer Co. (GF) of Switzerland for microstructural characterization. The materials from GF are from a previous study of long-term aging behavior of cast stainless steel.[1] The data on chemical composition, ferrite content, hardness, ferrite morphology, and grain structure of the experimental and commercial heats have been reported earlier.[2-6] The chemical composition, hardness, and ferrite content and distribution of the cast materials are given in Table 1. The results of microstructural characterization and mechanical-property data from Charpy-impact, tensile, and J-R curve tests on 16 heats of cast stainless steel aged up to 30,000 h at temperatures between 290 and 450°C have also been presented earlier.[7-21]

Work at Argonne National Laboratory (ANL) and elsewhere[1,22-28] has shown that embrittlement of cast stainless steel components will occur during the reactor lifetime of 40 y. Thermal aging at reactor temperatures increases the tensile strength and decreases the impact energy and fracture toughness of the steels. The Charpy transition curve shifts to

Table 1. Product form, chemical composition, hardness, and ferrite morphology of various heats of cast stainless steel

Heat	Grade	Chemical Composition (wt.%)									Ferrite[a] (%)		Hardness	Ferrite Spacing
		Mn	Si	P	S	Mo	Cr	Ni	N	C	Calc.	Meas.	R_B	(μm)
							Keel Blocks[b]							
50	CF-3	0.60	1.10	0.016	0.007	0.33	17.89	9.14	0.079	0.034	3.0	4.4	80.1	194
49	CF-3	0.60	0.95	0.010	0.007	0.32	19.41	10.69	0.065	0.010	4.4	7.2	76.6	185
48	CF-3	0.60	1.08	0.009	0.006	0.30	19.55	10.46	0.072	0.011	5.1	8.7	78.1	127
47	CF-3	0.60	1.06	0.007	0.006	0.59	19.81	10.63	0.028	0.018	8.4	16.3	79.7	68
52	CF-3	0.57	0.92	0.012	0.005	0.35	19.49	9.40	0.052	0.009	10.3	13.5	81.6	69
51	CF-3	0.63	0.86	0.014	0.005	0.32	20.13	9.06	0.058	0.010	14.3	18.0	83.8	52
58	CF-8	0.62	1.12	0.010	0.005	0.33	19.53	10.89	0.040	0.056	3.2	2.9	77.1	303
54	CF-8	0.55	1.03	0.011	0.005	0.35	19.31	9.17	0.084	0.063	4.1	1.8	83.3	317
57	CF-8	0.62	1.08	0.009	0.004	0.34	18.68	9.27	0.047	0.056	4.4	4.0	80.2	138
53	CF-8	0.64	1.16	0.012	0.009	0.39	19.53	9.23	0.049	0.065	6.3	8.7	83.1	92
56	CF-8	0.57	1.05	0.007	0.007	0.34	19.65	9.28	0.030	0.066	7.3	10.1	82.5	84
59	CF-8	0.60	1.08	0.008	0.007	0.32	20.33	9.34	0.045	0.062	8.8	3.5	83.2	75
61	CF-8	0.65	1.01	0.007	0.007	0.32	20.65	8.86	0.080	0.054	10.0	13.1	85.3	82
60	CF-8	0.67	0.95	0.008	0.006	0.31	21.05	8.34	0.058	0.064	15.4	21.1	86.7	63
62	CF-8M	0.72	0.56	0.007	0.005	2.57	18.29	12.39	0.030	0.063	2.8	4.5	78.1	140
63	CF-8M	0.61	0.58	0.007	0.006	2.57	19.37	11.85	0.031	0.055	6.4	10.4	81.6	81
66	CF-8M	0.60	0.49	0.012	0.007	2.39	19.45	9.28	0.029	0.047	19.6	19.8	85.3	41
65	CF-8M	0.50	0.48	0.012	0.007	2.57	20.78	9.63	0.064	0.049	20.9	23.4	89.0	43
64	CF-8M	0.60	0.63	0.006	0.005	2.46	20.76	9.40	0.038	0.038	29.0	28.4	89.7	41
							76-mm Slabs[c]							
69	CF-3	0.63	1.13	0.015	0.005	0.34	20.18	8.59	0.028	0.023	21.0	23.6	83.7	35
73	CF-8	0.72	1.09	0.028	0.016	0.25	19.43	8.54	0.053	0.070	7.0	7.7	78.8	253
68	CF-8	0.64	1.07	0.021	0.014	0.31	20.64	8.08	0.062	0.063	14.9	23.4	84.6	87
70	CF-8M	0.55	0.72	0.021	0.016	2.30	19.17	9.01	0.049	0.066	14.2	18.9	86.5	96
74	CF-8M	0.54	0.73	0.022	0.016	2.51	19.11	9.03	0.048	0.064	15.5	18.4	85.8	90
75	CF-8M	0.53	0.67	0.022	0.012	2.58	20.86	9.12	0.052	0.065	24.8	27.8	89.5	69
							Reactor Components[d]							
P3	CF-3	1.06	0.88	0.017	0.014	0.01	18.89	8.45	0.168	0.021	2.8	1.9	82.2	–
P2	CF-3	0.74	0.94	0.019	0.006	0.16	20.20	9.38	0.040	0.019	12.5	15.6	83.8	69
I	CF-3	0.47	0.83	0.030	0.011	0.45	20.20	8.70	0.032	0.019	20.4	17.1	81.0	65
C1	CF-8	1.22	1.18	0.033	0.008	0.65	19.00	9.37	0.040	0.039	7.8	2.2	79.5	–
P1	CF-8	0.59	1.12	0.026	0.013	0.04	20.49	8.10	0.056	0.036	17.7	24.1	84.9	90
P4	CF-8M	1.07	1.02	0.019	0.015	2.05	19.64	10.00	0.151	0.040	5.9	10.0	83.1	182
205	CF-8M	0.93	0.63	0.019	–	3.37	17.88	8.80	–	0.040	21.0	15.9	–	79
758	CF-8M	0.91	0.62	0.018	–	3.36	17.91	8.70	–	0.030	24.2	19.2	–	62
							Reactor-Aged[e]							
KRB	CF-8	0.31	1.17	–	–	0.17	21.99	8.03	0.038	0.062	27.7	34.0	–	–

Table 1. (Contd.)l

Heat	Grade	Chemical Composition (wt.%) Mn	Si	P	S	Mo	Cr	Ni	N	C	Ferrite[a] (%) Calc.	Meas.	Hardness R_B	Ferrite Spacing (μm)
							Laboratory-Aged[f]							
280	CF-3	0.50	1.37	0.015	0.006	0.25	21.60	8.00	0.038	0.028	36.3	40.0	-	186
278	CF-8	0.28	1.00	0.008	0.019	0.13	20.20	8.27	0.030	0.038	18.5	15.0	-	174
292	CF-8	0.34	1.57	0.018	0.016	0.13	21.60	7.52	0.039	0.090	23.9	28.0	-	-
286	CF-8M	0.40	1.33	0.044	0.015	2.44	20.20	9.13	0.062	0.072	18.9	22.0	-	201

[a] Calculated from the composition with Hull's equivalent factor.
Measured by ferrite scope AUTO Test FE, Probe Type FSP-1.
[b] *Static Cast Keel Blocks:* Foundry ESCO; Size 180 x 120 x 90–30 mm.
[c] *Static Cast Slabs*: Foundry ESCO; Size 610 x 610 x 76 mm.
[d] *Centrifugally Cast Pipes*:
P3 Foundry SANDUSKY; Size 580 mm O.D.,76 mm wall.
P2 Foundry FAM, France; Size 930 mm O.D., 73 mm wall.
P1 Foundry ESCO; Size 890 mm O.D., 63 mm wall.
P4 Foundry SANDUSKY; Size 580 mm O.D., 32 mm wall.
205 Size 305 mm O.D., 25 mm wall.
Static Cast:
Elbow 758: Size 305 mm O.D., 30 mm wall.
Pump Impeller I: Foundry ESCO; Size 660 mm diameter.
Pump Casing C1: Foundry ESCO; Size 600 mm O.D., 57 mm wall.
[e] *KRB Reactor Pump Cover Plate*: Foundry GF; Size 890 mm diameter.
[f] Aged Material from George Fischer Co., Switzerland.

higher temperatures. Different heats exhibit different degrees of thermal embrittlement. For cast stainless steel of all grades, the extent of thermal embrittlement increases with an increase in ferrite content. The low-C CF-3 steels are the most resistant, and the Mo-bearing, high-C CF-8M steels are the least resistant to thermal embrittlement. The flow stress of fully aged CF-3 steels increases by ≈10% and that of CF-8 and CF-8M steels increases by ≈20%. The fracture toughness J_{IC} and average tearing modulus for heats that are sensitive to thermal aging (e.g., CF-8M steels) are as low as ≈90 kJ/m^2 and ≈60, respectively. Correlations have been developed for estimating the increase in flow stress of the steels from data on the kinetics of thermal embrittlement.[15]

The mechanisms of thermal embrittlement of cast duplex stainless steel have been discussed.[12] Embrittlement of cast stainless steels results in a brittle fracture associated with either cleavage of the ferrite or separation of the ferrite/austenite phase boundary. The degree of thermal embrittlement is controlled by the amount of brittle fracture. Cast stainless steels with poor impact strength exhibit >80% brittle fracture. In some cast steels, a fraction of the material may fail in a brittle fashion but the surrounding austenite provides ductility and toughness. Such steels have adequate impact strength even after long-term aging. A predominantly brittle failure occurs when either the ferrite phase is continuous, e.g., in cast material with a large ferrite content, or the ferrite/austenite phase boundary provides an easy path for crack propagation, e.g., in high-C grades of cast steels with large phase-boundary carbides. Consequently, the amount, size, and distribution of the ferrite phase in the duplex structure, and the presence of phase-boundary carbides are important parameters in controlling the degree or extent of thermal embrittlement.

Thermal aging of cast stainless steels at <500°C (<932°F) leads to precipitation of additional phases in the ferrite, e.g., formation of a Cr-rich α' phase by spinodal decomposition; nucleation and growth of α'; precipitation of a Ni- and Si-rich G phase, $M_{23}C_6$ carbide, and γ_2 (austenite); and additional precipitation and/or growth of existing carbides at the ferrite/austenite phase boundaries.[18-21] The additional phases provide the strengthening mechanisms that increase strain hardening and local tensile stress. Consequently, the critical stress level for brittle fracture is achieved at higher temperatures. The effects of material variables on the thermal embrittlement of cast stainless steels have been evaluated.

Phase-boundary separation generally occurs in the high-C steels because of the presence of large $M_{23}C_6$ carbides at the phase boundaries. For CF-8 steels, the phase-boundary carbides form during production heat treatment of the casting. Consequently, the unaged CF-8 steels exhibit low lower-shelf energy and high mid-shelf Charpy transition temperature (CTT) relative to the CF-3 steels. The fracture mode for CF-8 steels in the lower-shelf or transition-temperature regime is predominantly phase-boundary separation.[7,8,12,13] In contrast, the CF-3 steels show dimpled ductile failure. Fracture by phase-boundary separation is observed in only a few heats of unaged CF-8M steels and is dependent on whether the material contains phase-boundary carbides. Materials aged at 450°C (842°F) show significant precipitation of phase-boundary carbides (also nitrides in high-N steels) and a large decrease in ferrite content of the material.[7,8,12,13] Such processes either do not occur or their kinetics are extremely slow at reactor temperatures. Consequently, data obtained at 450°C aging do not reflect reactor operating conditions, and extrapolation of the 450°C data to predict the extent of thermal embrittlement at reactor temperatures is not valid.

The chemical composition, production heat treatment, and the ferrite content and spacing of the steel are important parameters in controlling the extent and kinetics of thermal embrittlement. Ferrite morphology strongly affects the extent of thermal embrittlement, whereas material composition and production heat treatment influence the kinetics of embrittlement. Changes in the heat treatment or chemical composition of the steel can alter the kinetics of thermal embrittlement significantly; activation energies for embrittlement can range from 65 to 230 kJ/mole. The kinetics of thermal embrittlement of cast stainless steels is controlled primarily by the kinetics of strengthening of the ferrite, i.e., by the size and spacing of α' phase produced by the spinodal reaction. The log of the time of aging at 400°C (752°F) for a 50% reduction in Charpy-impact energy has been shown to be a useful parameter to characterize the kinetics of thermal embrittlement.[16] The aging behavior at 400°C varies significantly for the various heats of cast stainless steel. For example, the time of aging at 400°C required for 50% reduction in impact energy varies from 200 to 10,000 h for the various steels. Production heat treatment and possibly the casting process influence the aging behavior at 400°C and, therefore, the kinetics of thermal embrittlement. Activation energy for thermal embrittlement is high for those steels that show fast embrittlement at 400°C and is low for those that show slow embrittlement at 400°C. Precipitation of G phase in the ferrite has little or no effect on the kinetics of thermal embrittlement. Material parameters that influence the kinetics of thermal embrittlement also effect G-phase precipitation. However, activation energy for thermal embrittlement is generally low for cast stainless steels that contain G-phase. Estimation of the mechanical-property degradation suffered by cast stainless steel components, by extrapolation of the high-temperature data to reactor temperatures, requires not only the activation energy for thermal embrittlement of that specific material but also a reference aging behavior of the material at high temperatures, e.g., at 400°C.

This report presents a procedure and correlations for predicting fracture toughness of cast stainless steel components due to thermal aging during service in LWRs at 280–330°C (535–625°F). The correlations are validated with mechanical-property data obtained on cast stainless steel components from the decommissioned Shippingport reactor. The present analysis has focused on developing correlations for the fracture properties in terms of material information that can be determined from certified material test records (CMTRs) and on ensuring that the correlations are adequately conservative for static-cast and centrifugally cast components. Fracture toughness of a specific cast stainless steel is estimated from the extent and kinetics of thermal embrittlement. The extent of thermal embrittlement is characterized by the room-temperature "normalized" Charpy-impact energy (Charpy-impact energy per unit area). Based on the information available, two methods are presented for estimating the extent of thermal embrittlement at "saturation," i.e., the minimum impact energy that would be achieved by the material after long-term aging. The first method utilizes only the information available in the CMTRs, i.e., chemical composition of the steel. The second method is used when metallographic information on the ferrite morphology is also available, i.e., measured values of ferrite content and mean ferrite spacing of the steel are known.

Extent of thermal embrittlement as a function of time and temperature of reactor service is then estimated from the extent of thermal embrittlement at saturation and from the correlations describing the kinetics of thermal embrittlement, which are also given in terms of chemical composition. The fracture toughness J-R curve for the material is then obtained from the correlation between fracture toughness parameters and room-temperature Charpy-impact energy used to characterize the extent of thermal embrittlement. A common lower-bound J-R curve for cast materials with unknown chemical composition is also defined for a given material specification, ferrite content, and temperature.

Since the toughness of static-cast materials is generally lower than for centrifugally cast materials, the correlations tend to be fairly conservative for centrifugally cast materials. However, it was felt that at the present time the data base is not extensive enough to warrant the development of separate correlations for the two types of castings. Tests that should provide sufficient data to develop separate less conservative correlations are in progress. In this report, mechanical properties are expressed in SI units (see Nomenclature for units of measurements and conversion factors for British units).

2 Extent of Embrittlement at Saturation

Charpy-impact data obtained at room temperature indicate that, for a specific heat of cast stainless steel, a saturation value of minimum impact energy is reached after aging for 3,000–10,000 h at 400°C (752°F) or 30,000–60,000 h at 350°C (662°F). The variation of this saturation impact energy C_{Vsat} for different materials can be expressed in terms of a material parameter Φ that is determined from the chemical composition and ferrite morphology of the materials. It is well established that the extent of thermal embrittlement increases with an increase in the ferrite content of cast stainless steel. Furthermore, Charpy-impact data for several heats of CF-8 and CF-8M steels indicate that impact energy decreases with an increase in Cr content, irrespective of the ferrite content of the steel.[24] A better correlation is obtained when the total concentration of ferrite formers (i.e., Cr, Mo,

and Si) is considered.[24] A sharp decrease in impact energy occurs when either the Cr content exceeds 18 wt.% or the concentration of Cr+Mo+Si exceeds 23.5 wt.%. The concentration of Ni and Si in the steel, i.e., the elements that promote G–phase formation, also appear to increase the extent of thermal embrittlement of the Mo–bearing CF–8M steels. An increase in the concentration of C or N in the steel also increases the extent of thermal embrittlement because of the contribution to phase–boundary carbides or nitrides and the subsequent fracture by phase–boundary separation.

Based on the amount of information available, two different methods for estimating the material parameter and saturation impact energy are presented. The first method utilizes only the information available in the CMTRs, i.e., chemical composition of the material. The second method allows an estimate of saturation impact energy to be obtained when metallographic information on ferrite morphology is also available, i.e., the measured values of ferrite content and mean ferrite spacing of the steel are known.

2.1 Method A – When Only a CMTR Is Available

The saturation fracture toughness of a specific cast stainless steel, i.e., the minimum fracture toughness that would be achieved by the material after long–term aging, is estimated from the degree of thermal embrittlement at saturation. The degree of embrittlement is characterized in terms of room–temperature "normalized" Charpy–impact energy. The variation of the impact energy at saturation for different materials can be expressed in terms of a material parameter Φ, which is determined from the chemical composition.

The material parameter Φ is estimated from the information available in the CMTR, e.g., chemical composition. The ferrite content is calculated in terms of the Hull's equivalent factors[29]

$$Cr_{eq} = Cr + 1.21(Mo) + 0.48(Si) - 4.99 \quad (1)$$

and

$$Ni_{eq} = (Ni) + 0.11(Mn) - 0.0086(Mn)^2 + 18.4(N) + 24.5(C) + 2.77, \quad (2)$$

where chemical composition is in wt.%. The concentration of N is often not available in the CMTR; it is assumed to be 0.04 wt.% if not known. The ferrite content δ_c is given by

$$\delta_c = 100.3(Cr_{eq}/Ni_{eq})^2 - 170.72(Cr_{eq}/Ni_{eq}) + 74.22. \quad (3)$$

The measured and calculated values of ferrite content for the various heats used in studies at ANL,[7–16] Framatome (FRA),[26] Georg Fischer Co. (GF),[1] Electricité de France (EdF),[24] Central Electricity Generation Board (CEGB),[25] and Electric Power Research Institute (EPRI)[28] are shown in Fig. 1. The chemical composition, ferrite content, and room–temperature Charpy impact energy of the various materials are given in Tables 1 and 2. For most heats, the difference between the estimated and measured values is ±6% ferrite. The few heats for which the estimated ferrite contents are significantly lower than the measured values generally contain ≥10% nickel.

Table 2. Chemical composition and kinetics of thermal embrittlement for Georg Fischer and Framatome heats of cast stainless steels

	Chemical Composition (wt.%)							C_{Vsat}	Constants			Q
Heat	Cr	Mo	Si	Ni	Mn	C	N	(J/cm^2)	β	θ	α	(kJ/mole)
						Georg Fischer Co.						
277	20.5	0.06	1.81	8.13	0.54	0.052	0.019	33.5	0.488	3.65	0.55	88
278	20.2	0.13	1.00	8.27	0.28	0.038	0.030	68.3	0.381	4.05	0.47	63
279	22.0	0.22	1.36	7.85	0.37	0.040	0.032	23.8	0.586	3.21	0.69	92
280	21.6	0.25	1.37	8.00	0.50	0.028	0.038	24.4	0.591	3.30	0.73	87
281	23.1	0.17	0.45	8.60	0.41	0.036	0.053	26.6	0.560	3.76	0.42	93
282	22.5	0.15	0.35	8.53	0.43	0.035	0.040	30.0	0.525	3.73	0.43	98
283	22.6	0.23	0.53	7.88	0.48	0.036	0.032	23.8	0.580	3.65	0.43	83
284	23.0	0.17	0.52	8.23	0.28	0.025	0.037	23.8	0.560	3.71	0.41	87
291	19.6	0.66	1.59	10.60	0.28	0.065	0.054	121.9	0.235	3.89	0.79	77
292	21.6	0.13	1.57	7.52	0.34	0.090	0.039	22.2	0.392	3.08	0.46	99
285	18.8	2.35	0.86	9.49	0.48	0.047	0.039	64.3	0.347	3.76	0.34	82
286	20.2	2.44	1.33	9.13	0.40	0.072	0.062	20.5	0.571	3.11	0.62	106
287	20.5	2.58	0.51	8.46	0.50	0.047	0.033	23.8	0.563	3.52	0.42	92
288	19.6	2.53	1.70	8.40	0.47	0.052	0.022	19.4	0.643	3.02	0.64	106
289	19.7	2.30	1.44	8.25	0.48	0.091	0.032	21.1	0.571	3.32	0.39	90
290	20.0	2.40	1.51	8.30	0.41	0.054	0.050	21.1	0.602	3.49	0.11	81
						Framatome						
C	20.7	0.13	1.09	8.19	1.09	0.042	0.035	51.0	0.393	3.30	0.45	83
E	21.0	0.08	0.54	8.47	0.80	0.035	0.051	45.0	0.334	2.63	0.65	133
F	19.7	0.34	1.16	8.33	0.26	0.038	0.026	83.0	0.282	2.45	1.23	176
B	20.1	2.52	0.93	10.56	0.83	0.053	0.042	31.0	0.478	2.55	0.47	129
D	19.2	2.44	0.94	10.32	1.12	0.026	0.063	33.0	0.439	3.30	0.40	90

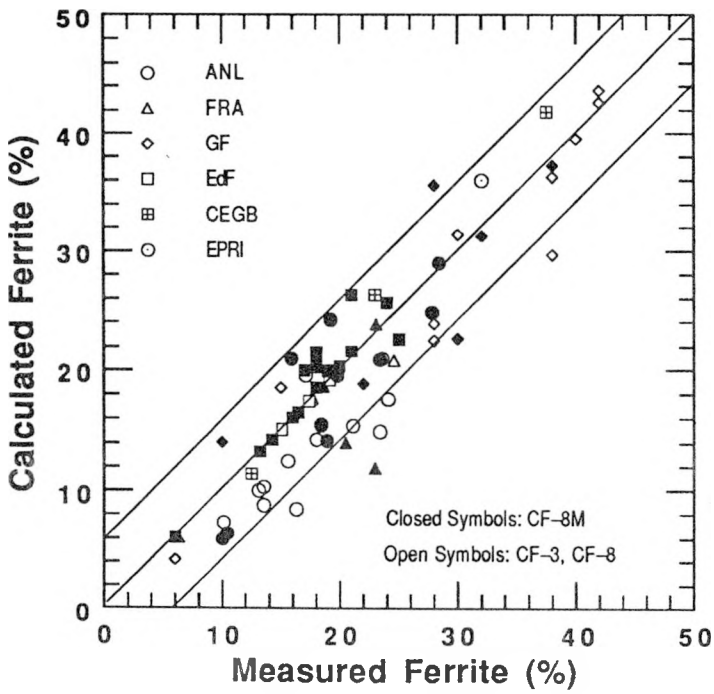

Figure 1. Measured and calculated ferrite contents for various heats of cast stainless steel. The dashed lines represent ±6% deviation.

Different correlations are used to estimate the saturation impact energy of the various grades of cast stainless steel. For CF–3 and CF–8 steels, the material parameter Φ is expressed as

$$\Phi = \delta_c(Cr + Si)(C + 0.4N) \quad (4)$$

and the saturation value of room–temperature normalized impact energy C_{Vsat} is given by

$$\log_{10}C_{Vsat} = 1.15 + 1.374\exp(-0.0365\Phi). \quad (5)$$

For the Mo–bearing CF–8M steels, the material parameter Φ is expressed as

$$\Phi = \delta_c Cr(C + 0.4N)(Ni + Si)^2/100 \quad (6)$$

and the saturation value of room–temperature normalized impact energy C_{Vsat} is given by

$$\log_{10}C_{Vsat} = 1.15 + 1.532\exp(-0.0467\Phi). \quad (7)$$

In Eqs. 4 and 6 N content can be assumed to be 0.04 wt.% if the value is not known.

The saturation values of room–temperature impact energy predicted by Eqs. 4 and 5 and those observed experimentally at ANL, FRA, GF, EdF, CEGB, and EPRI are shown in Fig. 2a. The difference between the predicted and observed values is $\leq \pm 15\%$ for most of the materials. The observed room–temperature impact energy at saturation and values predicted by Eqs. 6 and 7 are shown in Fig. 2b for the data from ANL, FRA, GF, and EdF studies. The difference between observed and predicted values for the CF–8M steel is larger than that for the CF–3 or CF–8 steels.

The correlations expressed in Eqs. 4–7 do not include Nb, and may not be conservative for Nb–bearing steels. Furthermore, for CF–8M steels with ≥10% Ni, the calculated ferrite content δ_c is often lower than the measured value. Consequently, for these steels, the measured ferrite content δ_m, if known, should be used instead of the calculated ferrite content δ_c in Eqs. 4 and 6.

2.2 Method B – When Metallographic Information Is Available

A common expression for material parameter for the various grades of steel can be obtained when the measured values of ferrite content and mean ferrite spacing of the steel are known. In this case, the material parameter Φ is representative of both the structure and the steel composition and is given by

$$\Phi = \delta_m^2(Cr + Mo + Si)(C + 0.4N)Ni\lambda/10^4, \quad (8)$$

where δ_m is the measured ferrite content (in %) and λ is the mean ferrite spacing (in μm). The saturation value of room–temperature impact energy C_{Vsat} is given by the relation

$$\log_{10}C_{Vsat} = 1.386 + 0.938\exp(-0.0205\Phi). \quad (9)$$

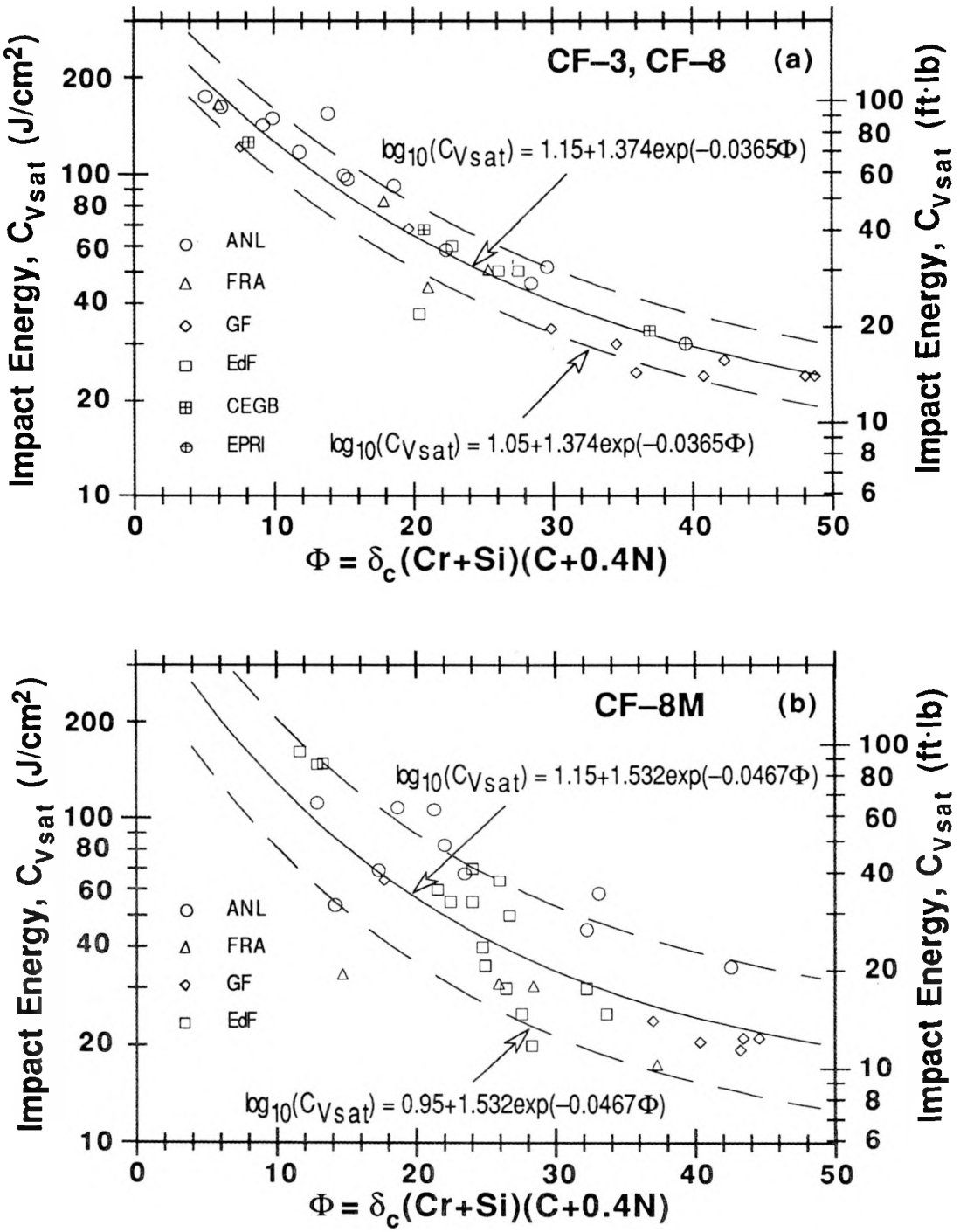

Figure 2. Correlation between room–temperature Charpy–impact energy at saturation and material parameter Φ (Method A) for CF–3, CF–8, and CF–8M steels. The dashed lines represent ±26% and ±58% deviation from the predicted values in Figs. 2a and 2b, respectively.

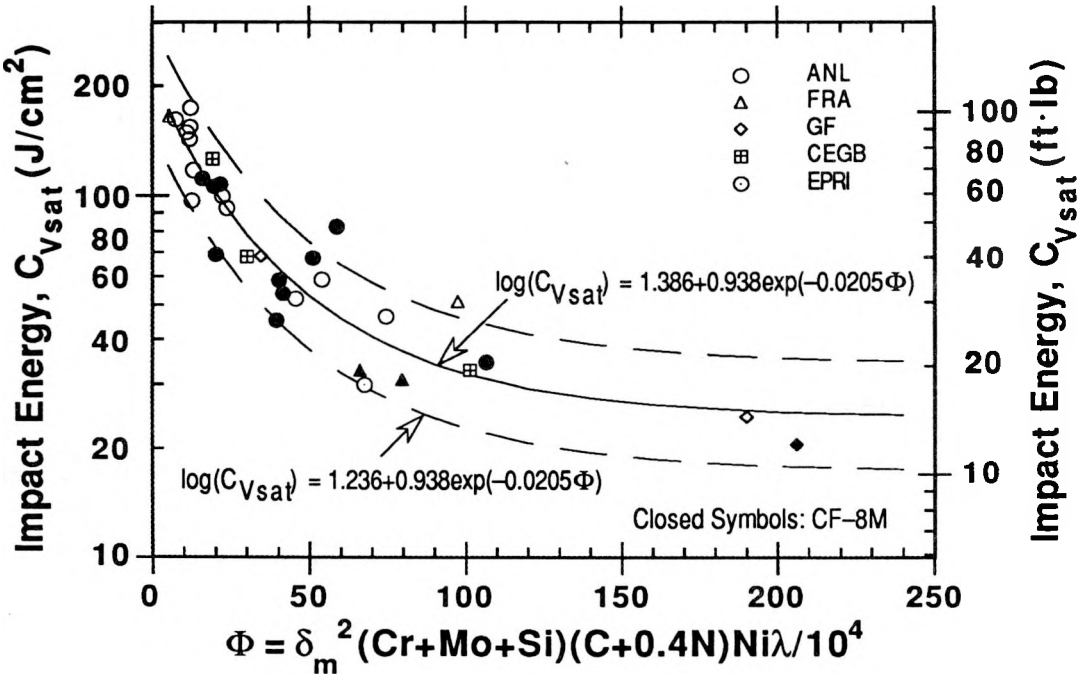

Figure 3. Correlation between room-temperature Charpy-impact energy at saturation and material parameter Φ (Method B) for all grades of cast stainless steels. The dashed lines represent ±41% deviation from the predicted values.

In the field, δ_m would have to be measured with a magne-gage or a ferrite scope (nonsaturation magnetic induction principle) and λ would be determined from metallographic replicas of the actual component. The N content is assumed to be 0.04 wt.% if not known.

Plots of room-temperature impact energy and the material parameter Φ, calculated from Eqs. 8 and 9, are shown in Fig. 3, together with data from studies at ANL, FRA, GF, CEGB, and EPRI. The saturation impact energies predicted from Eqs. 8 and 9 for CF-3 or CF-8 steels are comparable to those estimated from Eqs. 4 and 5; those for CF-8M steel are better than those estimated from Eqs. 6 and 7. As discussed in the previous section, Eq. 8 also does not consider the effects of Nb on thermal embrittlement and, hence, may not be conservative for Nb-bearing cast stainless steels.

3 Kinetics of Embrittlement

The results from room-temperature Charpy-impact tests on the various heats, aged up to 30,000 h at 290, 320, 350, 400, and 450°C (554, 608, 662, 752, and 842°F), were analyzed to determine the kinetics of thermal embrittlement. The variation of the Charpy-impact energy C_V (J/cm^2) with time can be expressed as

$$\log_{10}C_V = \log_{10}C_{Vsat} + \beta\{1 - \tanh[(P - \theta)/\alpha]\}, \quad (10)$$

Table 3. Kinetics of thermal embrittlement for ANL heats of cast stainless steel

Heat	Parameter Φ[a]	C_{Vsat} (J/cm^2)	Constants β	θ	α	Q (kJ/mole (kcal/mole)) Average	95% Confidence Limit
47	12.0	174.2	0.063	2.35	1.40	187 (44.7)	73–300 (17.5–71.8) [b]
51	10.8	149.2	0.083	3.00	0.76	221 (52.8)	123–320 (29.3–76.4) [b]
69	12.4	96.9	0.202	3.05	0.93	167 (40.0)	120–215 (28.7–51.3) [b]
59	22.2	99.8	0.166	3.12	1.40	229 (54.7)	156–301 (37.4–72.0)
60	45.5	52.0	0.288	2.95	0.89	227 (54.2)	186–267 (44.4–63.9)
68	74.4	46.4	0.348	3.00	0.74	169 (40.5)	136–204 (32.4–48.2)
P1	53.5	58.7	0.282	2.38	0.75	249 (59.6)	210–289 (50.2–69.1)
63	15.8	111.7	0.155	3.20	1.40	119 (28.4)	67–170 (16.0–40.7)
64	39.4	45.2	0.304	2.75	0.62	156 (37.4)	131–181 (31.4–43.2)
65	40.3	58.5	0.269	2.93	0.94	191 (45.7)	154–228 (36.8–54.6)
66	19.5	106.3	0.149	3.02	1.30	203 (48.4)	125–280 (29.9–66.9) [b]
75	106.4	34.7	0.422	2.76	0.53	146 (34.8)	127–165 (30.3–39.4)
P4	41.5	53.8	0.325	2.95	0.89	143 (34.2)	115–171 (27.6–40.8)

[a] Calculated from Eq. 8.

[b] Standard deviation is large because of the relatively small decrease in impact energy and a large scatter in data.

where C_{Vsat} (J/cm^2) is the saturation minimum impact energy reached after long-term aging, β is half the maximum change in $\log C_V$, θ is the log of the time to achieve β reduction in impact energy at 400°C (752°F), α is a shape factor, and P is the aging parameter defined by

$$P = \log_{10}(t) - \frac{1000Q}{19.143}\left(\frac{1}{T_s + 273} - \frac{1}{673}\right), \qquad (11)$$

where Q is the activation energy (kJ/mole) and t and T_s are time (h) and temperature (°C), respectively. The values of the constants in Eqs. 10 and 11 for the GF and FRA heats are given in Table 2 and for the ANL heats in Table 3. The constant β can be determined from the initial impact energy of the unaged material C_{Vint} and the saturation impact energy C_{Vsat}, thus

$$\beta = (\log_{10}C_{Vint} - \log_{10}C_{Vsat})/2. \qquad (12)$$

The results for the kinetics of thermal embrittlement indicate that the shape factor α increases linearly with C_{Vsat}. The best fit of the data for the various heats yields the expression

$$\alpha = -0.821 + 0.947\log_{10}C_{Vsat}. \qquad (13)$$

C_{Vsat} can be calculated from correlations presented in the Section 2 if the chemical composition is known. In practice, the initial impact energy is unlikely to be available. Mechanical-property data indicate that Charpy-impact energy of cast stainless steels is typically 200 ±20 J/cm^2, however, it can be as low as 60 J/cm^2 for some steels.[12,15]

Activation energy for the thermal embrittlement process has been expressed in terms of the chemical composition of the cast material. The earliest correlation, proposed by FRA, was based on GF data[1] for 16 heats of cast stainless steel. Activation energy was expressed as a function of the concentrations (wt.%) of Cr, Mo, and Si in the steel; thus,

$$Q \text{ (kJ/mole)} = -182.6 + 19.9\ Si + 11.08\ Cr + 14.4\ Mo. \quad (14)$$

The activation energy calculated from Eq. 14 for the process of thermal embrittlement ranges from 65 to 105 kJ/mole for the various grades of cast stainless steel. However, the estimated activation energies for ANL or CEGB heats are a factor of 2 lower than the experimental values. The GF data set covers a relatively narrow range of compositions, and the ferrite contents of most heats are above 30%; therefore, they are not representative of compositions defined by ASTM Specification A 351.

The correlations developed by ANL were based on a larger data base. Two separate correlations were proposed: one for the ANL[8,12] and FRA data[26] (15 heats), given by

$$Q \text{ (kJ/mole)} = 90.54 + 9.62\ Cr - 8.12\ Ni - 7.53\ Mo + 20.59\ Si - 123.0\ Mn + 317.7\ N, \quad (15)$$

and the other for the GF data[1] (16 heats), given by

$$Q \text{ (kJ/mole)} = -66.65 + 6.90\ Cr - 5.44\ Ni + 8.08\ Mo + 17.15\ Si + 44.1\ Mn + 297.1\ N, \quad (16)$$

where the constituent elements are given in wt.%. For a specific material composition, the activation energies predicted from Eqs. 14 and 16 are comparable, whereas those from Eq. 15 are higher. The ANL data used in developing these correlations represented only high-temperature aging; the results for long-term aging (i.e., 30,000 h) at 290 or 320°C (554 or 608°F) were not included in the analyses. Thus, the calculated activation energies primarily represent the kinetics of thermal embrittlement at temperatures between 350 and 450°C (662 and 842°F). These values are 15–20% lower than those determined from aging data at temperatures between 290 and 400°C (554 and 752°F).[13–15]

The results from Charpy-impact tests and microhardness measurements of the ferrite phase indicate that the kinetics of thermal embrittlement of cast stainless steels is controlled primarily by the kinetics of strengthening of the ferrite, i.e., by the size and spacing of α' phase produced by the spinodal reaction. The log of the time of aging at 400°C for a 50% reduction in Charpy-impact energy (i.e., value of the constant θ) has been shown to be a useful parameter to characterize the kinetics of thermal embrittlement.[16] The value of θ varies between ≈2.0 and 4.0 for the various heats of cast stainless steels. Limited data indicate that the production heat treatment and possibly the casting process influence the aging behavior at 400°C and, therefore, the kinetics of thermal embrittlement. In general, activation energy increases with a decrease in the value of θ, i.e., activation energy for thermal embrittlement is high for heats that show fast kinetics at 400°C and is low for heats with slow kinetics at 400°C. Precipitation of G phase in the ferrite has little or no effect on the kinetics of thermal embrittlement.[16] Material parameters that influence the kinetics of thermal embrittlement also effect G-phase precipitation. However, activation energy for thermal embrittlement is generally low for cast stainless steels that contain G-phase.

Charpy data for the kinetics of thermal embrittlement were reanalyzed to develop a general correlation for activation energy that would be applicable for all chemical compositions within ASTM Specification A 351 and valid for the entire temperature range of extrapolation, i.e., 280–400°C (536–752°F). Activation energy for thermal embrittlement was expressed in terms of both chemical composition and the constant θ to incorporate the effects of heat treatment and the casting process on the kinetics of thermal embrittlement. The best fit of the data from ANL, FRA, GF, and CEGB studies (36 heats) yields the expression

$$Q\ (\text{kJ/mole}) = 10\,[74.06 - (7.66 - 0.46\,I_1)\,\theta - 4.35\,Si + 1.38\,I_2\,Mo - 1.67\,Cr - (2.22 + 3.56\,I_1)\,Mn + (108.8 - 75.3\,I_1)\,N], \qquad (17)$$

where the indicators $I_1 = 0$ and $I_2 = 1$ for CF-3 or CF-8 steels and assume the values of 1 and 0, respectively, for CF-8M steels. The estimated and observed values of Q for the ANL,[8,12-15] FRA,[26] CEGB,[25] and GF[1] heats are plotted in Fig. 4. The predicted values are

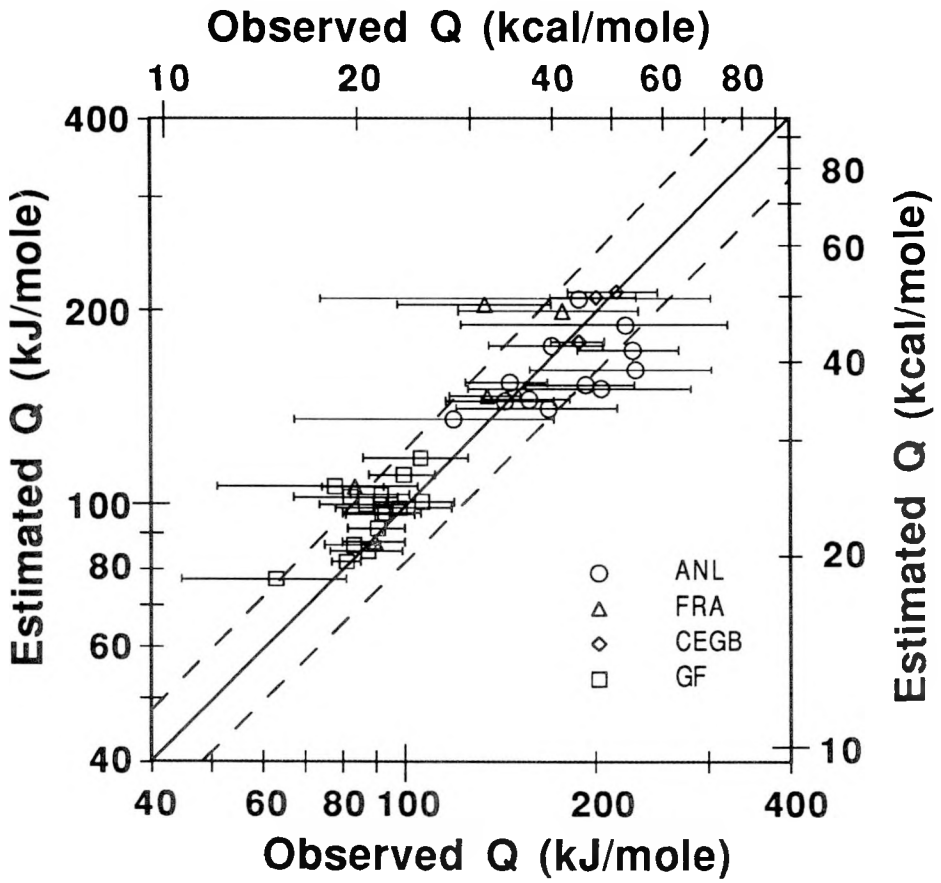

Figure 4. Observed and estimated activation energy for thermal embrittlement of cast stainless steels. Error bars represent 95% confidence limits for the observed values of Q and dashed lines represent ±20% range.

within the 95% confidence limits for all the heats. Equation 17 is applicable for compositions within ASTM Specification A 351, with a upper limit of 1.2 wt.% for Mn content. Actual Mn content is used up to 1.2 wt.% and is assumed to be 1.2 for steels containing >1.2 wt.% Mn. Furthermore, the values of Q predicted from Eq. 17 should be between 65 kJ/mole minimum and 250 kJ/mole maximum; Q is assumed to be 65 kJ/mole if the predicted values are lower and 250 kJ/mole if the predicted values are higher.

4 Estimation of Impact Energy

The room-temperature Charpy-impact energy of a specific cast stainless steel can be estimated from the correlations in Sections 2 and 3. Based on the information available, imapct energy at saturation C_{Vsat} can be determined from the two methods described in Section 2. The first method utilizes only the information available in the CMTRs, i.e., chemical composition of the steel. The second method is used when metallographic information on the ferrite morphology is also available, i.e., measured values of ferrite content and mean ferrite spacing of the steel are known. The saturation value represents the minimum impact energy that would be achieved by the material after long-term aging. Estimation of the decrease in impact energy as a function of time and temperature of service requires additional information, namely, the initial impact energy of the unaged material and the aging behavior at 400°C, i.e., the value of constant θ.

The estimated and observed impact energies for some of the ANL, FRA, and GF heats aged at temperatures between 300 and 350°C (572 and 662°F), are shown in Figs. 5 and 6. For each heat, the impact energy at saturation was determined first, from Eqs. 1–7, i.e., Method A. The activation energy for thermal embrittlement was obtained from Eq. 17; observed values of θ were used for all the heats. Then, the change in impact energy with time and temperature of aging was estimated from Eqs. 10–13. The measured value of C_{Vint}, i.e., initial impact energy of the unaged material, was used in Eq. 12 to determine β. The estimated change in impact energy shows good agreement with the observed aging behavior for most of the heats. For some heats, the estimated C_{Vsat} is higher than the observed value, e.g., Heat B. Such discrepancies are caused by underestimation of the ferrite content of the steel. As mentioned earlier, the ferrite contents estimated from Eqs. 1–3 for heats containing ≥10 wt.% Ni, are always lower than the measured values. A non-conservative value for C_{Vsat} can be avoided by using the lower-limit expressions for Eqs. 5 and 7, i.e., the lower-bound curves shown by the dashed line in Figs. 2 and 3.

The values of θ are not available for cast stainless steel components in the field, and can only be obtained from aging archive material for 5,000–10,000 h at 400°C (752°F). Parametric studies show that the aging response at reactor temperatures is relatively insensitive to the values of θ. Varying θ between 2.3 and 3.3 results in identical aging behavior at 300°C (572°F). At 330°C (626°F), a low value of θ predicts slightly faster kinetics and at 280°C (536°F), a high value of θ predicts faster kinetics. A median value of 2.9 for θ can be used to estimate thermal embrittlement at reactor temperatures, i.e., 280–330°C. Charpy-impact tests have been conducted on reactor-aged components from the Shippingport reactor to benchmark the laboratory data and validate these correlations.[30] The results show good agreemant with the estimated values and are presented in Section 7.

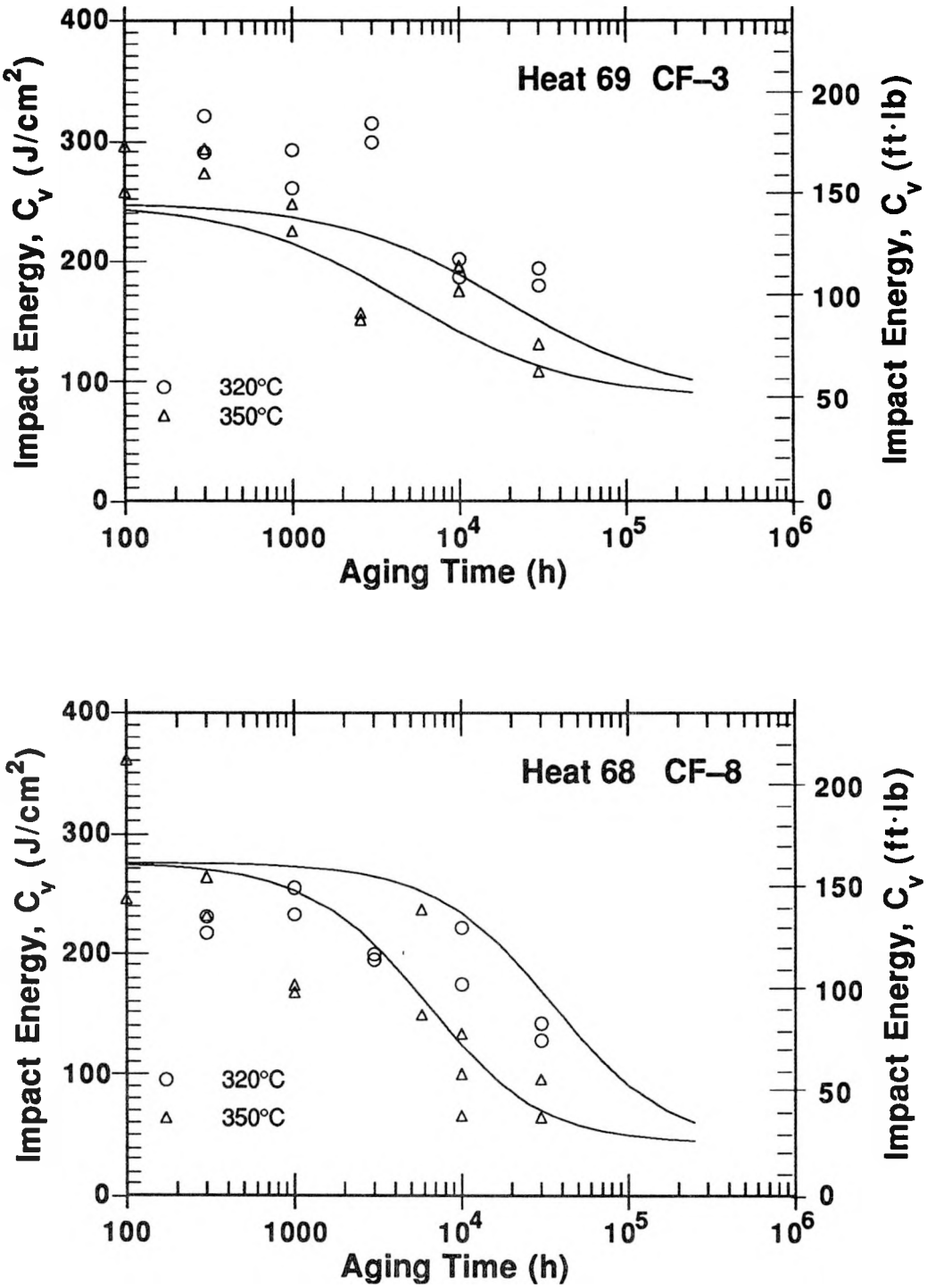

Figure 5. Observed and estimated room–temperature Charpy–impact energy for one heat of aged CF–3 and three heats of aged CF–8 cast stainless steel

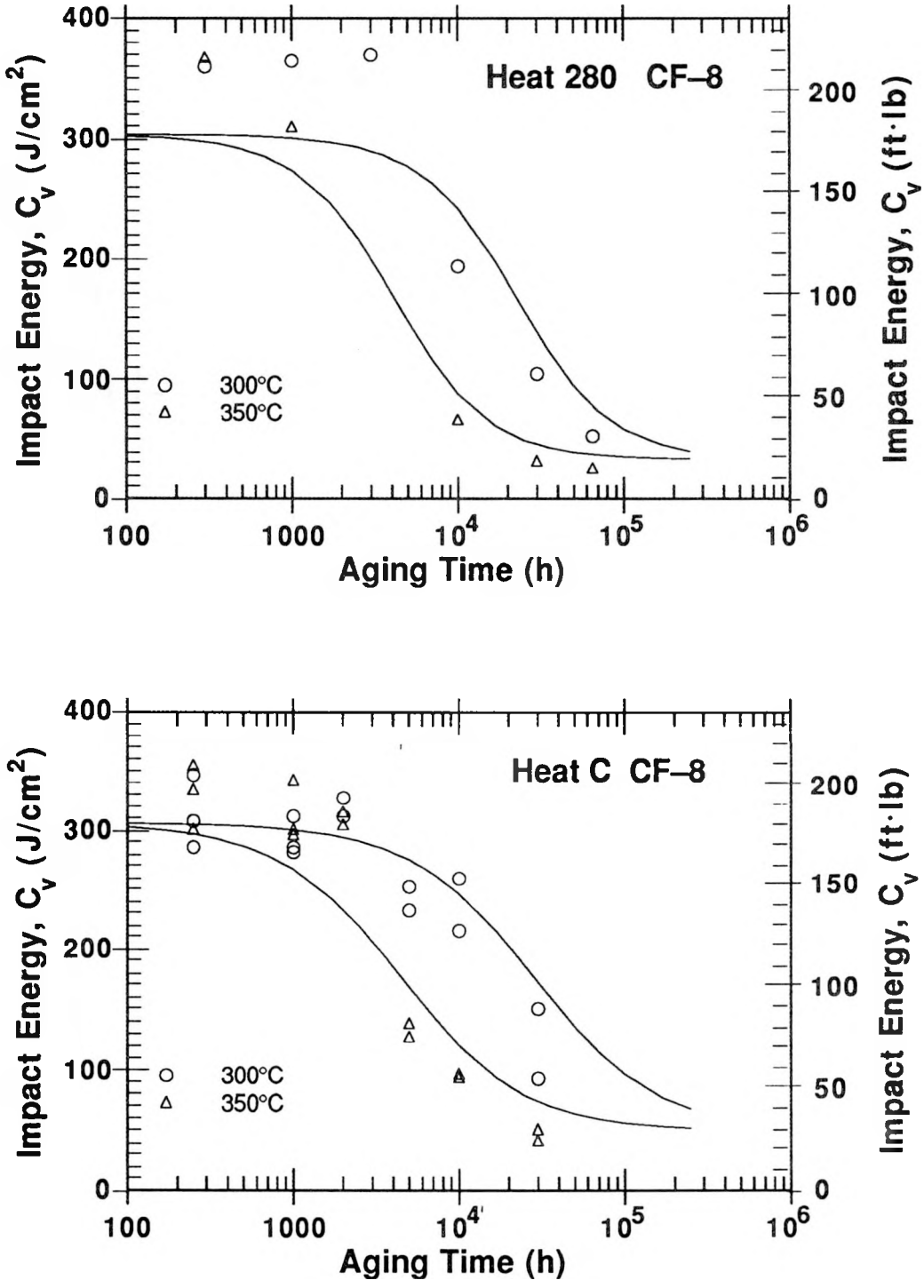

Figure 5. (Contd.)

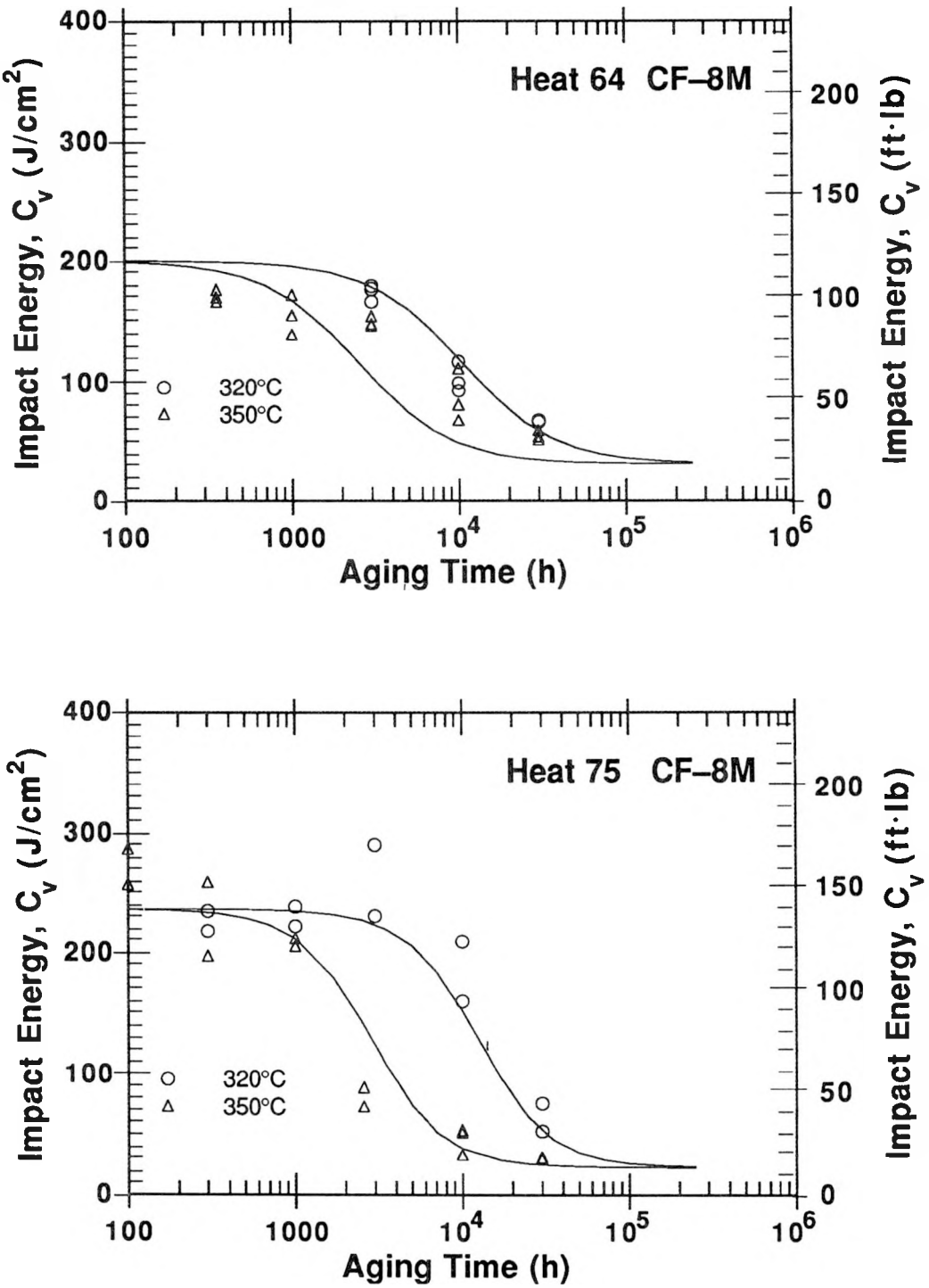

Figure 6. Observed and estimated room-temperature Charpy-impact energy for four heats of aged CF-8M cast stainless steel

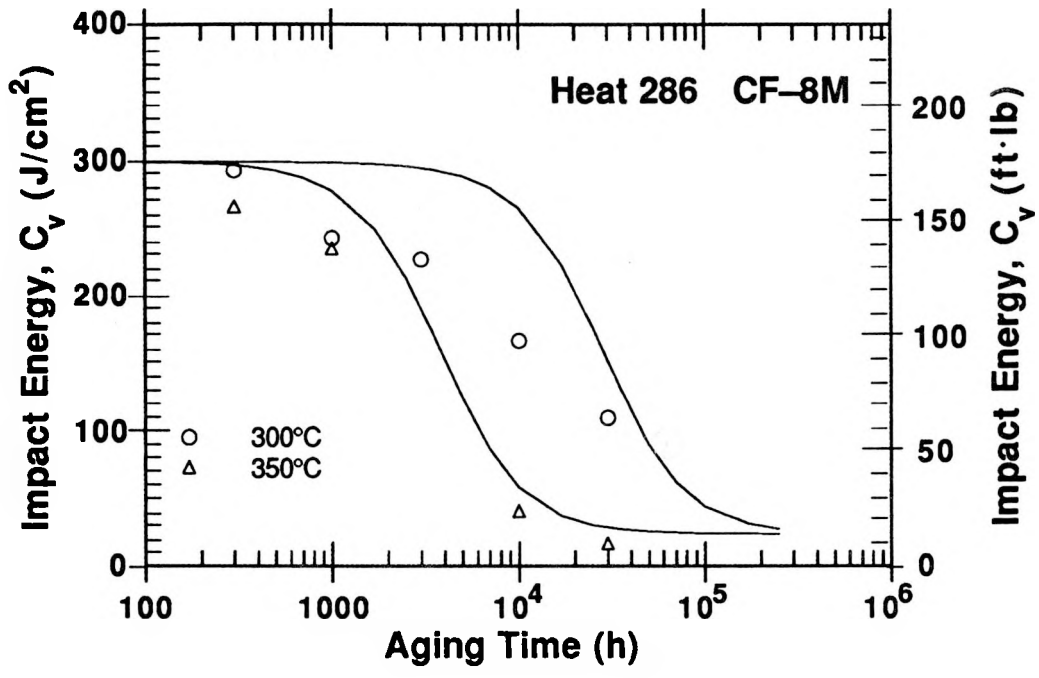

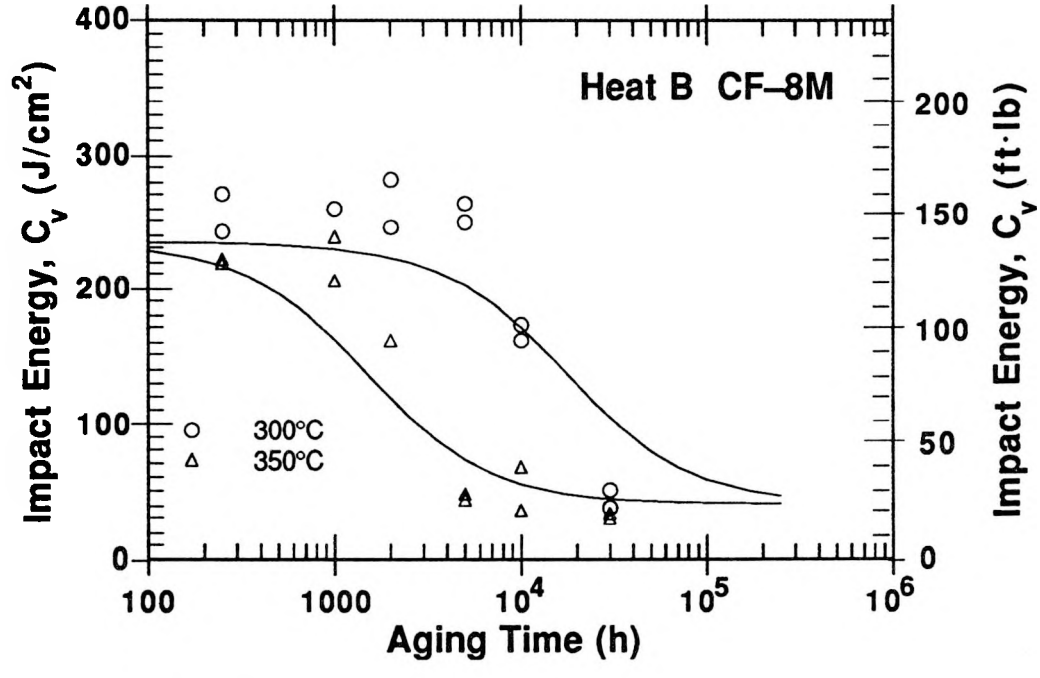

Figure 6. (Contd.)

5 Estimation of Fracture Toughness

5.1 Saturation Fracture Toughness

Thermal aging of cast stainless steels decreases their fracture toughness at room temperature as well as at reactor temperatures, i.e., 280–330°C (536–626°F). The fracture toughness results are consistent with the Charpy-impact data, i.e., unaged and aged materials that show low impact strength also exhibit lower fracture toughness. The saturation fracture toughness J–R curve for a specific cast stainless steel, i.e., the minimum toughness that would be achieved by the material, can be estimated from its room-temperature impact energy at saturation. The J–R curve is expressed by the power-law relation $J_d = C\Delta a^n$, where J_d is deformation J per ASTM Specifications E 813–85 and E 1152, Δa is the crack extension, and C and n are constants. The coefficient C at room and reactor temperatures and the room-temperature normalized Charpy-impact energy, C_V for aged and unaged cast stainless steels are plotted in Fig. 7. Fracture toughness data from ANL,[8,12] FRA,[26,27] and EPRI[28] studies are included in the figure. At both temperatures, the coefficient C decreases with a decrease in impact energy. Separate correlations are obtained for CF–3 or CF–8 steels and for CF–8M steel; the latter shows a larger decrease in fracture toughness for a given impact energy. The correlations used to estimate J–R curves were obtained by subtracting the value of σ (standard deviation for the fit to the data) from the best-fit curve. They are shown in dash/dot lines in Fig. 7, and help ensure that the estimated J–R curve is conservative for all material and aging conditions. The saturation fracture toughness J–R curve at room temperature for CF–3 and CF–8 steels is given by

$$J_d = 49[C_{Vsat}]^{0.52}[\Delta a]^n; \quad (18)$$

for CF–8M steel, it is given by

$$J_d = 16[C_{Vsat}]^{0.67}[\Delta a]^n. \quad (19)$$

At 290–320°C (554–608°F), the saturation J–R curve for CF–3 and CF–8 steels is given by

$$J_d = 82[C_{Vsat}]^{0.34}[\Delta a]^n; \quad (20)$$

for CF–8M steel, it is given by

$$J_d = 35[C_{Vsat}]^{0.49}[\Delta a]^n. \quad (21)$$

The exponent n of Δa is correlated to the coefficient C, Fig. 8. The correlations shown in the figure were obtained by subtracting standard deviation from the best-fit curves, and help ensure that the estimated J–R curves are conservative. These correlations and the best-fit curves in Fig. 7 are used to obtain the relationship between exponent n and saturation room-temperature impact energy. At room temperature, the exponent n for CF–3 and CF–8 steels is given by

$$n = 0.32 + 0.0131[C_{Vsat}]^{0.52}; \quad (22)$$

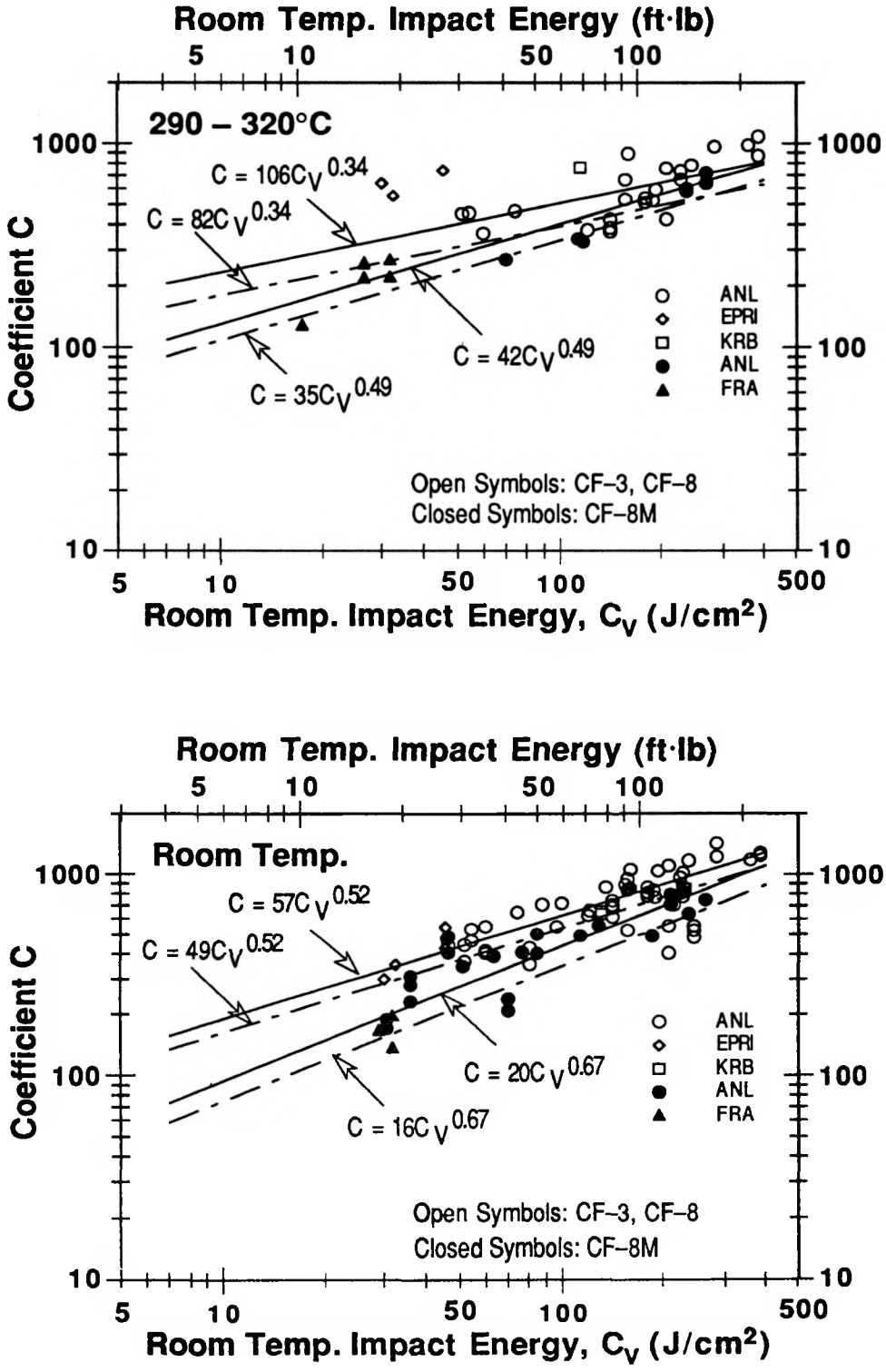

Figure 7. Correlation between room-temperature Charpy-impact energy and coefficient C at 290–320°C and room temperature for cast stainless steels

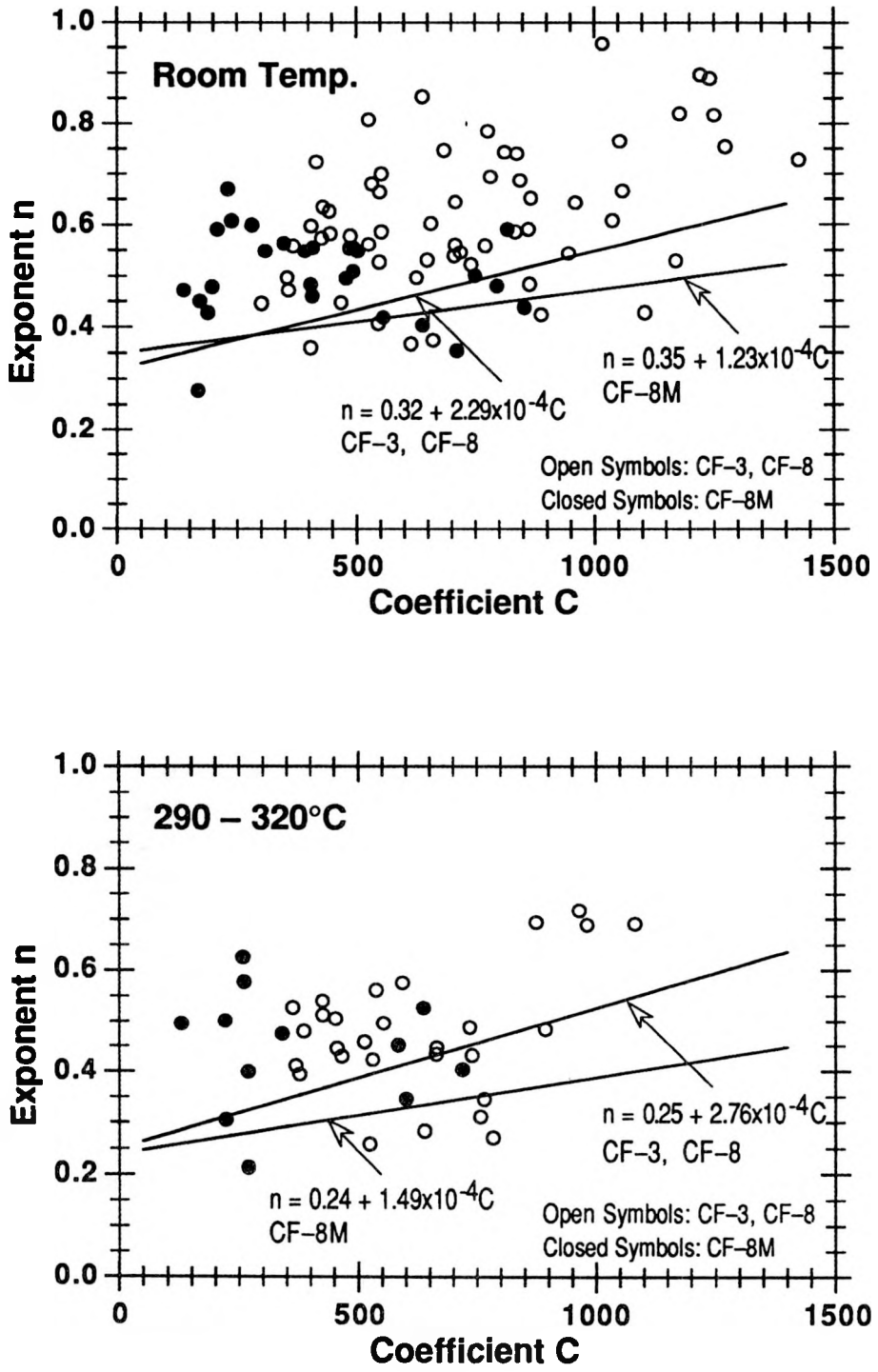

Figure 8. Correlation between coefficient C and exponent n of the power-law J–R curve at 290–320°C and room temperature for cast stainless steels

for CF–8M steel, it is given by

$$n = 0.35 + 0.0025[C_{Vsat}]^{0.67}. \quad (23)$$

At 290–320°C (554–608°F), the exponent n for CF–3 and CF–8 steels is given by

$$n = 0.25 + 0.0293[C_{Vsat}]^{0.34}; \quad (24)$$

for CF–8M steel, it is given by

$$n = 0.24 + 0.0063[C_{Vsat}]^{0.49}. \quad (25)$$

The values of J at any other intermediate temperature can be linearly interpolated from the values at room temperature and 290°C (554°F). The fracture toughness J–R curve at saturation for a specific cast stainless steel can be obtained from its chemical composition by using the correlations for saturation impact energy given in Section 2 and Eqs. 18–25. Examples of the experimental data and estimated J–R curves at saturation, i.e., the minimum fracture toughness that would be achieved by the material by thermal aging, are shown in Figs. 9–15. For most heats, the saturation fracture toughness is achieved after aging for ≥5,000 h at 400°C (752°F). Experimental data and estimated J–R curves for the unaged materials are also shown for comparison; the J–R curves were estimated from the measured initial room–temperature impact energy of the unaged materials. The estimated J–R curves show good agreement with the experimental results in many cases and are essentially conservative. The room–temperature J–R curves for unaged static–cast Heats 69 and 75 (Figs. 11, and 13) are non–conservative. The fracture toughness of unaged static–cast slabs (e.g., Heats 68, 69, 74, and 75) is exceptionally low, although their Charpy–impact energy is comparable to other similar heats of cast stainless steel. The poor fracture toughness for these unaged static–cast slabs is due to residual stresses introduced in the material during the casting process or production heat treatment. Annealing these heats for a short time at temperatures between 290–400°C (554–752°F) increases the fracture toughness and decreases the tensile stress without significantly affecting their impact energy. An example of this is Heat 69, which was aged for 2,570 h at 350°C (662°F) and is shown in Fig. 11. The experimental J–R curve for the short–term–aged material is significantly higher than that for the unaged material. Consequently, the fracture toughness of these heats would initially increase during reactor service before it decreases due to thermal aging. Furthermore, the overestimation for unaged Heats 68, 69, 74, and 75 is not considered important because the materials have adequate fracture toughness, i.e., J_{IC} values >250 kJ/m^2.

The fracture–toughness data for unaged cast stainless steels indicate that the J–R curve for some heats are lower than those for wrought stainless steels. The available J–R–curve data at 290–320°C (554–608°F) for unaged cast stainless steels are shown in Fig. 16a. The static–cast pump casing ring (Heat C1 with δ_c = 8%) shows the lowest and centrifugally cast pipes (Heat P2 with δ_c = 12% and Heat C1488 with δ_c = 21%) have the highest fracture toughness. Fracture toughness J–R curves for wrought stainless steels are higher than the J–R curve for static–cast pump casing ring, Fig. 16b.[31–36] The fracture toughness of unaged cast stainless steels at room temperature is slightly higher than at 290–320°C. At temperatures up to 320°C, a lower–bound J–R curve for unaged static–cast stainless steels can be expressed as

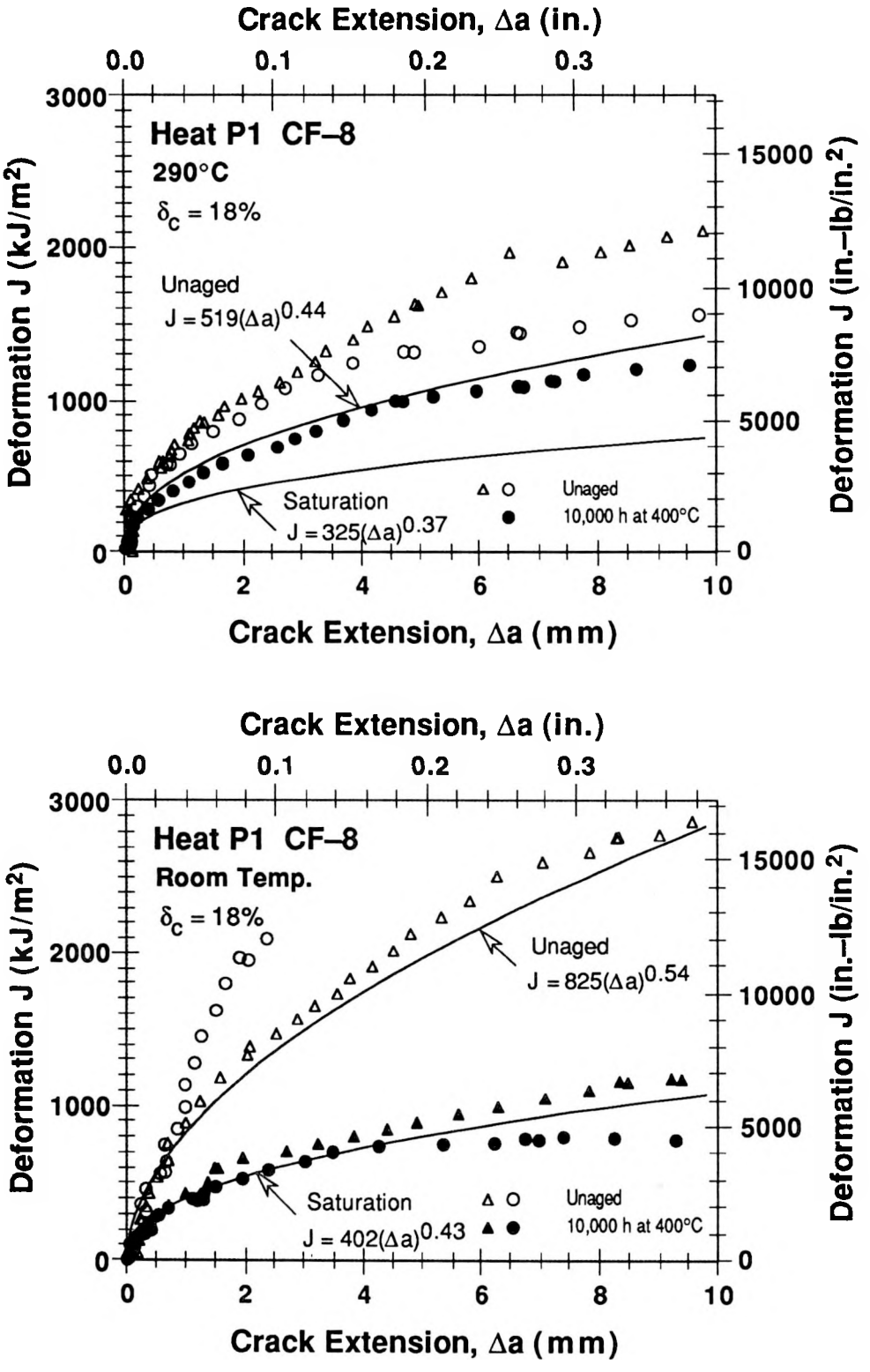

Figure 9. Experimental data and estimated J–R curves for unaged and fully aged centrifugally cast pipe of CF–8 steel

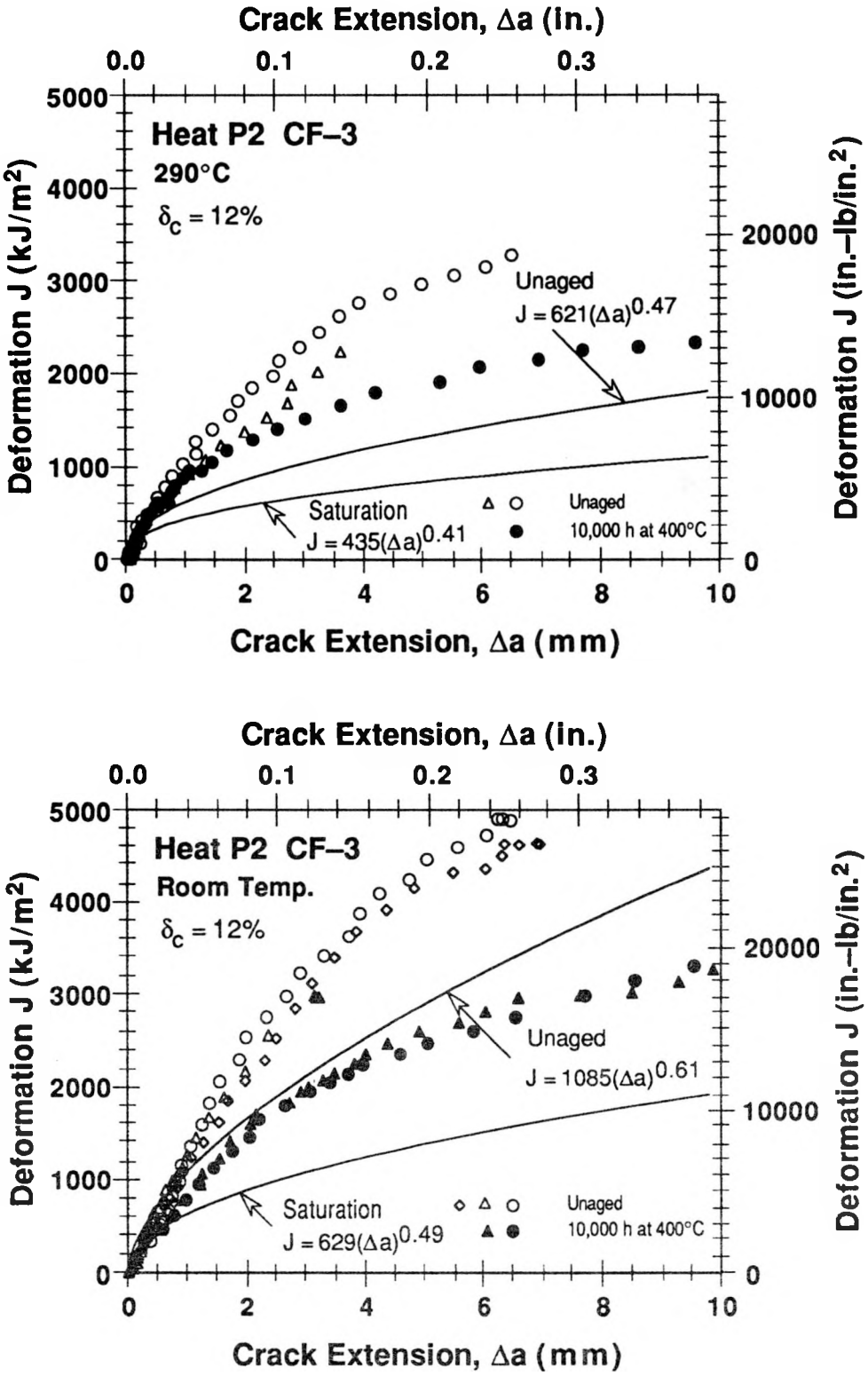

Figure 10. Experimental data and estimated J–R curves for unaged and fully aged centrifugally cast pipe of CF–3 steel

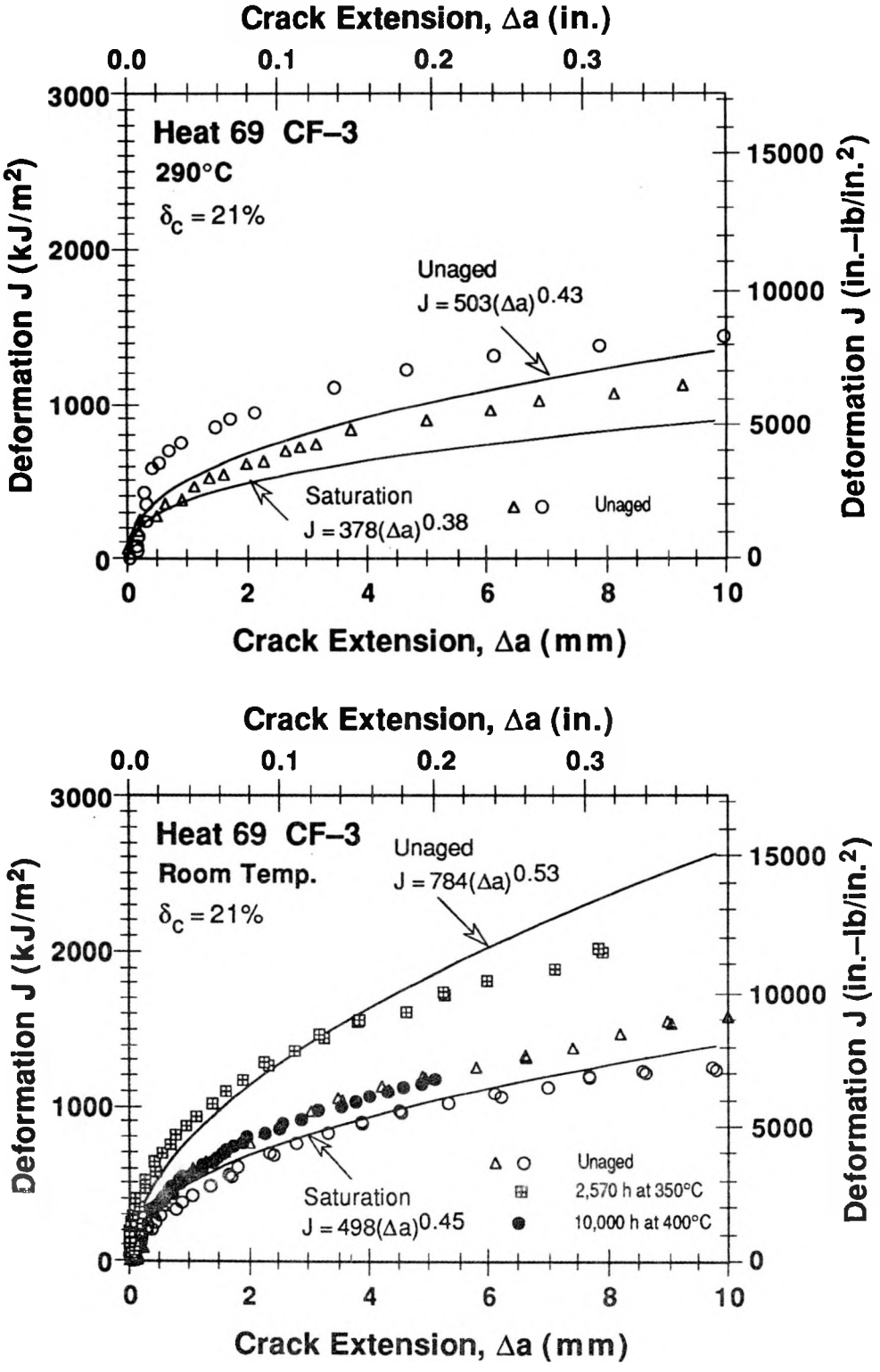

Figure 11. Experimental data and estimated J–R curves for unaged and fully aged static-cast slab of CF–3 steel

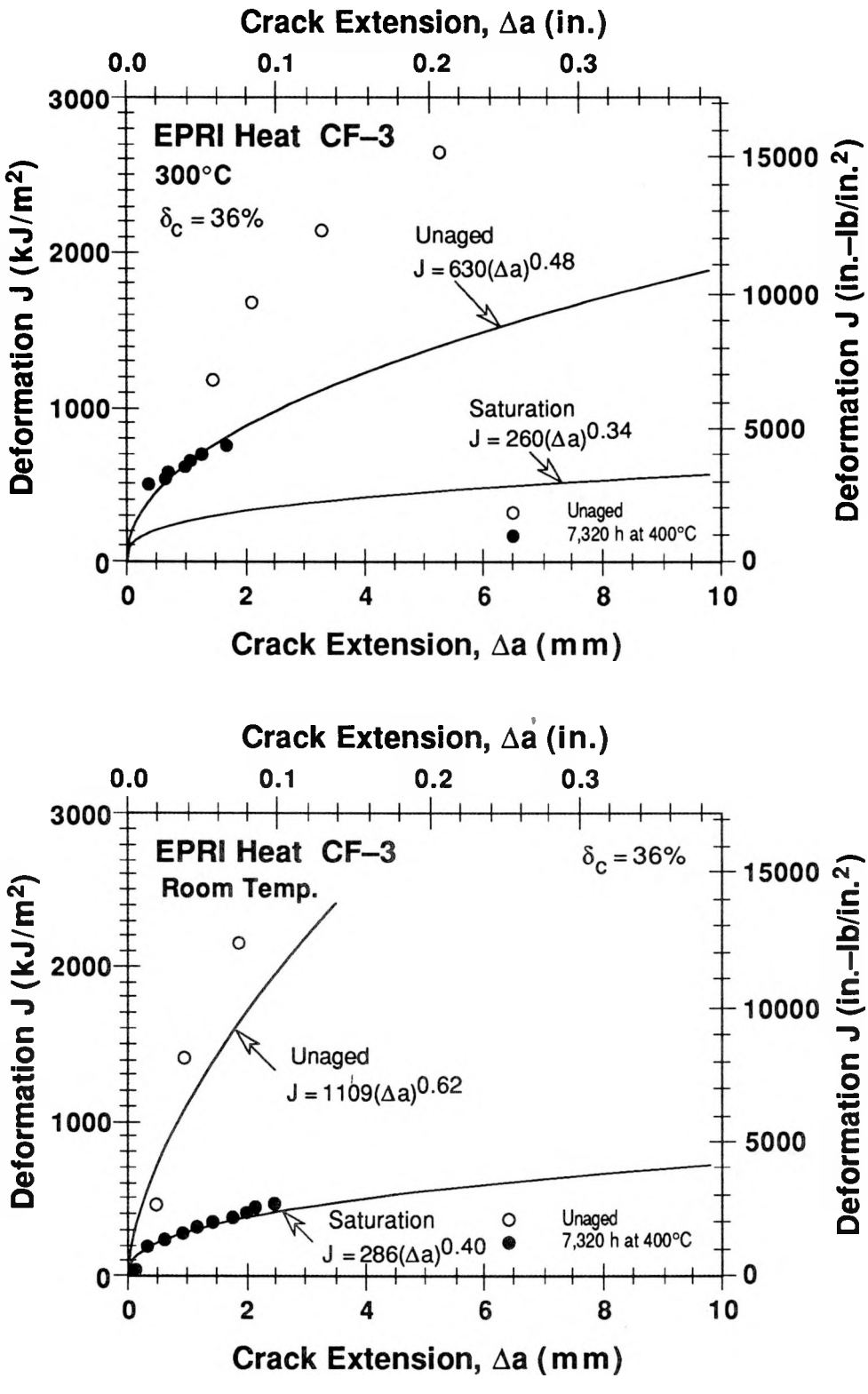

Figure 12. Experimental data and estimated J–R curves for unaged and fully aged static-cast plate of CF-3 steel (Ref. 28)

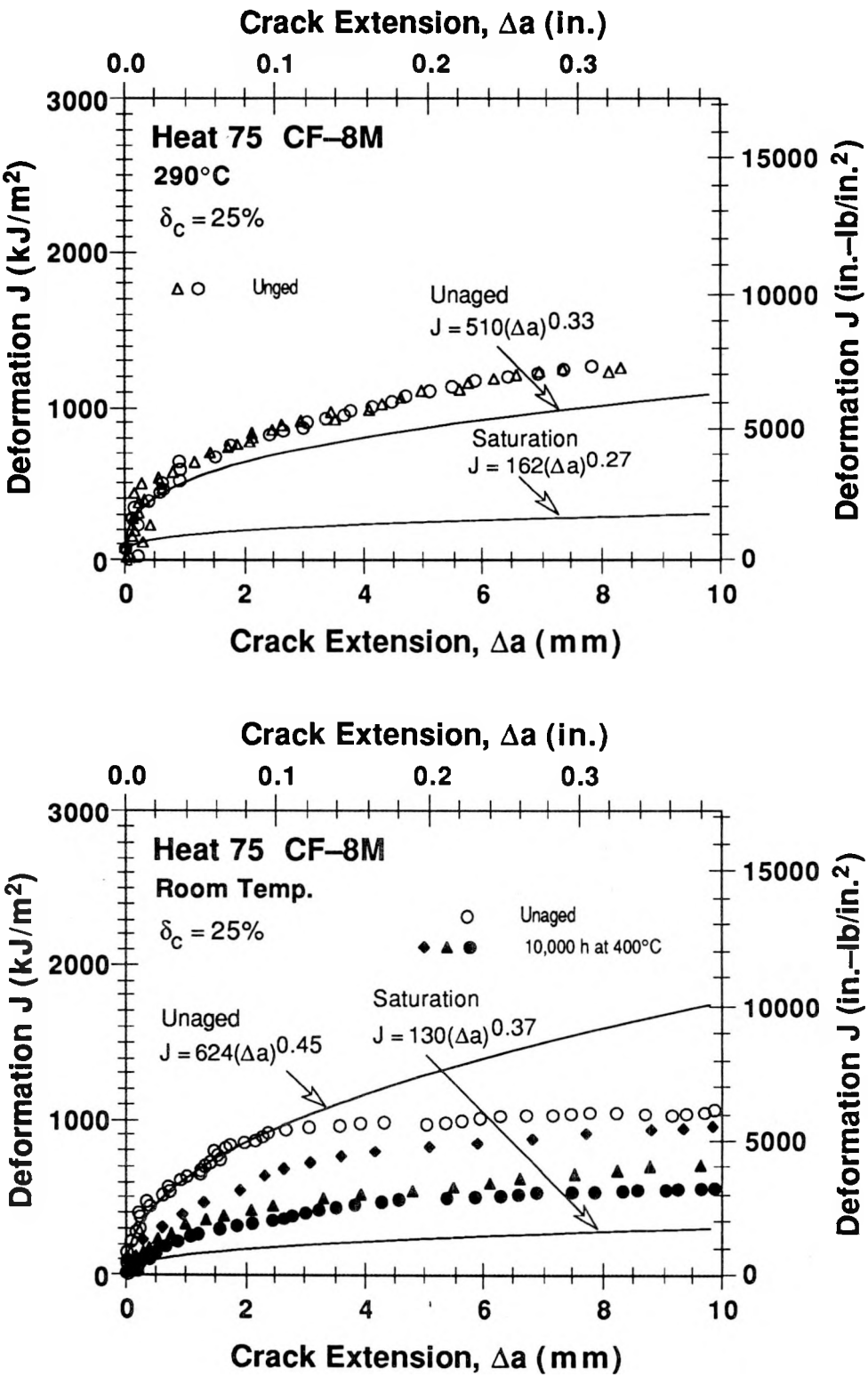

Figure 13. Experimental data and estimated J–R curves for unaged and fully aged static–cast slab of CF–8M steel

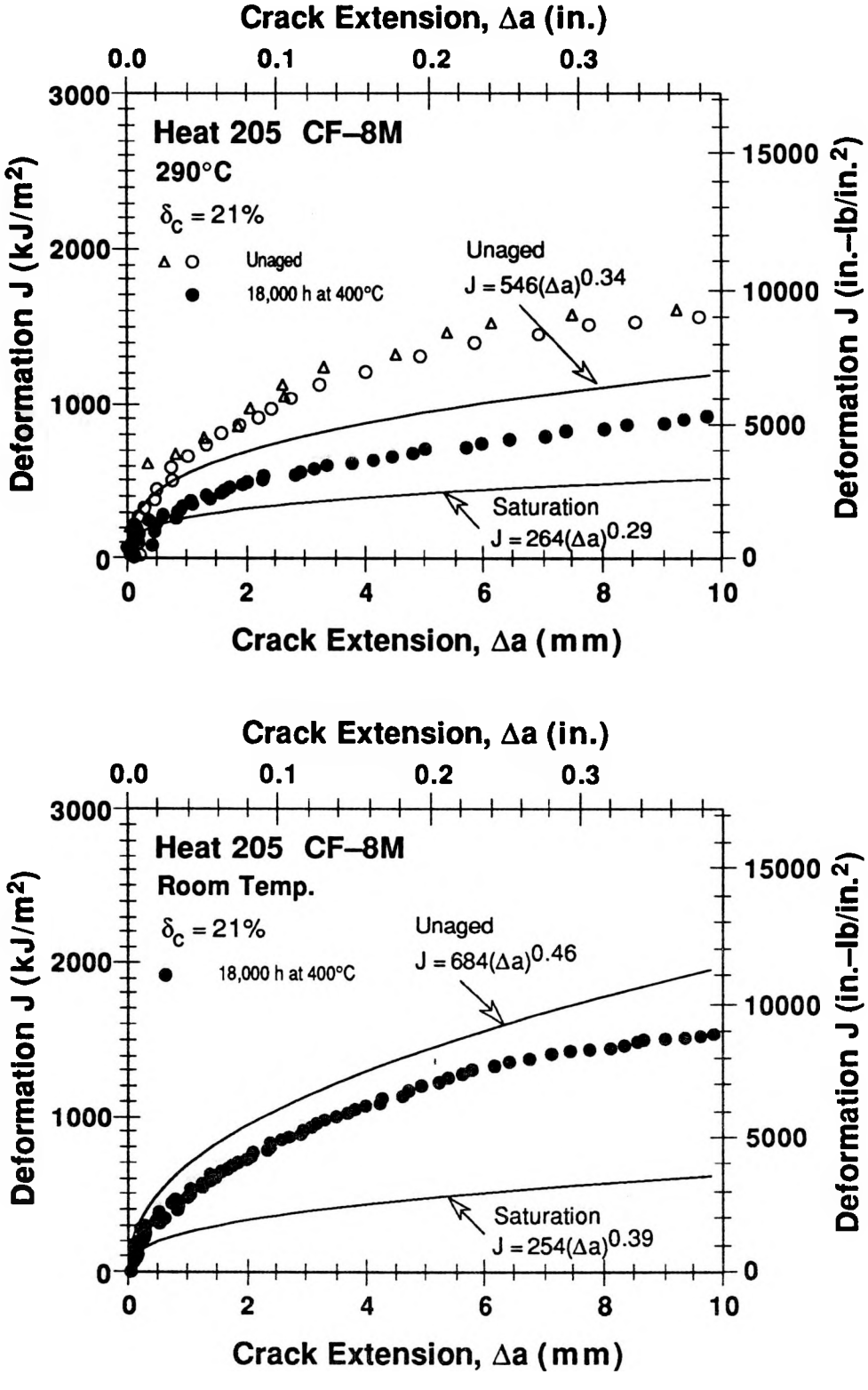

Figure 14. Experimental data and estimated J–R curves for unaged and fully aged centrifugally cast pipe of CF–8M steel

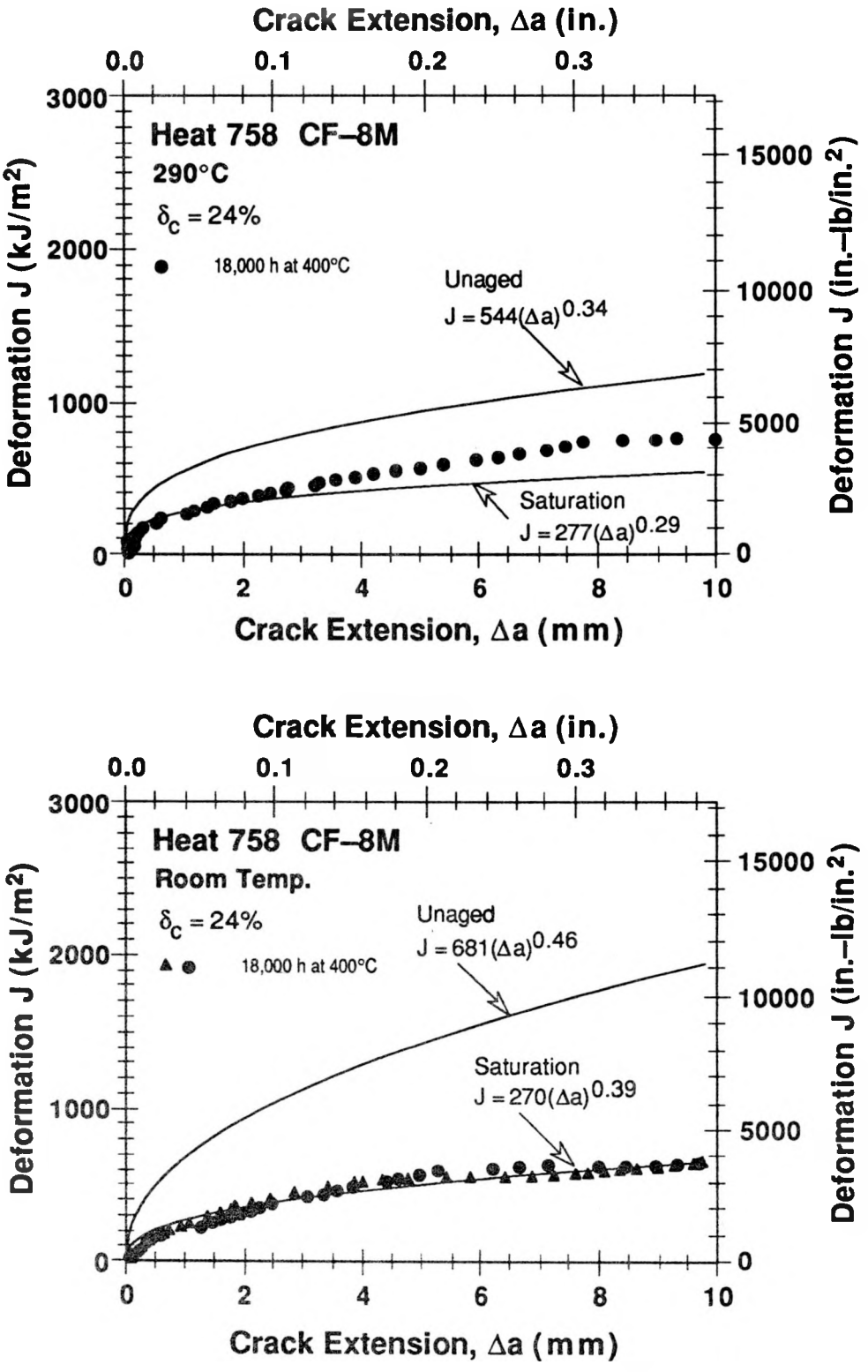

Figure 15. Experimental data and estimated J–R curves for unaged and fully aged static-cast elbow of CF–8M steel

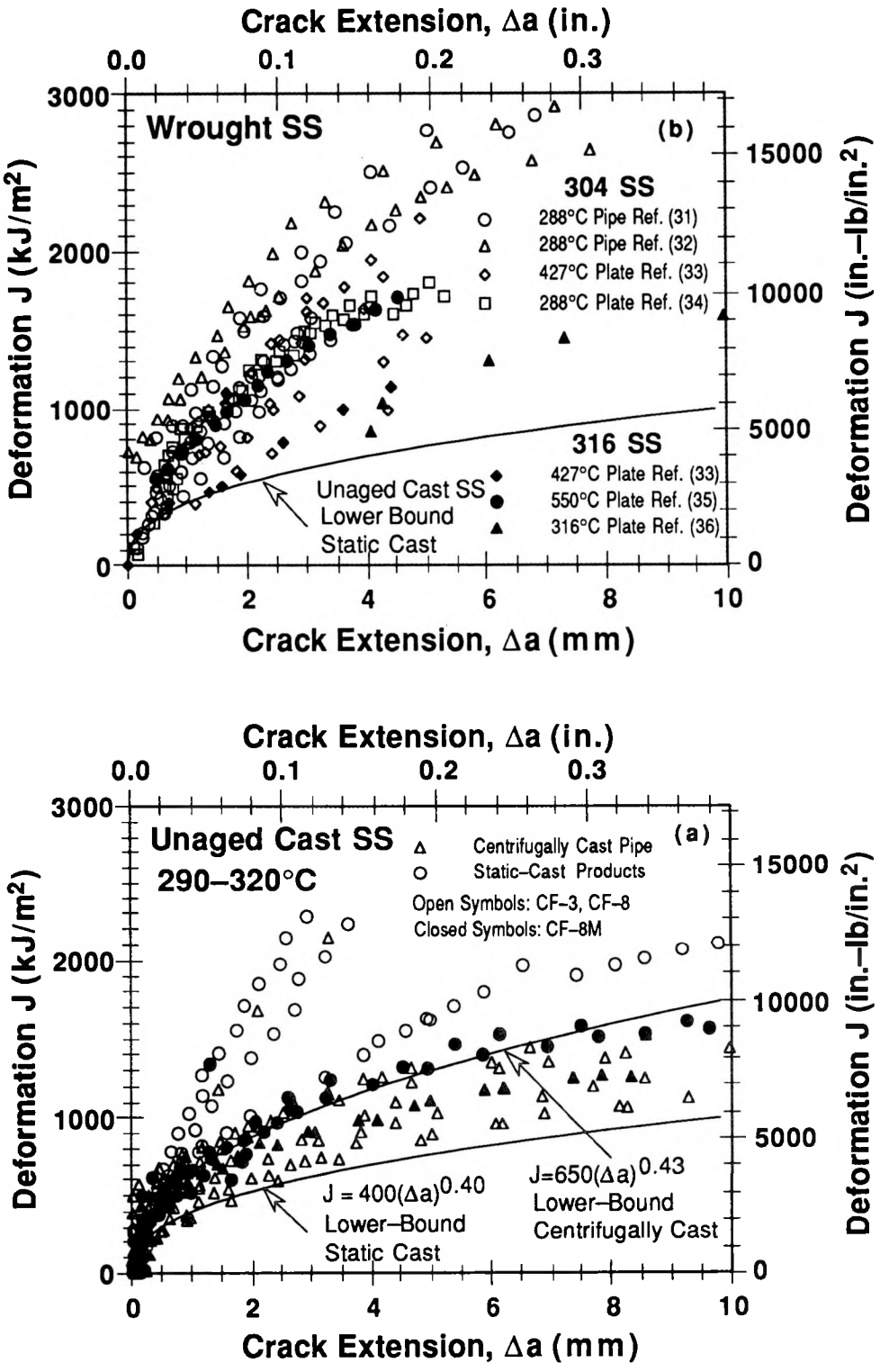

Figure 16. Fracture toughness J–R curves for (a) unaged cast stainless steels and (b) wrought stainless steels at temperatures ≥290°C

$$J_d = 400[\Delta a]^{0.40}; \quad (26)$$

for centrifugally cast stainless steels it can be expressed as

$$J_d = 650[\Delta a]^{0.43}. \quad (27)$$

The correlations given in Eqs. 10–25 account for the degradation of toughness due to thermal aging. They do not explicitly consider the initial fracture properties of the original unaged material. To take this into account, when no information is available on the fracture toughness of the unaged material, the lower bound estimate given by Eqs. 26 or 27 is used as upper bound for the predicted fracture toughness of the aged material, i.e., Eqs. 26 or 27 are used when fracture toughness predicted by Eqs. 10–15 is higher than that predicted by Eqs. 26 or 27. If the actual fracture toughness of the unaged material or the initial Charpy-impact energy is known, use of the higher value may be justified.

5.2 Service–Time Fracture Toughness

The emphasis to this point has been on the saturation values of the fracture toughness, i.e., the lowest values that would ever be obtained. These, of course, represent conservative estimates of the fracture toughness at any given time. Less conservative estimates of fracture toughness can be obtained by considering the kinetics of thermal embrittlement. As in the case of the saturation toughness, the thermal embrittlement for a specific time and temperature is characterized in terms of the room-temperature impact energy C_V, which is estimated by the correlations described in Section 3. Once C_V is known, the service-time J–R curve is determined from correlations described in Section 5.1. For convenience, they are repeated here. The J–R curve at room temperature for CF–3 and CF–8 steels is given by

$$J_d = 49[C_V]^{0.52}[\Delta a]^n; \quad (28)$$

for CF–8M steel, it is given by

$$J_d = 16[C_V]^{0.67}[\Delta a]^n. \quad (29)$$

At 290–320°C (554–608°C), the saturation J–R curve for CF–3 and CF–8 steels is given by

$$J_d = 82[C_V]^{0.34}[\Delta a]^n; \quad (30)$$

for CF–8M steel, it is given by

$$J_d = 35[C_V]^{0.49}[\Delta a]^n. \quad (31)$$

At room temperature the exponent n for CF–3 and CF–8 steels is given by

$$n = 0.32 + 0.0131[C_{Vsat}]^{0.52} \quad (32)$$

for CF–8M steel, it is given by

$$n = 0.35 + 0.0025[C_{Vsat}]^{0.67}. \quad (33)$$

At 290–320°C (554–608°C) the exponent n for CF–3 and CF–8 steels is given by

$$n = 0.25 + 0.0293[C_{Vsat}]^{0.34} \quad (34)$$

for CF–8M steel, it is given by

$$n = 0.24 + 0.0063[C_{Vsat}]^{0.49}. \quad (35)$$

As described in Section 5.1, the J values at intermediate temperatures can be obtained by linear interpolation between the values at room temperature and at 290°C (554°F). The fracture toughness J–R curve for a specific material and aging condition can be obtained from the correlations expressed in Eqs. 28–35, the saturation room–temperature impact energy C_{Vsat} estimated from Eqs. 1–7, and the kinetics of thermal embrittlement expressed in Eqs. 10–13 and 17. Comparisons of the experimental and estimated J_d values at 0.5–, 1.0–, 2.5–, and 5.0–mm crack extensions are shown in Figs. 17 and 18. The estimated J_d values are always lower but within a factor of 2 of the experimental values of J_d. The estimated room–temperature J_d values for unaged static–cast slabs alone are higher than the experimental values. As discussed in Section 5.1, these heats have poor fracture toughness because of residual stresses in the material. Fracture toughness of the static–cast slabs would initially increase during reactor service before it decreases due to thermal aging.

Examples of the experimental and estimated J–R curves for several partially aged cast stainless steels are shown in Figs. 19–24. The estimated J–R curves show good agreement with the experimental results and are essentially conservative. Estimations for centrifugally cast steels in particular are quite conservative. As discussed in Section 5.1, when no information is available on the fracture toughness of the unaged material and a typical value of 200 J/cm^2 is assumed for room–temperature impact energy, lower bound fracture toughness of the unaged material (Eqs. 26 or 27) is used if the fracture toughness predicted by Eqs. 28–35 is higher than that predicted by Eqs. 26 or 27. J–R curves estimated from Eqs. 28–35 should only be used when initial Charpy–impact energy C_{Vint} is known in Eq. 12.

The kinetics of thermal embrittlement were estimated using the actual experimental values of θ in Eqs. 10 and 17. A value of 2.9 for θ can be used to estimate thermal embrittlement at temperatures between 280–330°C (536–626°F). With a assumed value of 2.9 for θ, estimations of fracture toughness before saturation, may be non–conservative for service temperatures >330 and <280°C (>626 and <536°F). Comparisons of the coefficient C at 290°C (554°F), computed using the actual value of θ and θ = 2.9 are shown in Figs. 25 and 26, respectively, for Heats 278, 281, and 287 (measured θ value 3.5–4.0) and Heats EPRI, KRB, and B (measured θ value 2.1–2.5). For all heats the two estimates are essentially the same at a service temperature of 300°C (572°F). With θ = 2.9, estimated values of C are up to 20% higher at 280–300°C (536–572°F) for heats with θ >2.9 (Fig. 25) and at 300–330°C (572–626°F) for heats with θ <2.9 (Fig. 26). A θ value of 2.5 should be used for estimating fracture toughness at 330–360°C (626–680°F) and 3.3 for estimating at <280°C (<536°F).

The estimated J–R curves at 290–320°C (554–608°F) for some of the heats after service for 16, 32, and 48 effective full power years (efpy) at 290 and 320°C are shown in Figs. 27–32. The saturation fracture toughness for the specific cast stainless steel and the

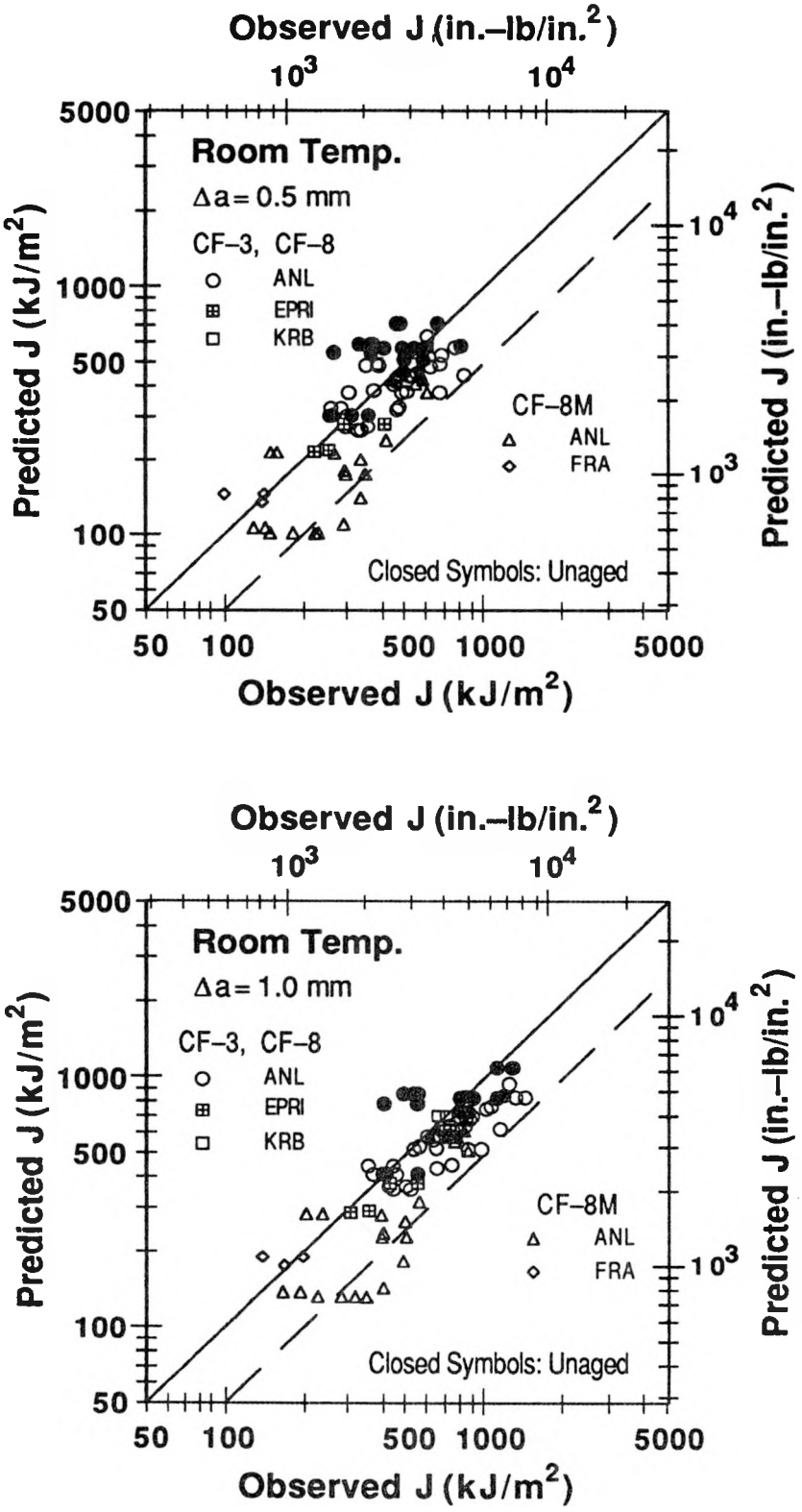

Figure 17. Estimated and observed J values at room temperature and 0.5–, 1.0–, 2.5–, and 5.0–mm crack extensions for aged cast stainless steels

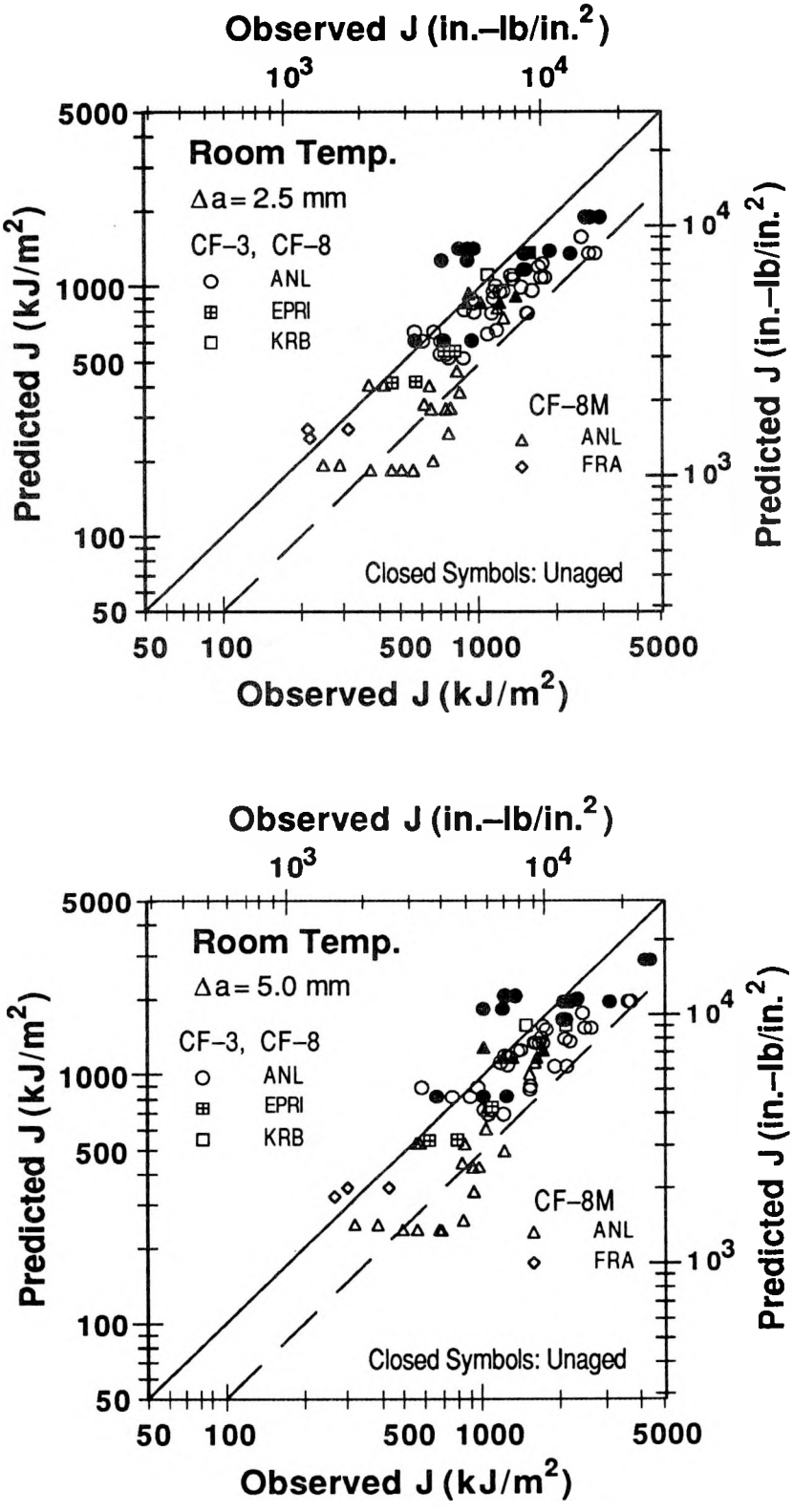

Figure 17. (Contd.)

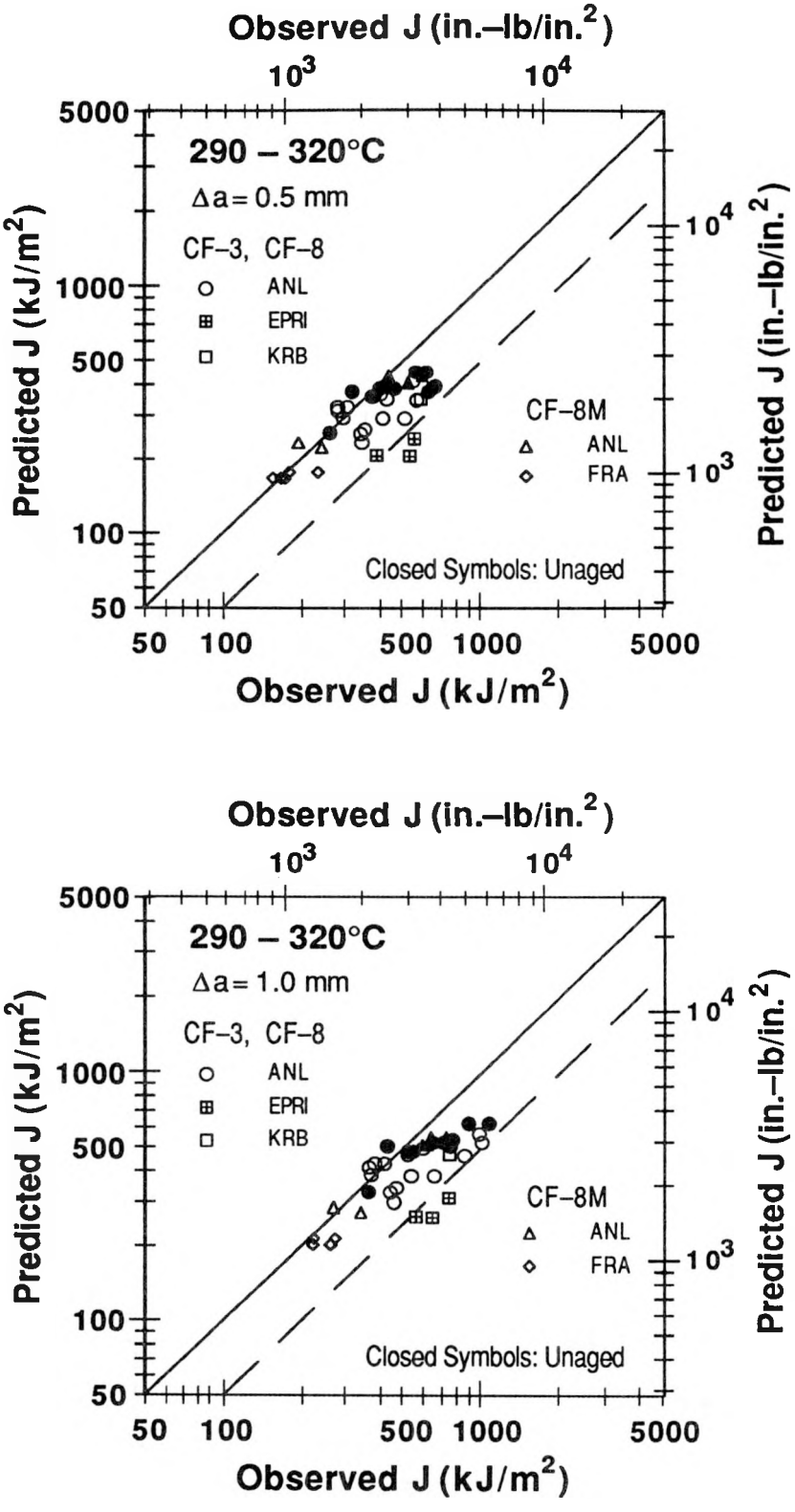

Figure 18. Estimated and observed J values at 290°C and 0.5–, 1.0–, 2.5–, and 5.0–mm crack extensions for aged cast stainless steels

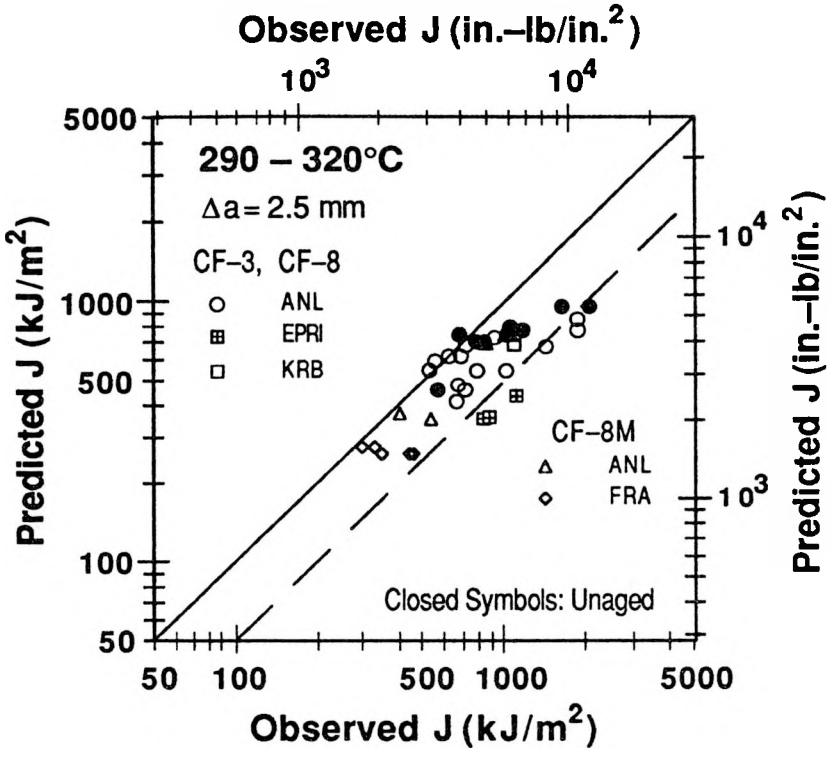

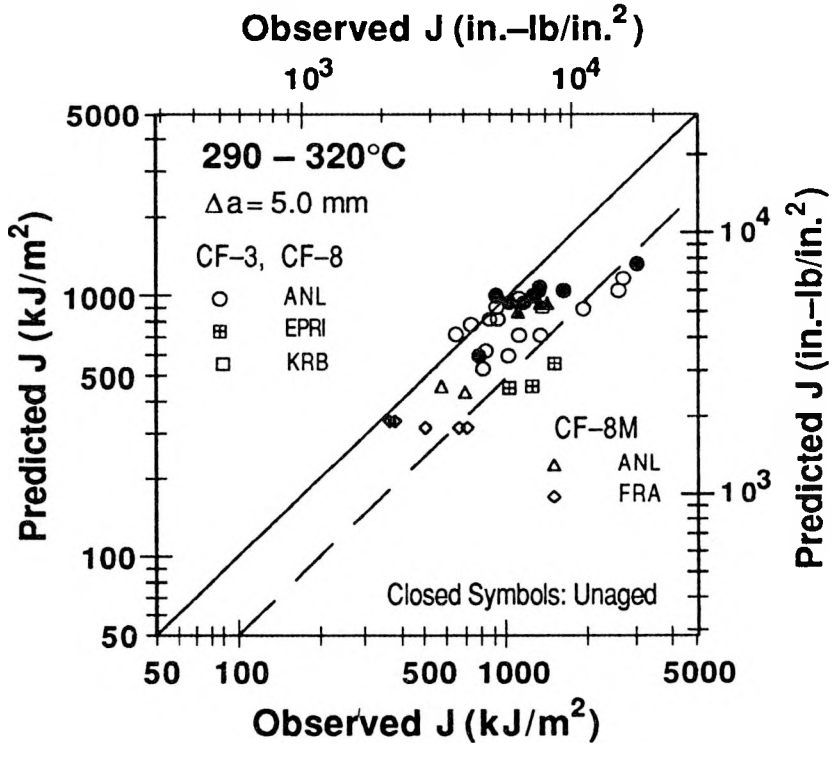

Figure 18. (Contd.)

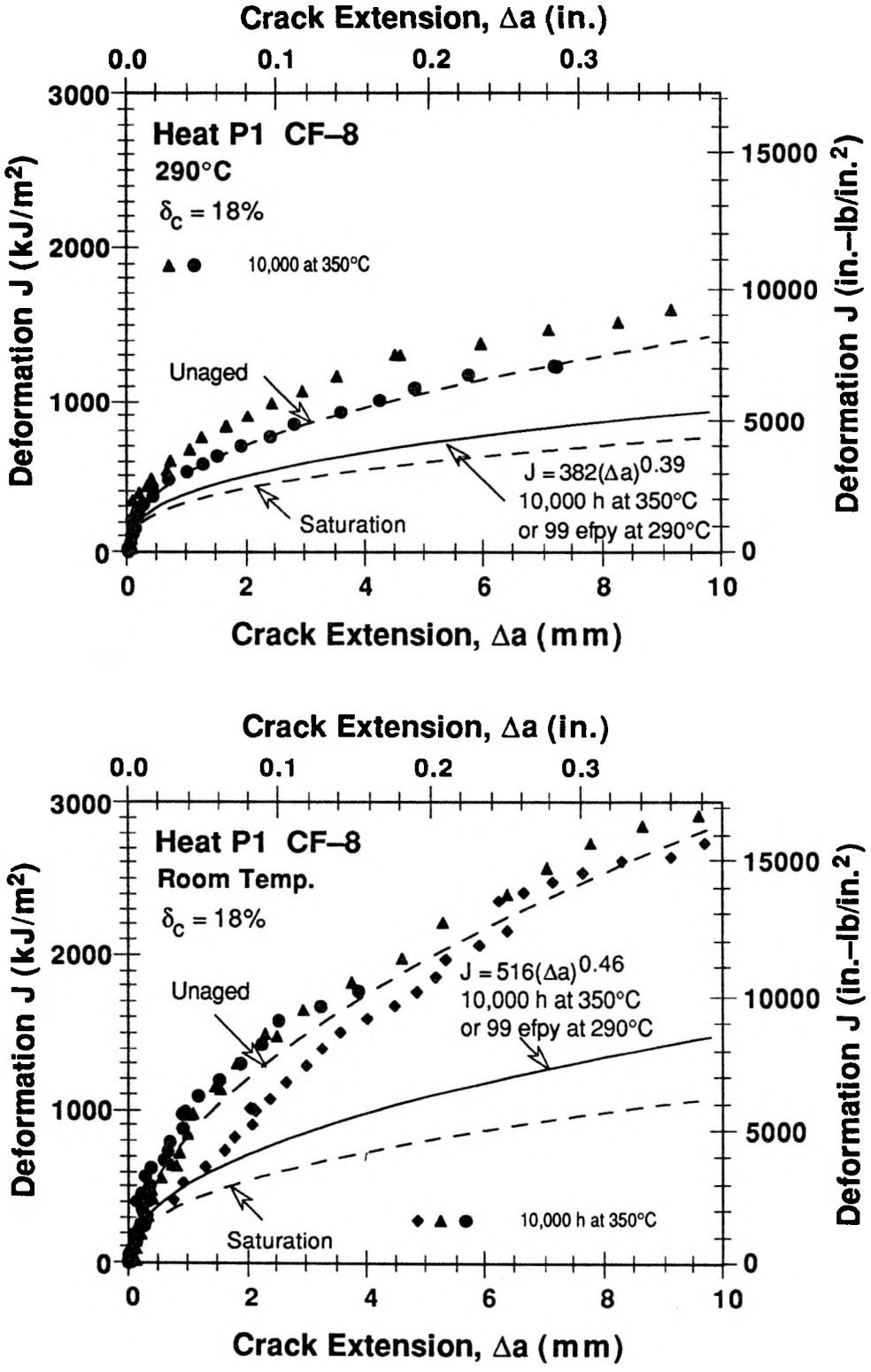

Figure 19. Experimental data and estimated J–R curves for a partially aged centrifugally cast pipe of CF–8 steel

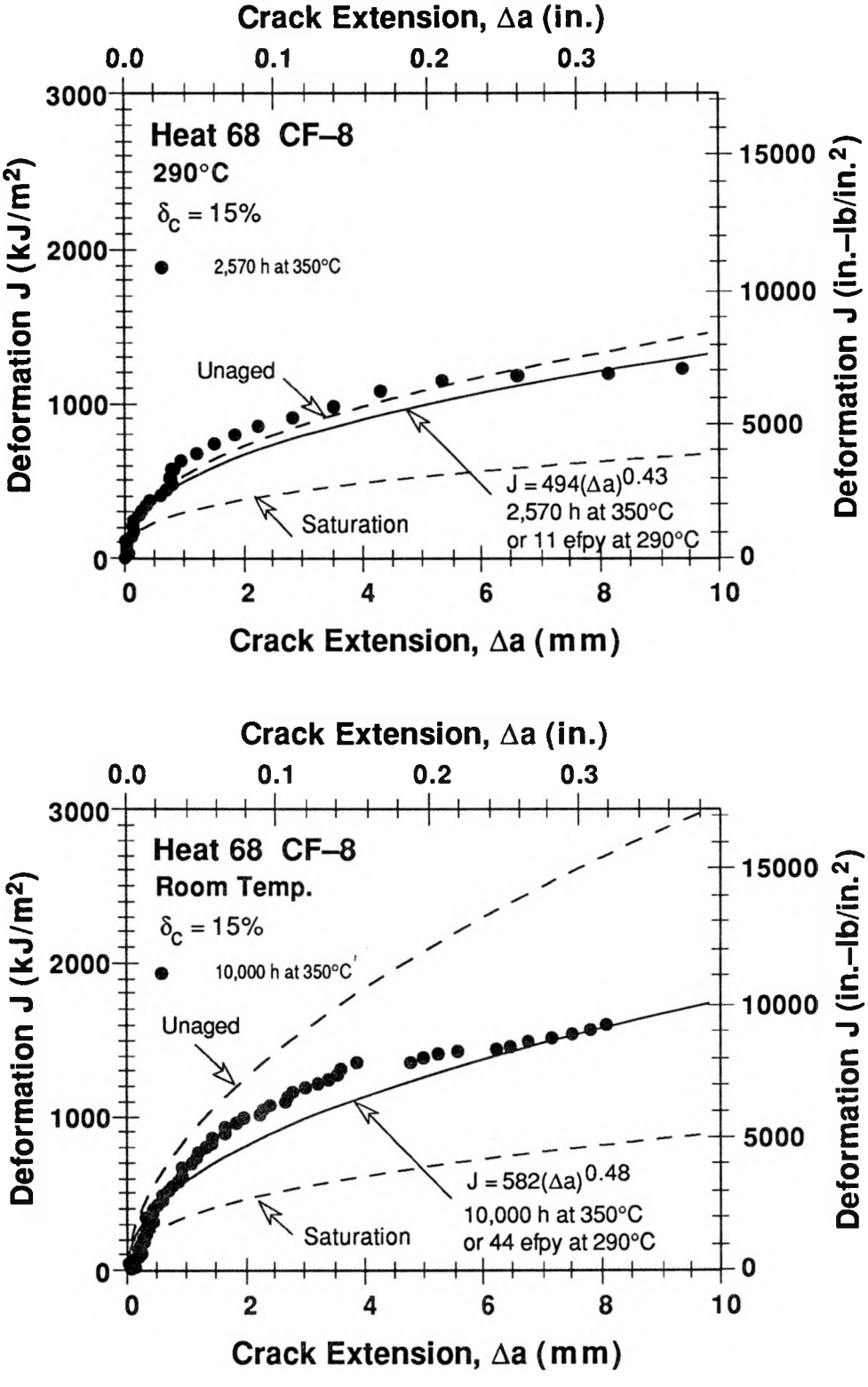

Figure 20. Experimental data and estimated J–R curves for a partially aged static-cast slab of CF–8 steel

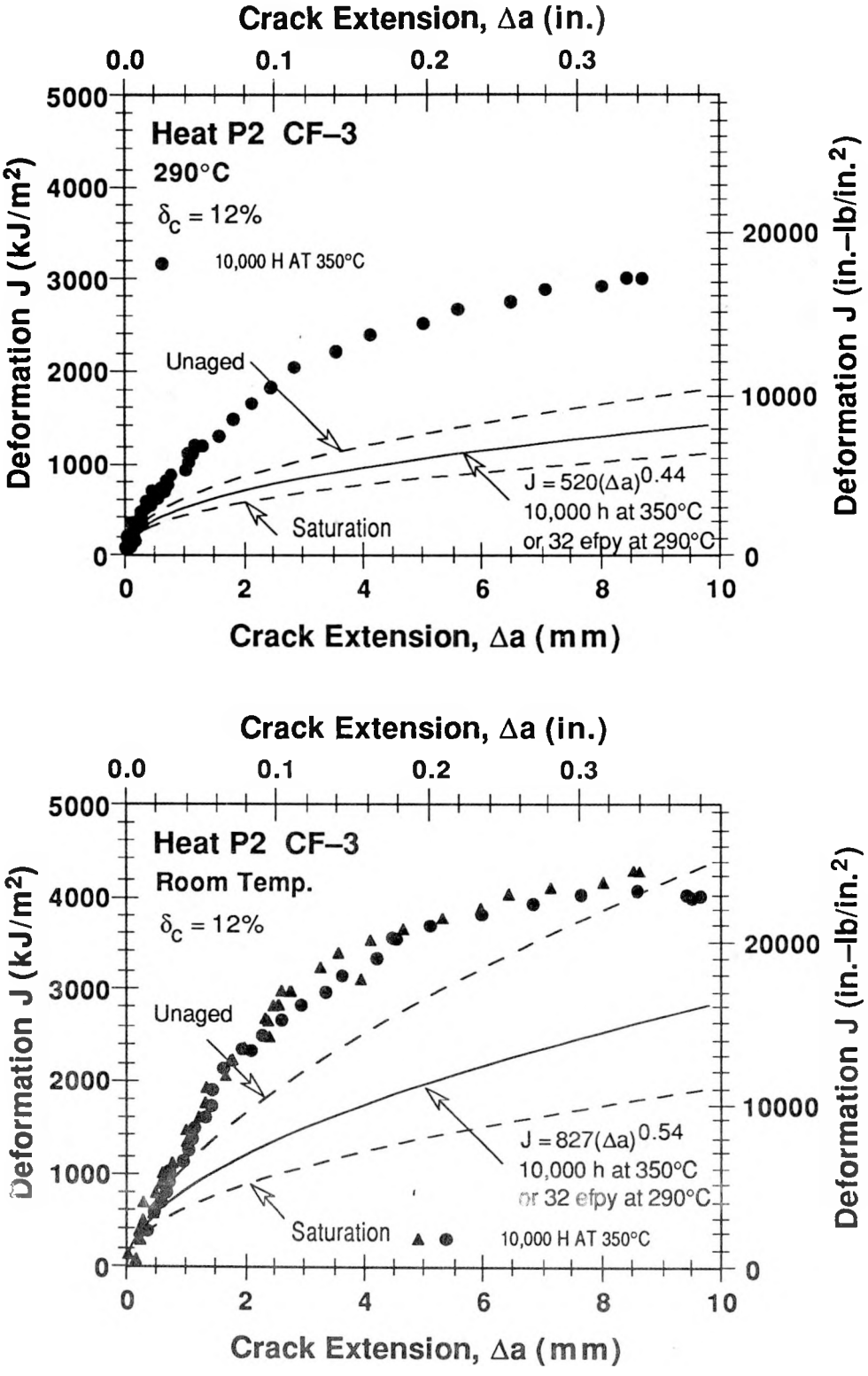

Figure 21. Experimental data and estimated J–R curves for a partially aged centrifugally cast pipe of CF–3 steel

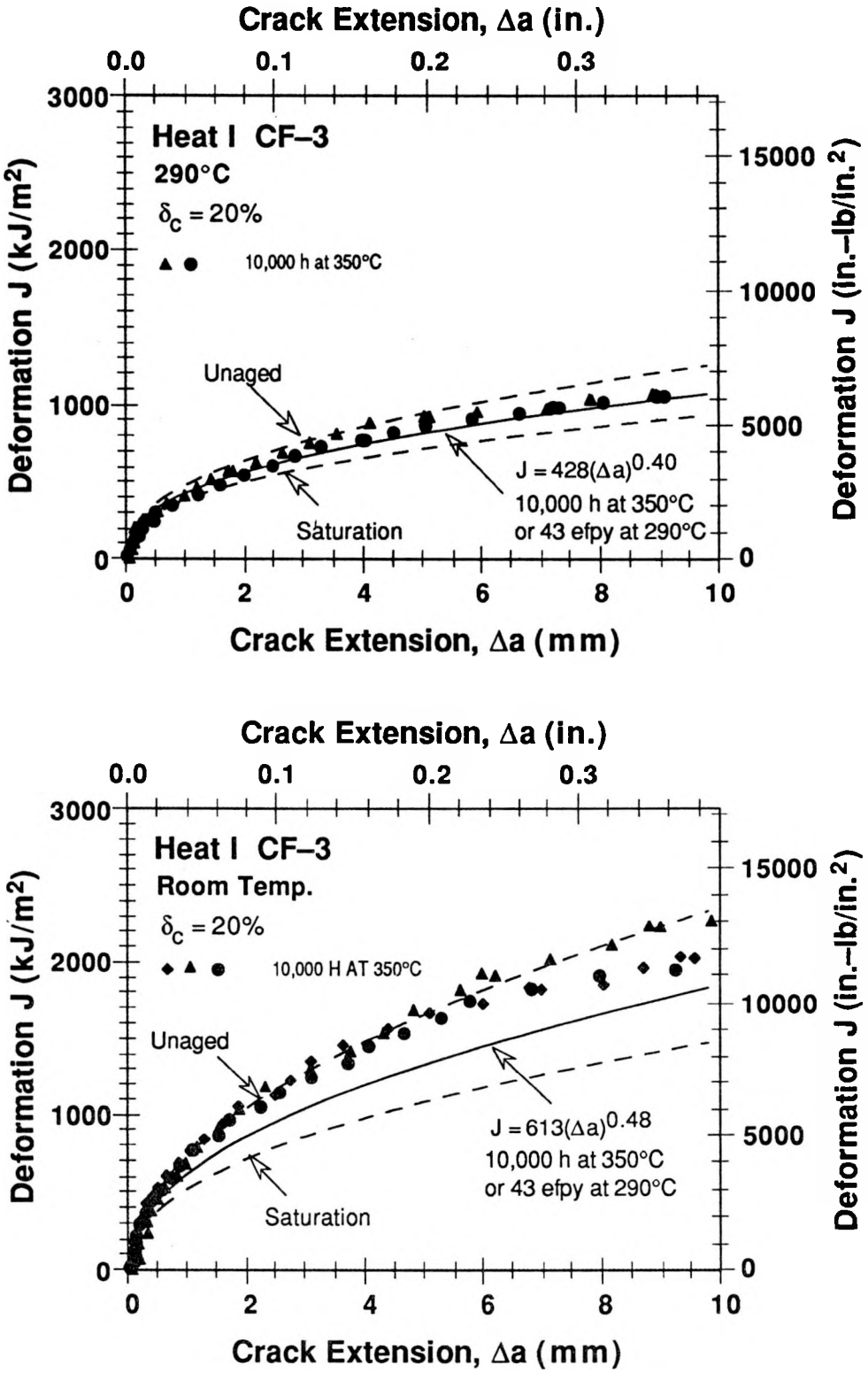

Figure 22. Experimental data and estimated J–R curves for a partially aged static-cast pump impeller of CF-3 steel

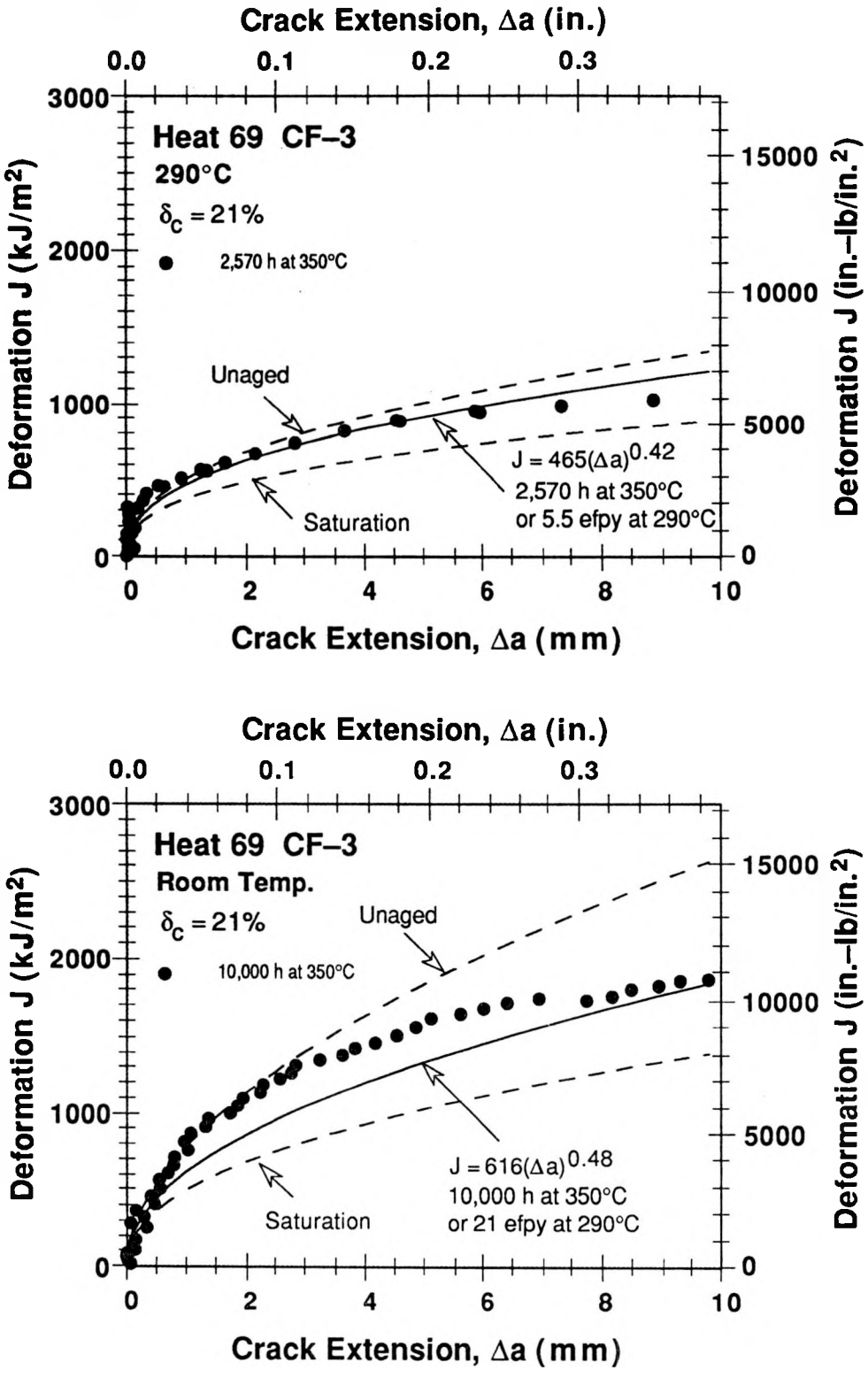

Figure 23. Experimental data and estimated J–R curves for a partially aged static-cast slab of CF-3 steel

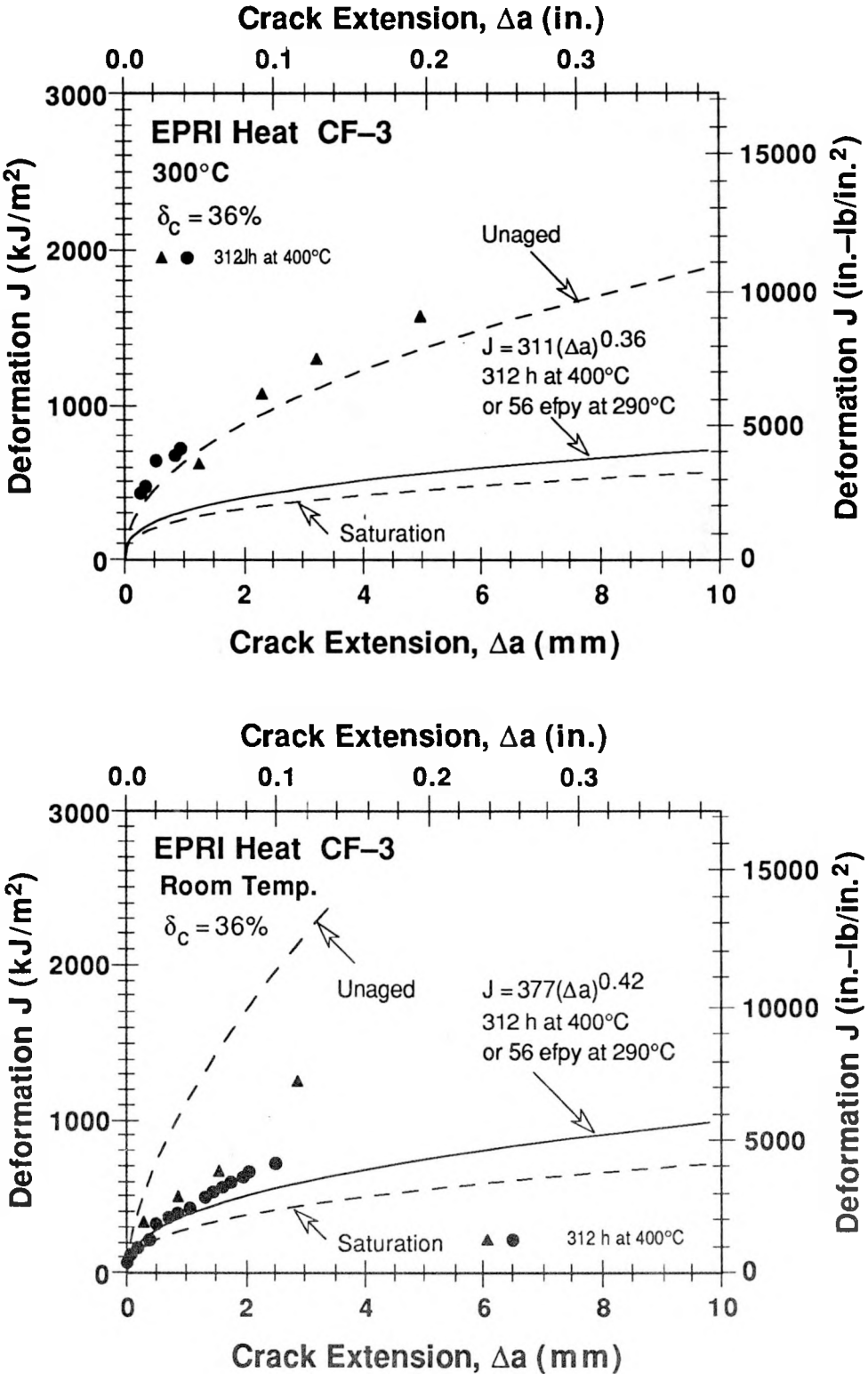

Figure 24. Experimental data and estimated J–R curves for a partially aged static-cast plate of CF–3 steel (Ref. 28)

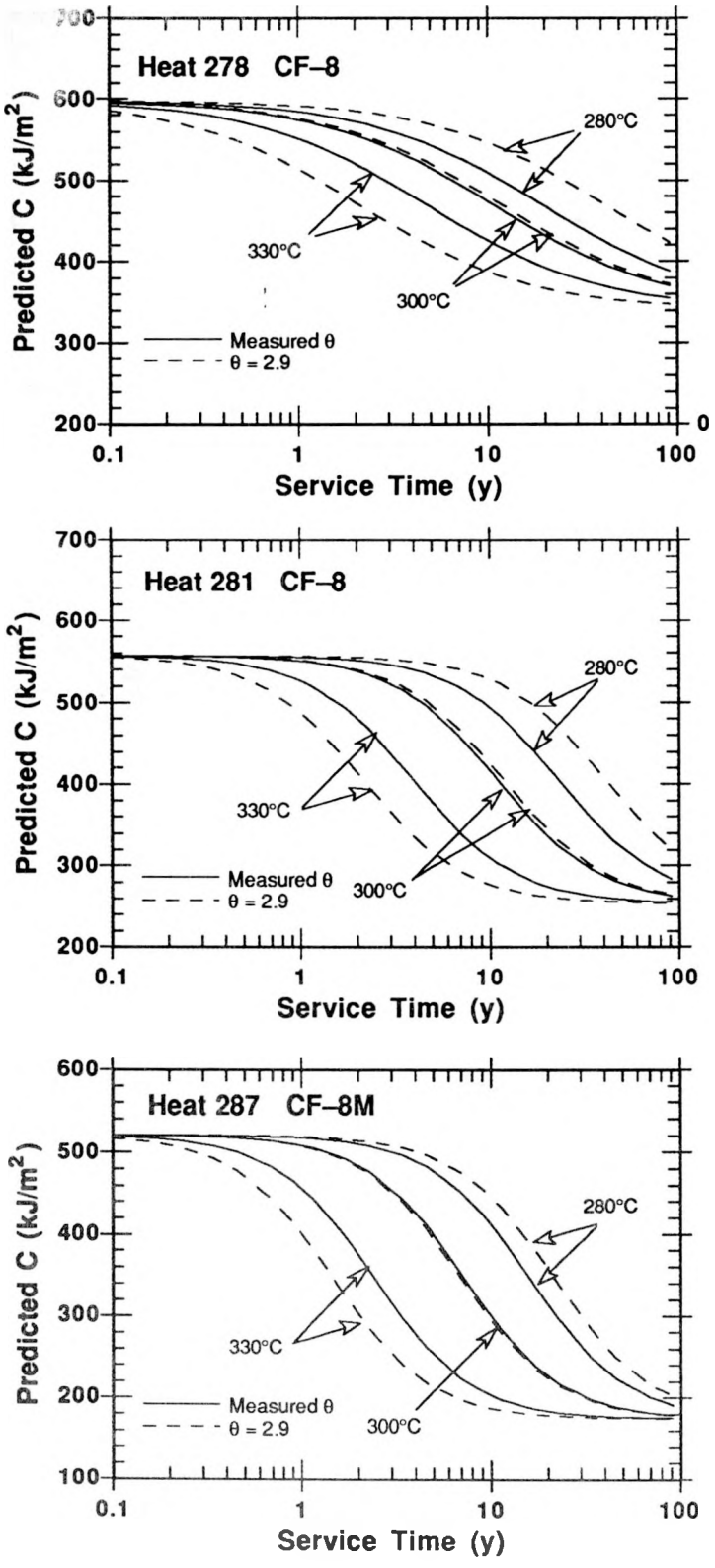

Figure 25. Coefficient C at 290°C estimated from actual and assumed values of θ for aged cast stainless steels with θ >2.9

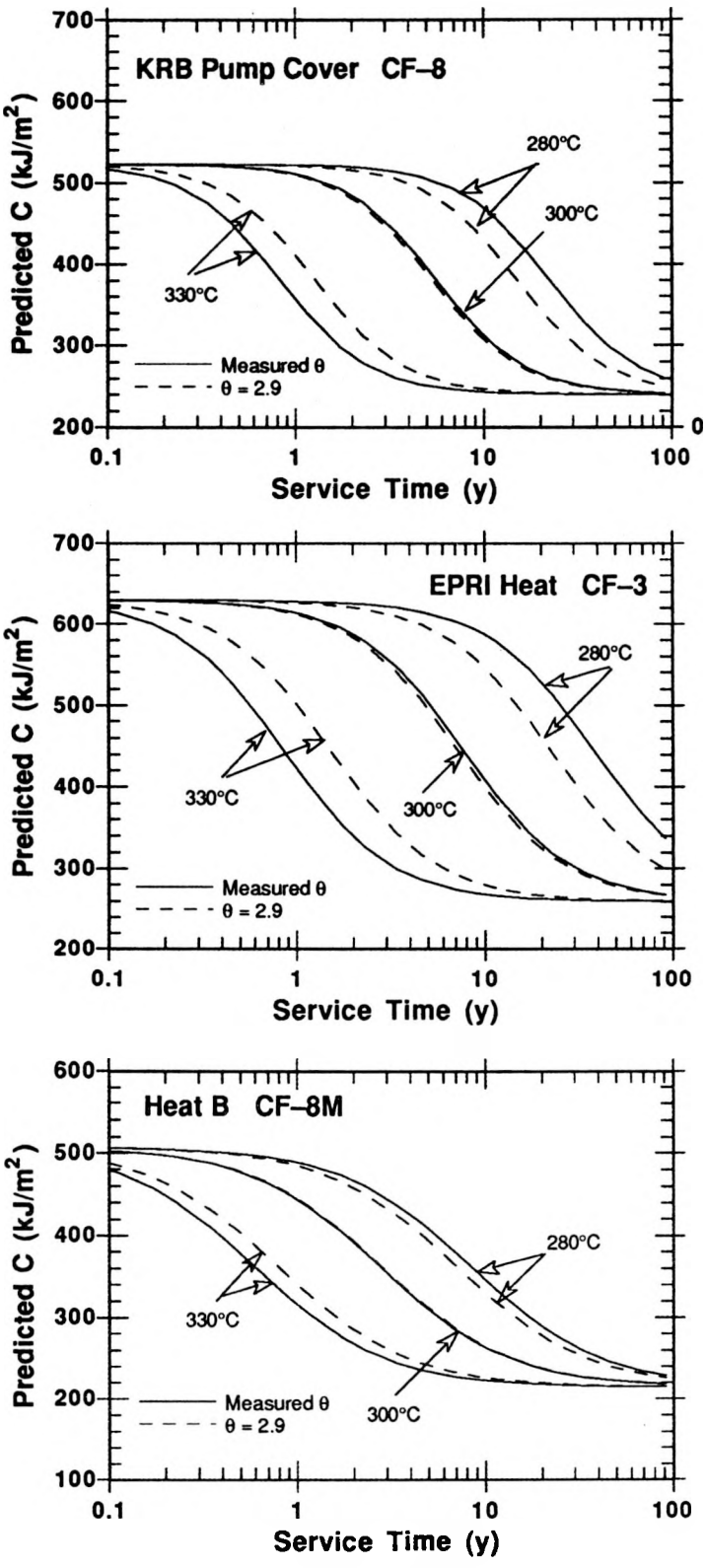

Figure 26. Coefficient C at 290°C estimated from actual and assumed values of θ for aged cast stainless steels with θ <2.9

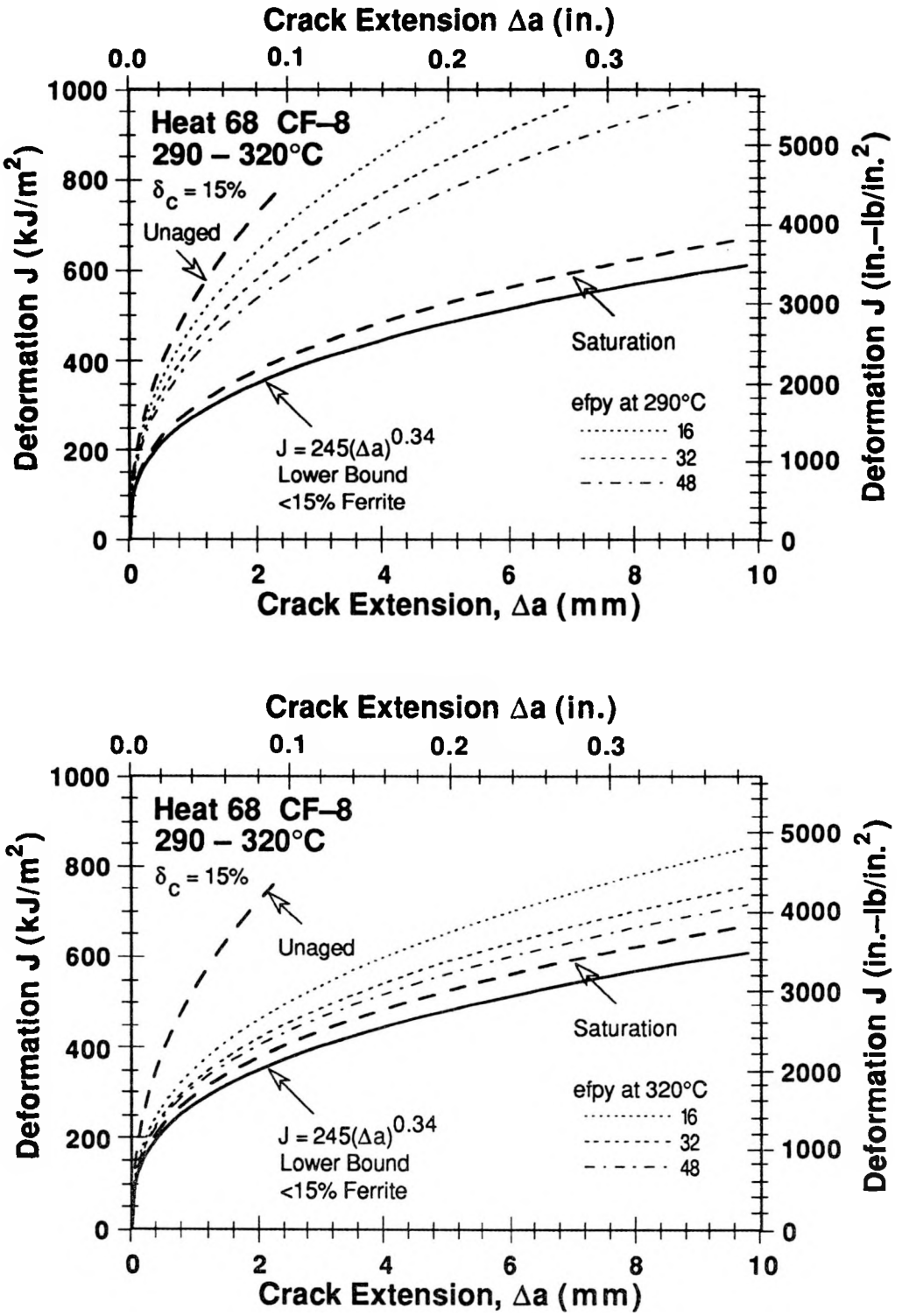

Figure 27. Comparison between lower-bound J-R curve and J-R curves after 16, 32, and 48 efpy at 290 and 320°C for static-cast slab of CF-8 steel

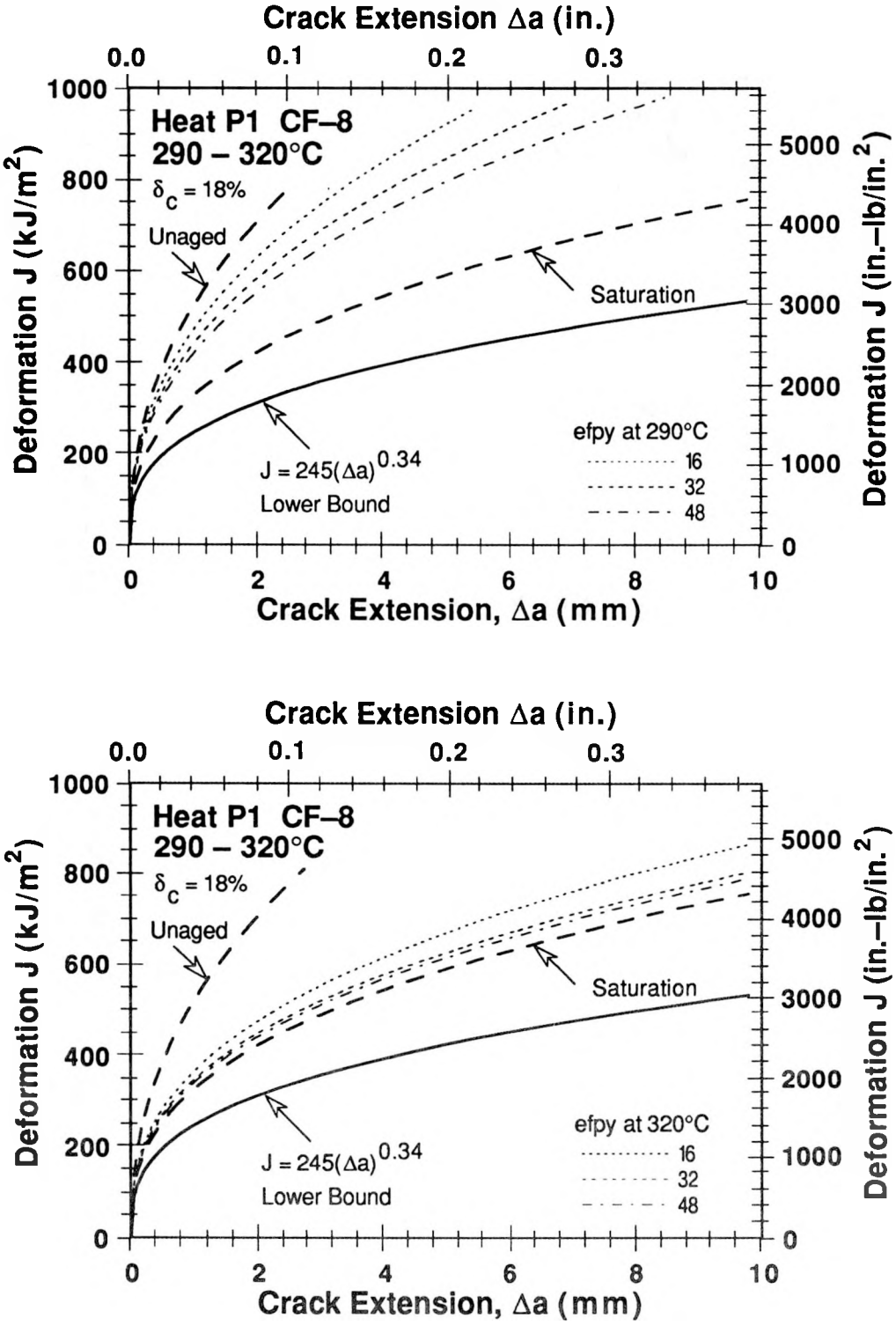

Figure 28. Comparison between lower-bound J-R curve and J-R curves after 16, 32, and 48 efpy at 290 and 320°C for centrifugally cast pipe of CF-8 steel

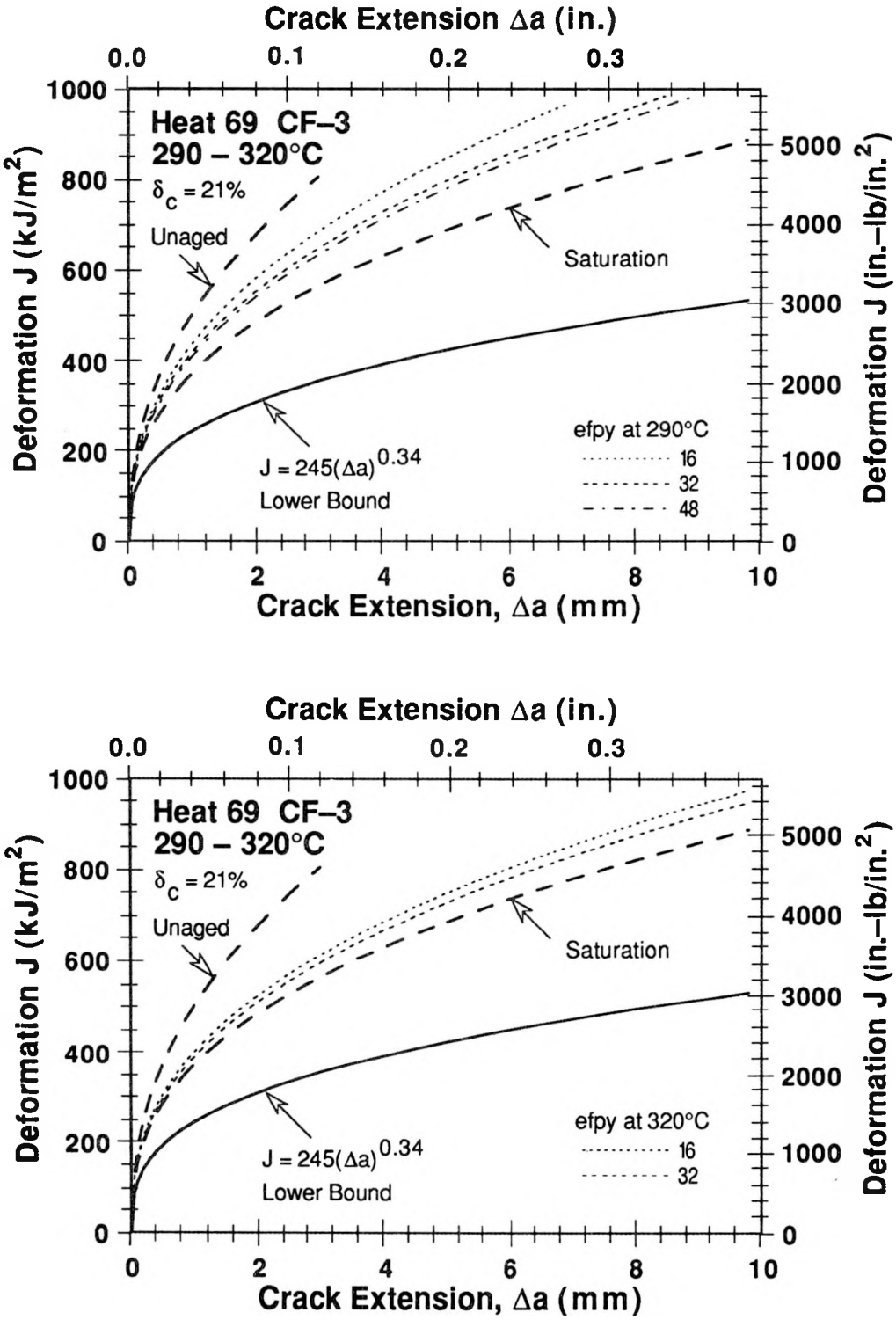

Figure 29. Comparison between lower-bound J–R curve and J–R curves after 16, 32, and 48 efpy at 290 and 320°C for static-cast slab of CF–3 steel

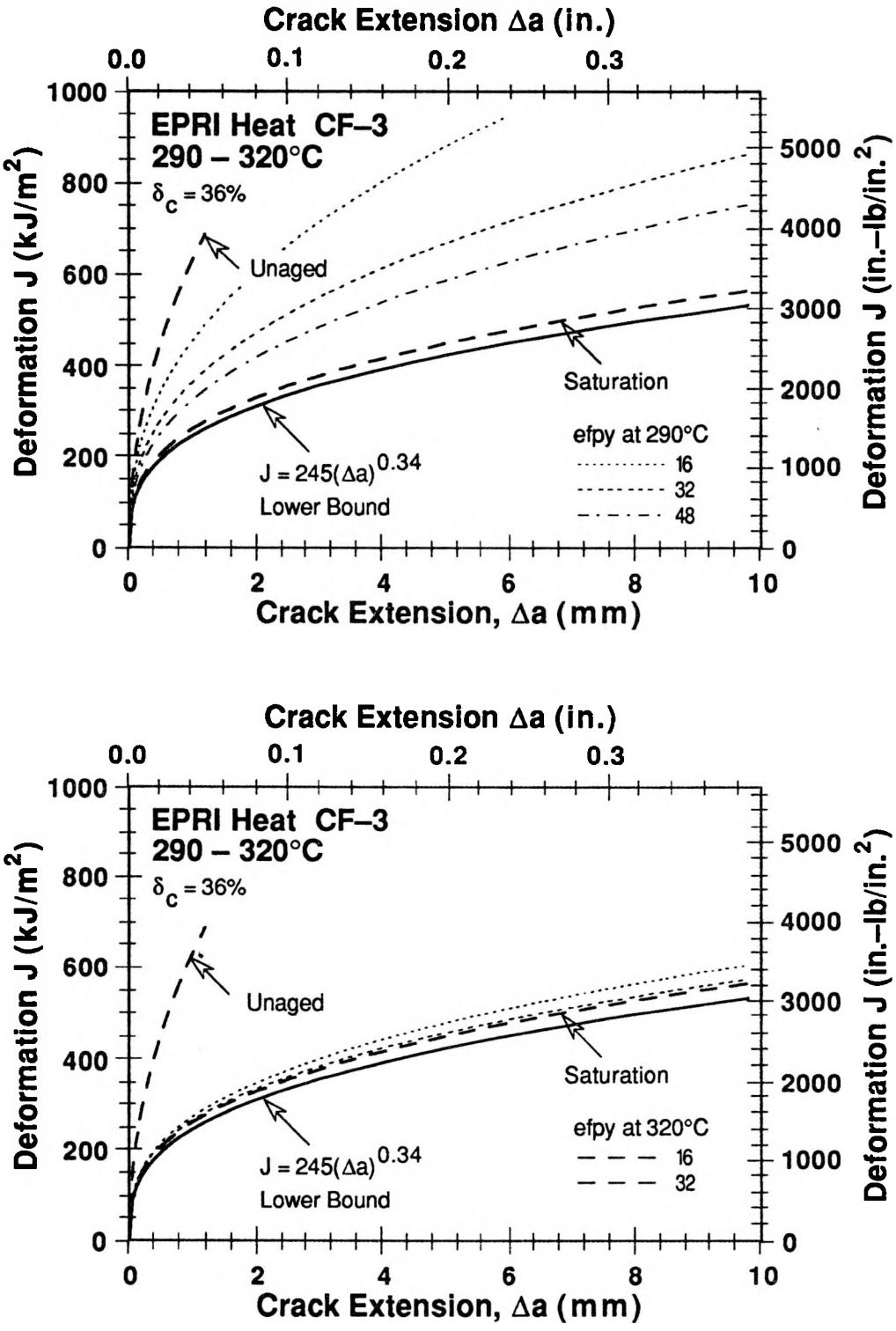

Figure 30. Comparison between lower-bound J-R curve and J-R curves after 16, 32, and 48 efpy at 290 and 320°C for static-cast plate of CF-3 steel

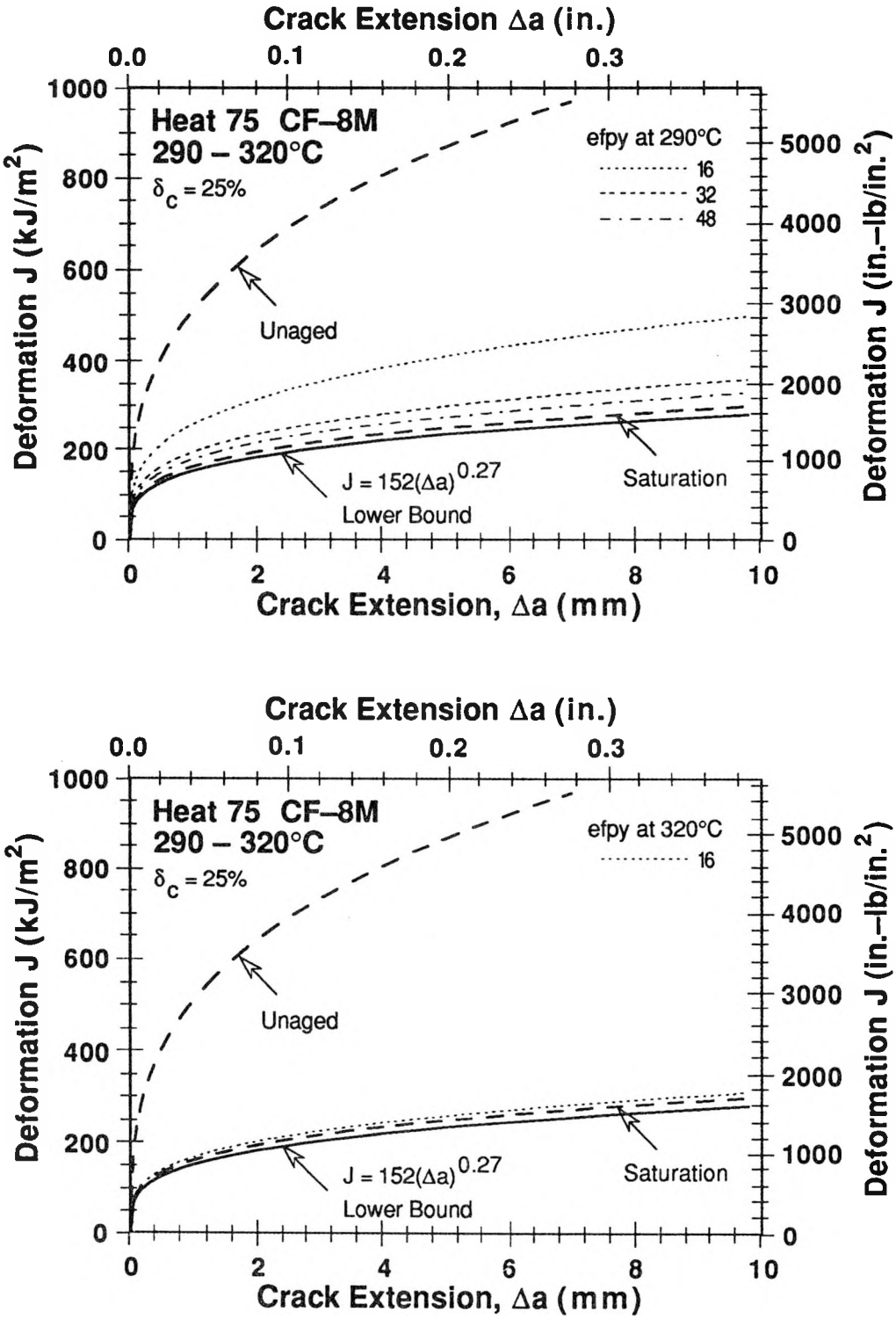

Figure 31. Comparison between lower-bound J–R curve and J–R curves after 16, 32, and 48 efpy at 290 and 320°C for static-cast slab of CF-8M steel

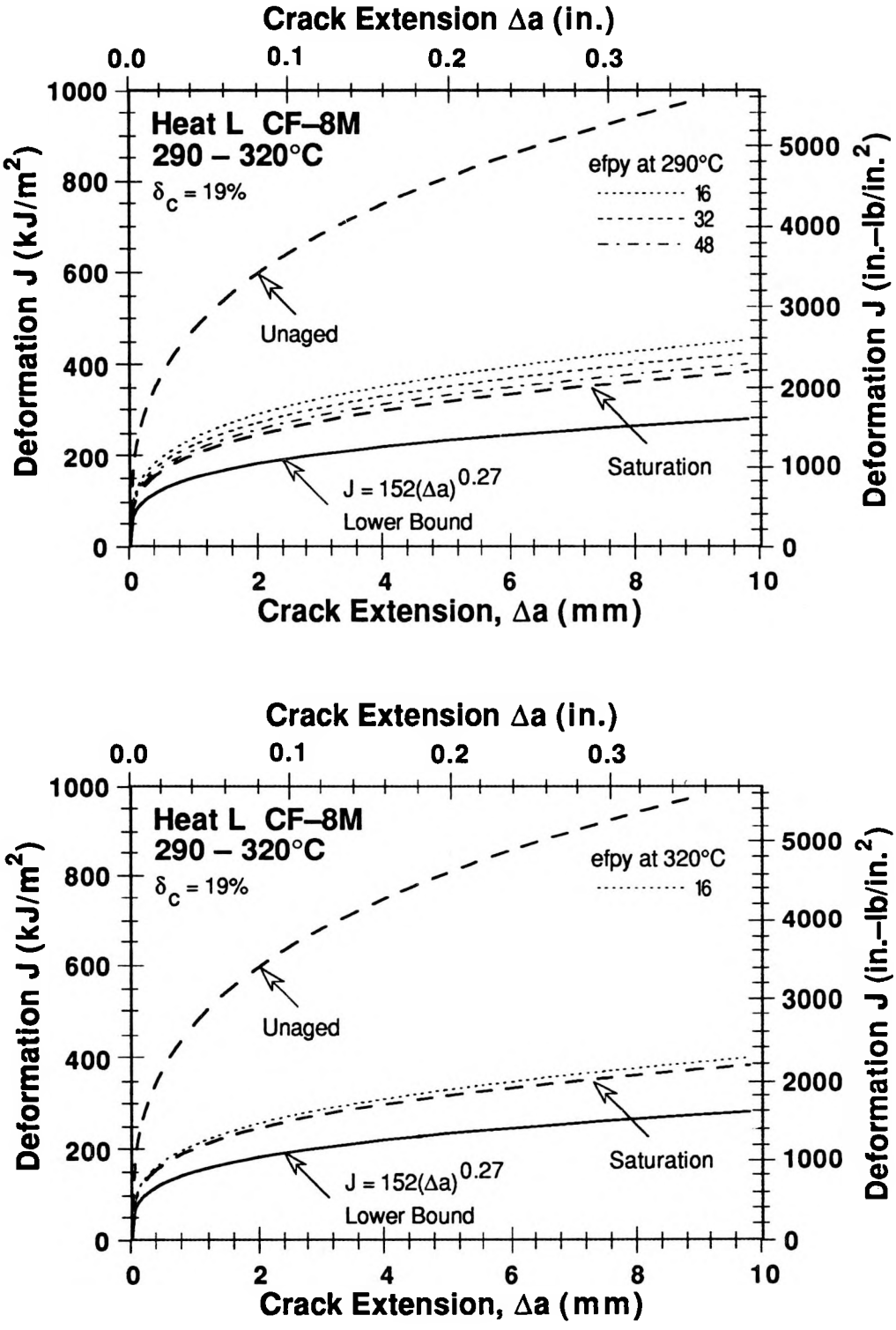

Figure 32. Comparison between lower-bound J-R curve and J-R curves after 16, 32, and 48 efpy at 290 and 320°C for static-cast plate of CF-8M steel

lower bound fracture toughness defined in Section 5.3 are also shown for comparison. The results show the benefit of knowing the chemical composition of the steel. The saturation fracture toughness of only few heats, e.g., KRB and EPRI material and Heat 75, is close to the lower bound fracture toughness. Furthermore, depending on the service temperature, the saturation fracture toughness may not be achieved within the design lifetime of the reactor. For the EPRI material, saturation fracture toughness is reached after ≈16 efpy at 320°C (608°F) but not at 290°C (554°F) even after 48 efpy. Thermal embrittlement of Heats 75 and L is much faster; saturation fracture toughness is reached in 16–32 efpy at 290 and 320°C. Figure 27 shows that the saturation J–R curve for Heat 68 is close to the lower-bound J–R curve for cast stainless steels with ≤15% ferrite. However, the saturation fracture toughness is not achieved within the design lifetime.

5.3 Lower–Bound Fracture Toughness

For cast stainless steels of unknown chemical composition, lower-bound fracture toughness is defined for a given material specification and temperature. Charpy-impact data indicate that, for cast stainless steels within the ASTM Specification A 351, the saturation room-temperature impact energy can be as low as 25 J/cm^2 (≈15 ft·lb) for CF–3 and CF–8 steels and 20 J/cm^2 (≈12 ft·lb) for CF–8M steel. A lower-bound fracture toughness J–R curve at room temperature for CF–3 and CF–8 steels is given by

$$J_d = 261[\Delta a]^{0.39}; \tag{36}$$

for CF–8M steel, it is given by

$$J_d = 119[\Delta a]^{0.37}. \tag{37}$$

At 290–320°C (554–608°F), a lower-bound fracture toughness J–R curve for CF–3 and CF–8 steels is given by

$$J_d = 245[\Delta a]^{0.34}; \tag{38}$$

for CF–8M steel, it is given by

$$J_d = 152[\Delta a]^{0.27}. \tag{39}$$

The J–R curves predicted from Eqs. 36–39 are shown in Fig. 33. The cast stainless steels used in the U.S. nuclear industry generally have <15% ferrite. The lower-bound J–R curves represented by Eqs. 36–39 are based on the "worst case" chemical composition (>20% ferrite) and structurally "weak" cast stainless steels and are thus very conservative for most steels. Less conservative estimates of lower-bound J–R curves can be obtained if the ferrite content of the steel is known. The ferrite content of a cast stainless steel component can be measured in the field with a ferrite scope and a remote probe. When the ferrite content is ≤15%, a lower-bound fracture toughness J–R curve at room temperature for CF–3 and CF–8 steels is given by

$$J_d = 311[\Delta a]^{0.40}; \tag{40}$$

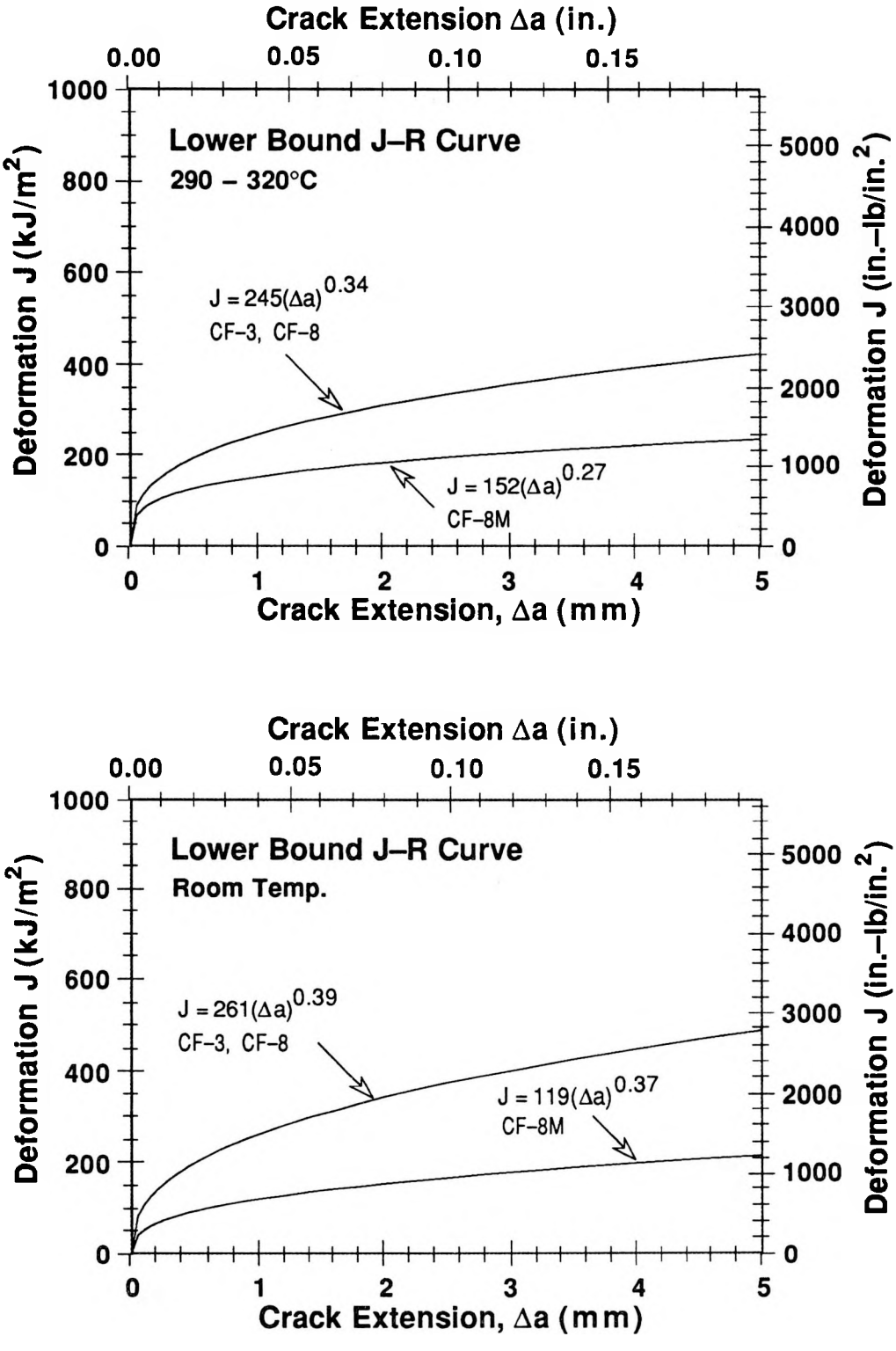

Figure 33. Lower-bound fracture toughness J-R curve at 290–320°C and room temperature for aged cast stainless steels

for CF–8M steel, it is given by

$$J_d = 135[\Delta a]^{0.37}. \quad (41)$$

At 290–320°C (554–608°F) a lower-bound fracture toughness J–R curve for CF–3 and CF–8 steels with ferrite content ≤15% is given by

$$J_d = 275[\Delta a]^{0.35}; \quad (42)$$

for CF–8M steel, it is given by

$$J_d = 166[\Delta a]^{0.27}. \quad (43)$$

When the ferrite content is ≤10%, a lower-bound fracture toughness J–R curve at room temperature for CF–3 and CF–8 steels is given by

$$J_d = 394[\Delta a]^{0.43}; \quad (44)$$

for CF–8M steel, it is given by

$$J_d = 186[\Delta a]^{0.38}. \quad (45)$$

At 290–320°C (554–608°F) a lower-bound fracture toughness J–R curve for CF–3 and CF–8 steels with ferrite content ≤10% is given by

$$J_d = 320[\Delta a]^{0.36}; \quad (46)$$

for CF–8M steel, it is given by

$$J_d = 211[\Delta a]^{0.28}. \quad (47)$$

Lower bound J–R curves for cast stainless steels with <15% and <10% ferrite are shown in Figs. 34 and 35, respectively. The limited data available[27] indicate that J values at any other intermediate temperature can be linearly interpolated from the values at room temperature and at 290–320°C.

6 Flow Diagram for Estimating Fracture Toughness

A flow diagram of the sequential steps required for estimating fracture toughness is shown in Fig. 36. Section A of Fig. 36 defines lower-bound fracture toughness J–R curves for cast stainless steels of unknown chemical composition ; Sections B and C present procedures for estimating J–R curves when some information is known about the material. Section B describes two methods for estimating saturation J–R curves, i.e., the lowest toughness that would be achieved by the material after long-term service. The first method utilizes only the information available in the CMTRs, i.e., chemical composition of the steel. The second method is used when measured values of ferrite content and mean ferrite spacing of the steel are also known. Nitrogen content is assumed to be 0.04 wt.% if not known. The lower-bound J–R curve for the unaged cast stainless steels is used as the

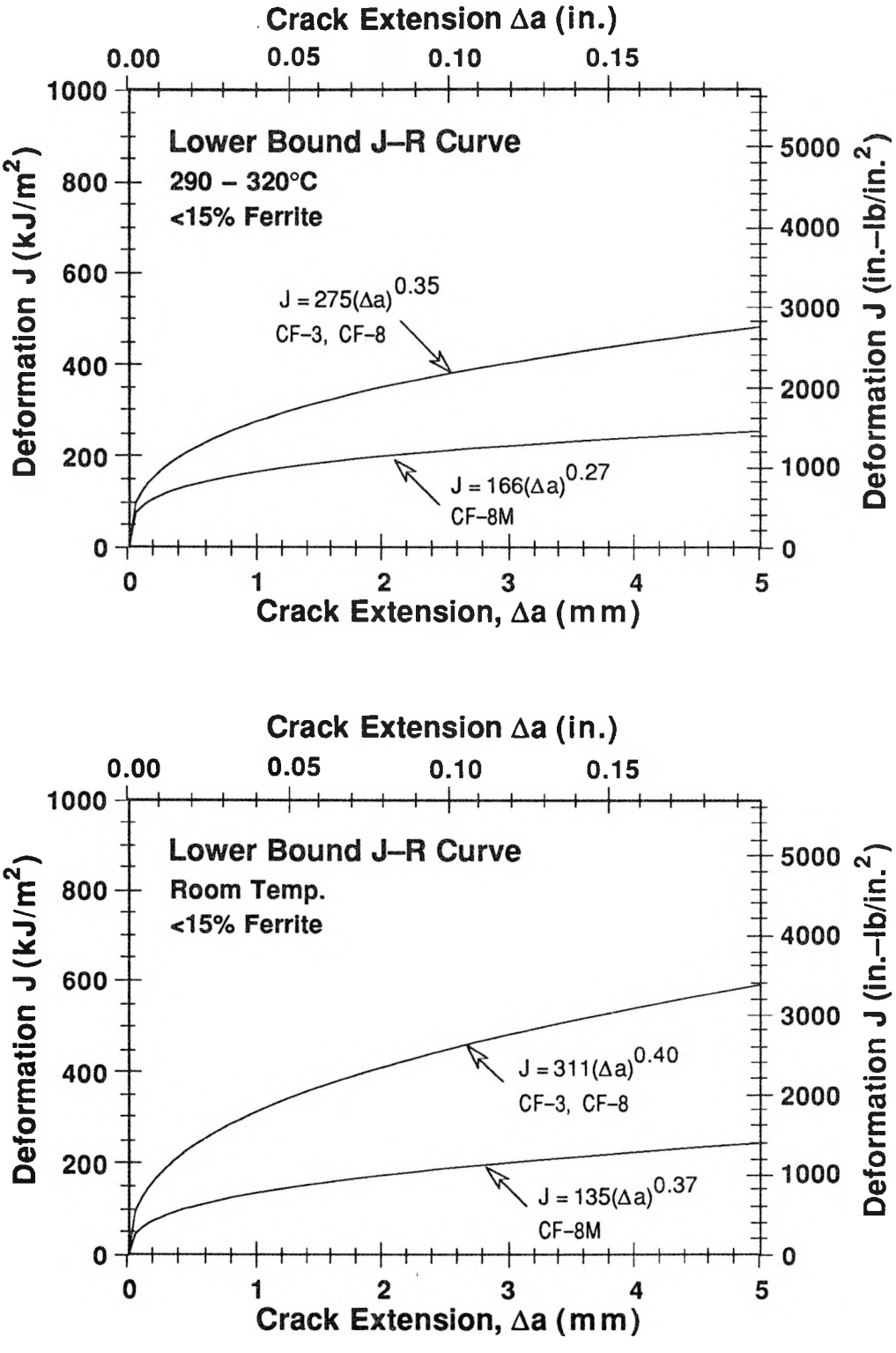

Figure 34. Lower-bound fracture toughness J-R curve at 290-320°C and room temperature for aged cast stainless steels with <15% ferrite

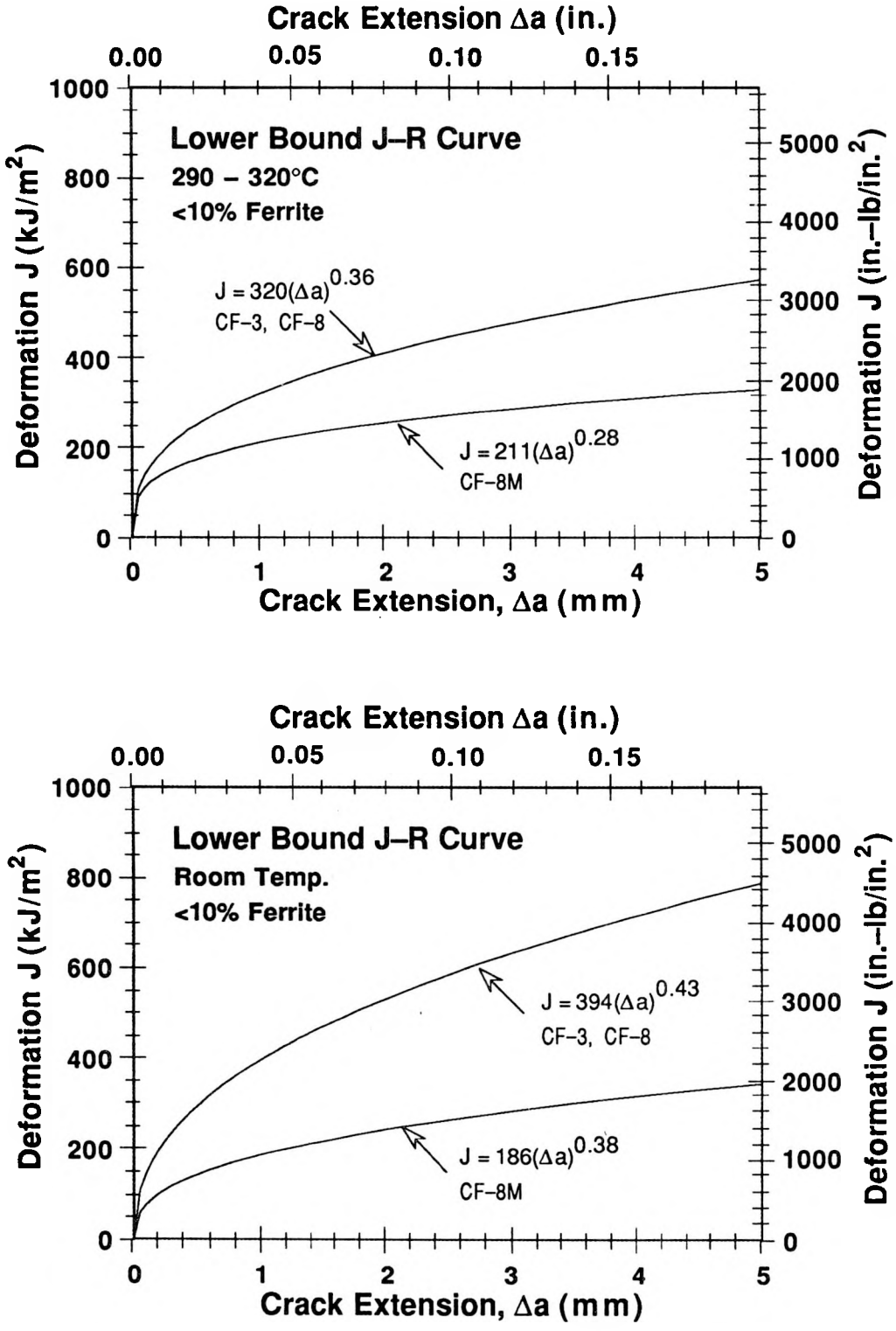

Figure 35. Lower-bound fracture toughness J-R curve at 290-320°C and room temperature for aged cast stainless steels with <10% ferrite

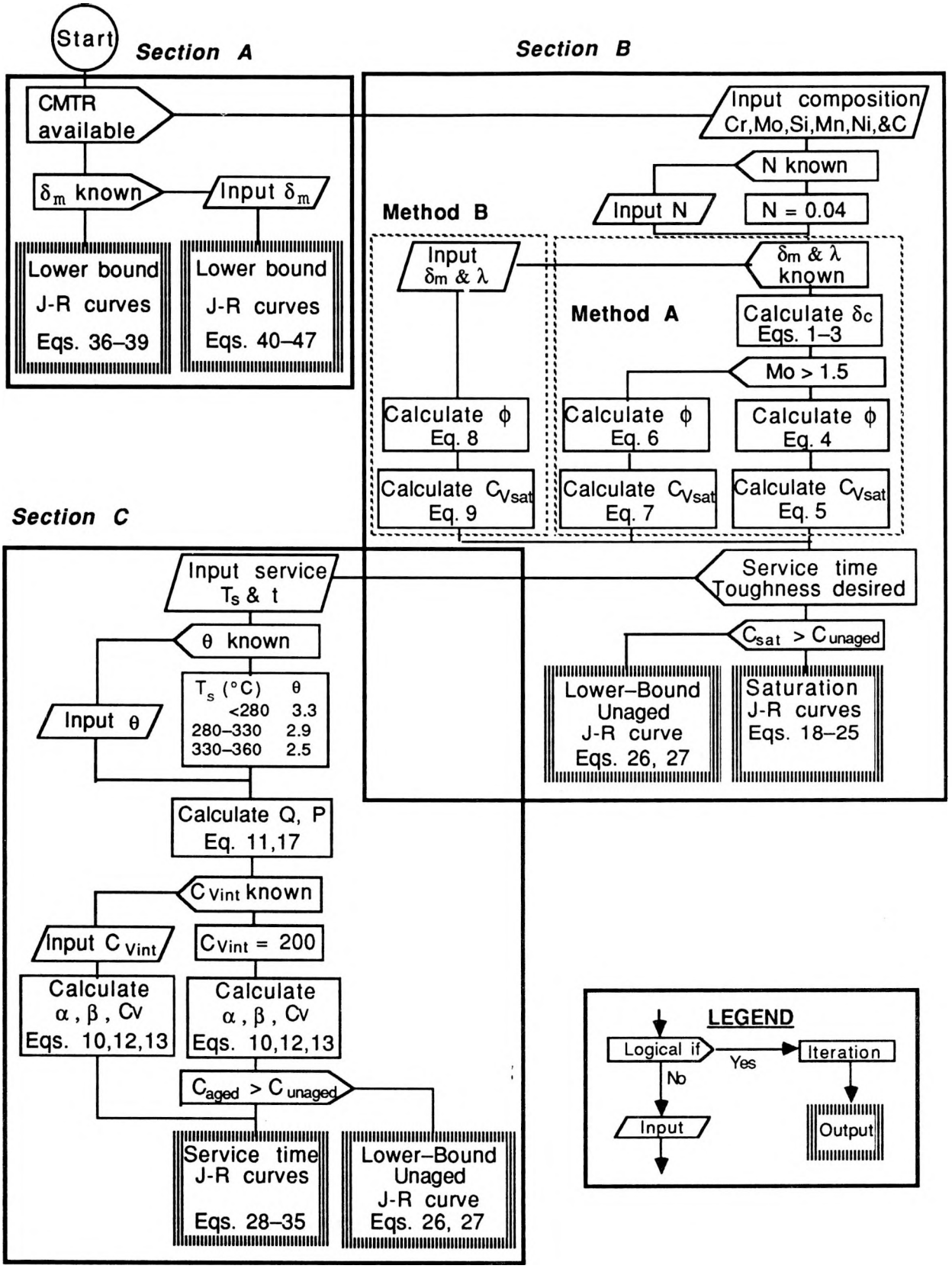

Figure 36. Flow diagram for estimating fracture toughness J–R curves of cast stainless steels in LWR systems

saturation J–R curve of a material when the J–R curve estimated from the chemical composition is higher than the lower-bound curve for the unaged material.

Estimation of service time J–R curves, i.e., fracture toughness at any given time and temperature of service, is described in Section C. The service time J–R curves depend on the kinetics of thermal embrittlement, i.e., the rate of decrease of fracture toughness as a function of reactor service time. The initial impact energy of the unaged material and the constant θ are also required for estimating the kinetics of thermal embrittlement. The impact energy can be assumed to be 200 J/cm^2 if not known. The value of θ depends on the service temperature; it is assumed to be 3.3 for <280°C (<535°F), 2.9 for 280–330°C (536–626°F), and 2.5 for 330–360°C (626–680°F). If the initial impact energy of the unaged material is not known, the lower-bound J–R curve for the unaged cast stainless steels is used when the J–R curve estimated from the chemical composition is higher than the lower bound for the unaged steel.

7 Cast Stainless Steels from the Shippingport Reactor*

7.1 Material Characterization

Cast stainless steel materials from the decommissioned Shippingport reactor offered a unique opportunity to validate the correlations and benchmark the laboratory studies. Cast stainless steel materials were obtained from four cold-leg check valves, two hot-leg main shutoff valves, and two pump volutes. One of the volutes is a "spare" that had seen service only during the first core loading, the other was in service for the entire life of the plant. The actual time at temperature for the materials was ≈13 y at ≈281°C for the hot-leg components and ≈264°C for the cold-leg components. The components were at a hot standby condition ≈204°C for an additional ≈2 y.

The various cast materials were characterized to determine their chemical composition, hardness, grain structure, and ferrite content and distribution. Samples were obtained from different locations of the casting and from different regions across the thickness of the wall. The chemical composition, hardness, and amount and distribution of ferrite for the cast materials are given in Table 4. All materials are CF–8 cast stainless steel. Hardness increases with an increased ferrite content. Some differences in hardness and ferrite content were observed for material from different locations in the casting. Such differences appear to be related to compositional variations.

The results of metallurgical characterization of the materials have been presented earlier.[37] All valve materials have a radially oriented columnar grain structure. Typical examples of the grain structure for the check valves and main shutoff valves are shown in Figs. 37 and 38, respectively. The inner surface of all the valves contained repair welds; an example is shown in Fig. 38. The pump volutes have a mixed grain structure of columnar and equiaxed grains (Fig. 39). The ferrite morphologies of the check valves and main shutoff valves are shown in Figs. 40 and 41, respectively. The materials contain a lacy ferrite with a

*Work performed under NRC FIN No. A22561

Table 4. Chemical composition, ferrite morphology, and hardness of cast stainless steel components from the Shippingport reactor

Mater.	Composition (wt.%)										Ferrite (%)		Ferrite Spacing	Hard-ness
ID[a]	C	N	Si	Mn	P	S	Ni	Cr	Mo	Cu	Calc.	Meas.	(μm)	(R_B)
						Cold Leg Check Valve[b]								
CA4	0.056	0.041	1.45	1.10	0.018	0.009	8.84	20.26	0.01	0.07	10.8	10.9	157	79.8
CA7	0.058	0.041	1.43	1.09	0.018	0.009	8.72	20.22	0.01	0.07	10.9	10.0	148	78.6
CB7	0.052	0.053	1.36	1.07	0.018	0.011	8.85	19.12	0.02	0.06	5.9	3.2	296	75.0
CC4	0.056	0.067	1.42	1.11	0.018	0.012	9.64	20.10	0.01	0.05	5.3	6.0	211	77.0
						Hot Leg Main Shutoff Valve[c]								
MA1	0.052	0.049	0.22	0.72	0.039	0.013	10.50	20.74	0.24	0.13	5.2	9.5	217	76.9
MA9	0.052	0.051	0.24	0.72	0.041	0.011	10.54	20.78	0.24	0.13	5.1	10.0	245	77.6
MB2	0.042	0.073	0.51	0.72	0.043	0.017	10.77	19.74	0.19	0.12	2.6	1.9	–	74.2
						Pump Volute								
VR[d]	0.046	0.049	1.14	0.50	0.027	0.017	9.56	20.79	0.04	0.07	9.8	16.2	181	82.9
PV	0.108	0.027	0.89	1.11	0.032	0.008	9.30	19.83	0.38	0.25	4.1	13.0	–	–

[a] For the valves, the second letter indicates the loop where the valve was located and the number designates the segment of the component from which the material was removed (Segments 1, 2, and 7 are from the top of the valve, Segment 4 is from the bottom, and Segment 9 is from a cooler region).
[b] In service for ≈13 y at 264°C.
[c] In service for ≈13 y at 281°C.
[d] Spare pump volute in service only during initial core loading.

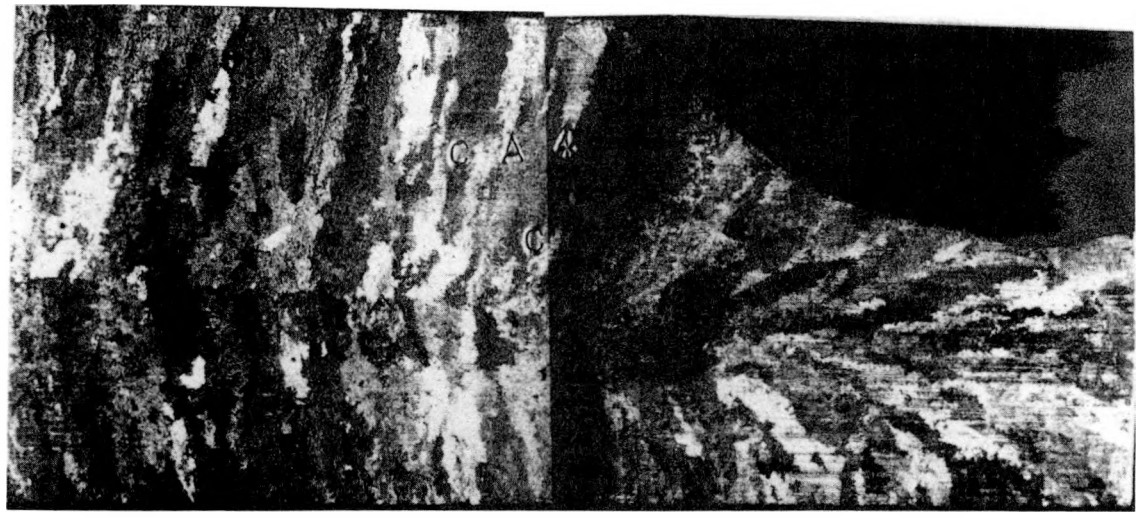

Figure 37. Microstructure along axial section of Loop A check valve from the Shippingport reactor

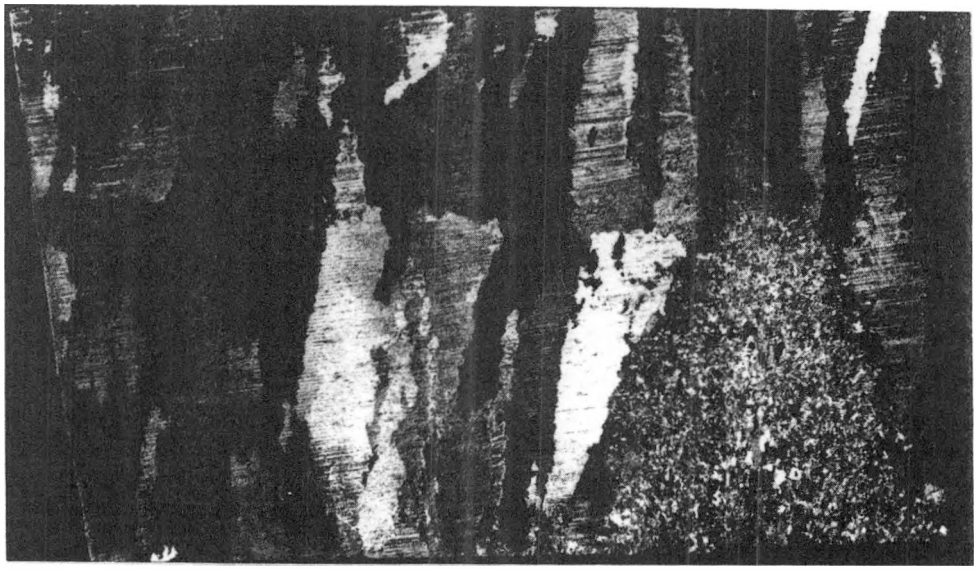

Figure 38. Microstructure along axial section of loop B main shutoff valve from the Shippingport reactor. A repair weld is also seen on the outer diameter of the valve.

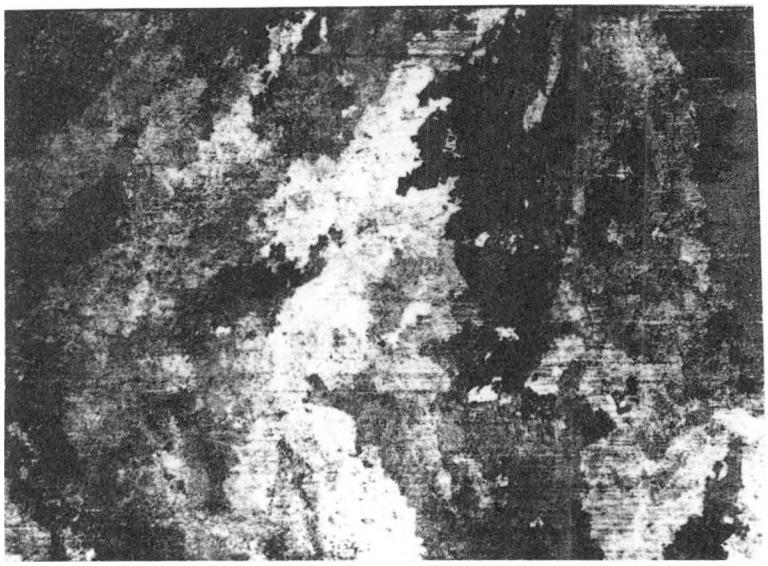

Figure 39. Microstructure along axial section of the spare volute from the Shippingport reactor

mean ferrite spacing in the range of 150–300 μm. The check valve materials show a significant amount of carbides at the ferrite/austenite phase boundaries. Also, most of the phase boundaries have migrated. The original phase boundaries are decorated with carbides, which most likely formed during production heat treatment of the casting.

Microstructural examination of the cast materials indicates that the mechanism of low-temperature thermal embrittlement is the same as that of the laboratory-aged materials.[20,21] All materials showed spinodal decomposition of the ferrite to form a Cr-rich α' phase. In addition, the check valve materials contained the Ni- and Si-rich G phase in the ferrite and $M_{23}C_6$ carbides at the austenite/ferrite phase boundary. An unexpected microstructural feature, i.e., σ phase precipitates on slip bands and stacking faults, was also observed in the austenite of the check valve material.[20,21] Precipitation of σ phase generally occurs at temperatures >550°C (1022°F). The presence of σ phase and phase boundary migration indicate significant differences between the production heat treatment of the check valves and that of the other materials.

7.2 Mechanical Properties

Specimens for Charpy-impact and tensile tests were obtained from different locations across the thickness of the various components. All specimens were in the LC orientation.* Impact tests were conducted on standard Charpy V-notch specimens machined according to ASTM Specification E 23. A Dynatup Model 8000A drop-weight impact machine with an

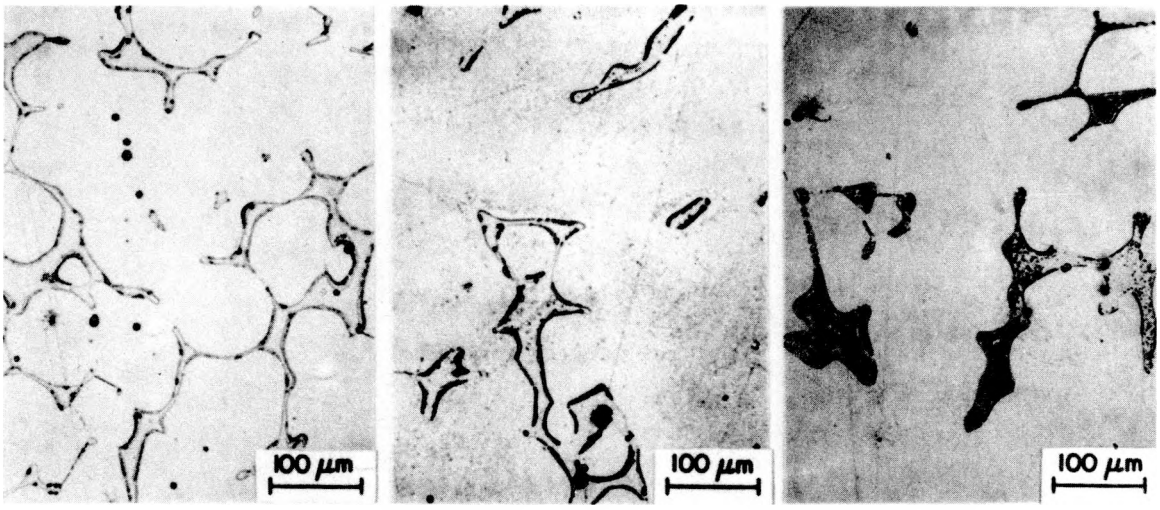

Loop A *Loop B* *Loop C*

Figure 40. Ferrite morphology of cast materials from Loops A, B, and C cold-leg check valves from the Shippingport reactor

*The first letter represents the direction normal to the plane of the crack; and the second indicates the direction of crack propagation; L = longitudinal; and C = circumferential.

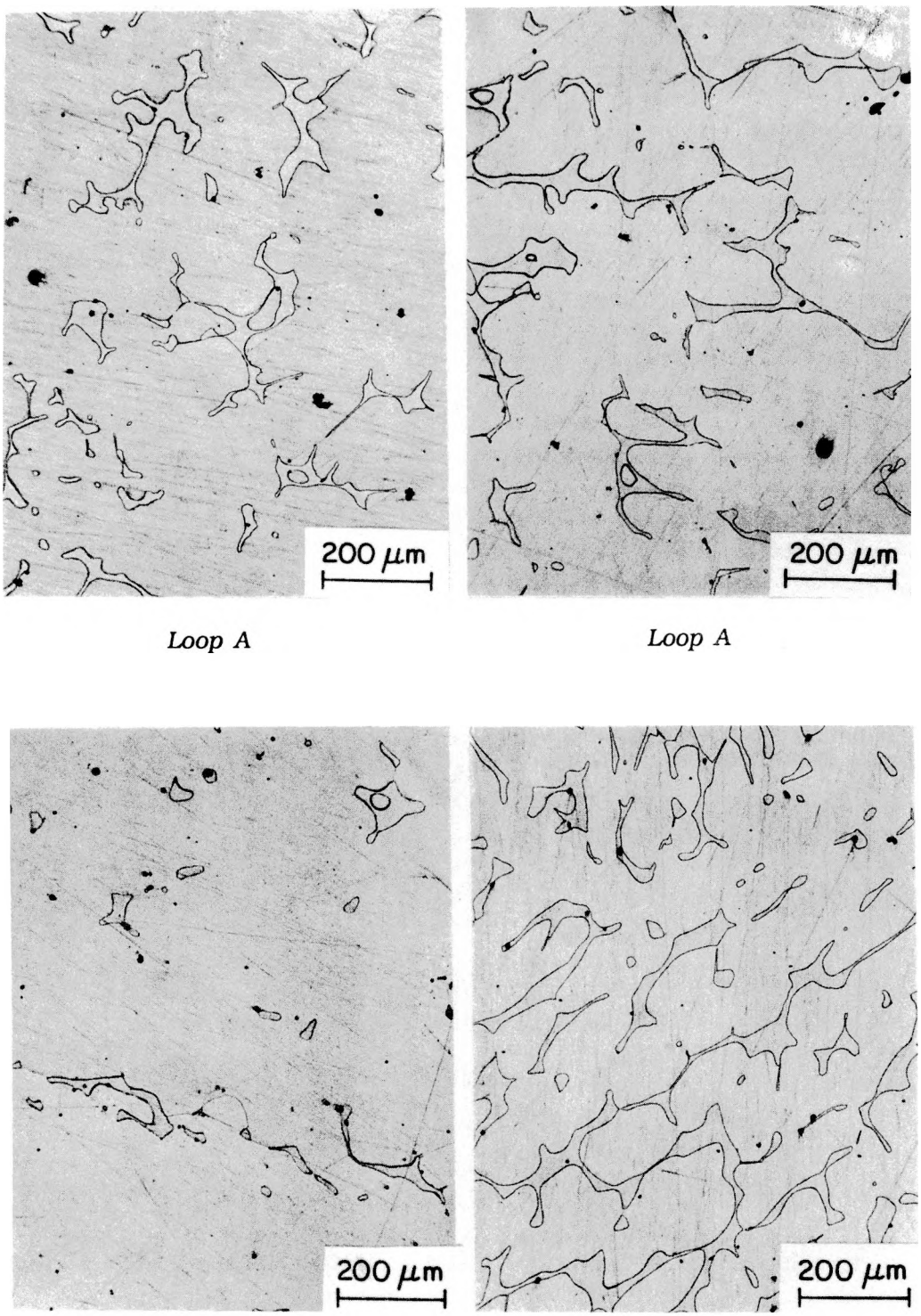

Loop A *Loop A*

Loop B *Loop C*

Figure 41. Ferrite morphology of cast materials from Loops A, B, and C hot-leg main shutoff valves

instrumented tup and data readout system was used for the tests. Tensile tests were performed on cylindrical specimens with a diameter of 5 mm and a gauge length of 20 mm. The tests were conducted at an initial strain rate of 4×10^{-4} s^{-1}.

7.2.1 Baseline Mechanical Properties

The baseline mechanical properties for the unaged materials must be known to establish the thermal-aging effects during reactor service. Microstructural and annealing studies[12-15,18-21] on laboratory and reactor-aged materials have been conducted to investigate the possibility of recovering the mechanical properties of embrittled materials. The results indicate that the formation of the α' phase by spinodal decomposition is the primary mechanism of thermal embrittlement. The α' phase is not stable at temperatures >550°C (1022°F). The mechanical properties can be recovered by annealing the embrittled cast stainless steels for 1 h at 550°C and then water-quenching to dissolve the α' phase while avoiding the formation of σ phase. The influence of annealing on the Charpy transition curves for three laboratory-aged heats and service-aged material from the KRB reactor is shown in Fig. 42. The results indicate an essentially complete recovery from thermal embrittlement; the transition curves for the annealed materials agree well with those for the unaged steel. Microstructural examination of the annealed material showed no α' phase, but the size and distribution of the G phase were the same as in the aged material.[18-21] The results indicate that baseline mechanical properties of unaged material can be determined from recovery-annealed material.

Charpy-impact tests were also conducted on material from a cooler region of the Shippingport Loop A main shutoff valve to obtain baseline properties. The Charpy transition curves for MA9 and recovery-annealed material from MA9 and MA1 are shown in Fig. 43. These materials are from the same valve, although MA9 is from a cooler region of the valve. The results indicate that MA9 material suffered little or no thermal-aging thermal embrittlement; annealing had no effect on the transition curves. The results for annealed MA1 material also show good agreement with the transition curve for MA9. The upper-shelf energy (USE) for both materials is not constant but decreases with an increase in temperature. The average impact energies at room temperature and at 290°C (554°F), respectively, are 356 and 253 J/cm^2 for MA9, and 320 and 254 J/cm^2 for annealed MA1.

The Charpy data were fitted with a hyperbolic tangent function of the form

$$C_V = K_o + B\{1 + \tanh [(T - C)/D]\}, \quad (48)$$

where K_o is the lower-shelf energy, T is the test temperature in °C, B is half the distance between upper- and lower-shelf energy, C is the mid-shelf CTT in °C, and D is the half-width of the transition region. The best-fit curves for MA9, with or without annealing, and for annealed MA1 indicate that the latter is marginally weaker; the CTT is ≈10°C higher and the average USE is ≈30 J/cm^2 lower for MA1. Such differences in impact energy are most likely due to minor variations in composition and structure of the materials from different locations of the casting. The Charpy data for MA9 and annealed MA1 may be represented by a single transition curve; the best-fit curve is shown in Fig. 43.

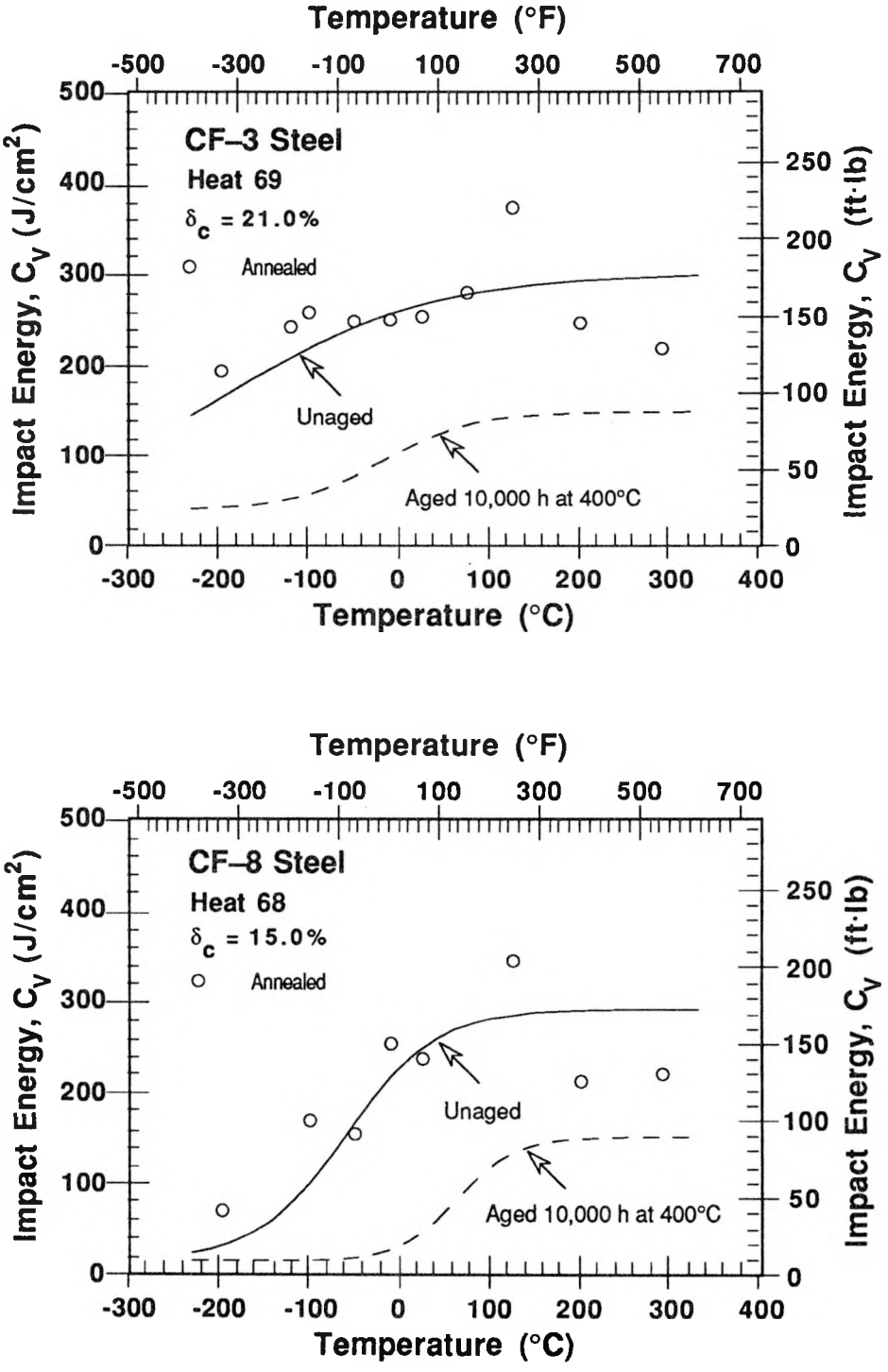

Figure 42. Effect of annealing on Charpy transition curves for thermally aged Heats 69, 68, and 75 and KRB pump cover plate. The dashed lines are the curves of embrittled laboratory heats.

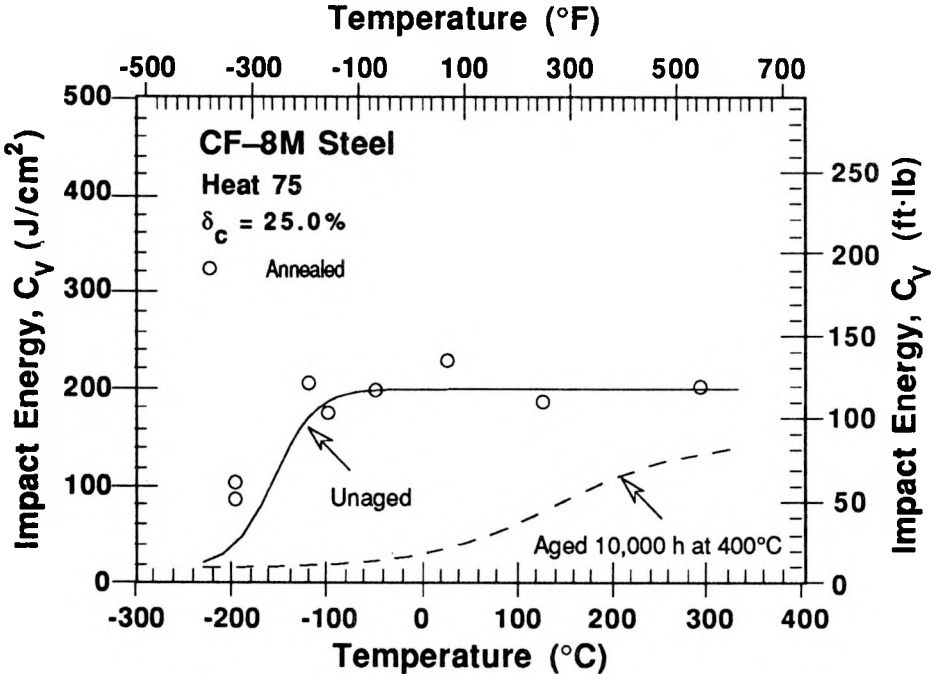

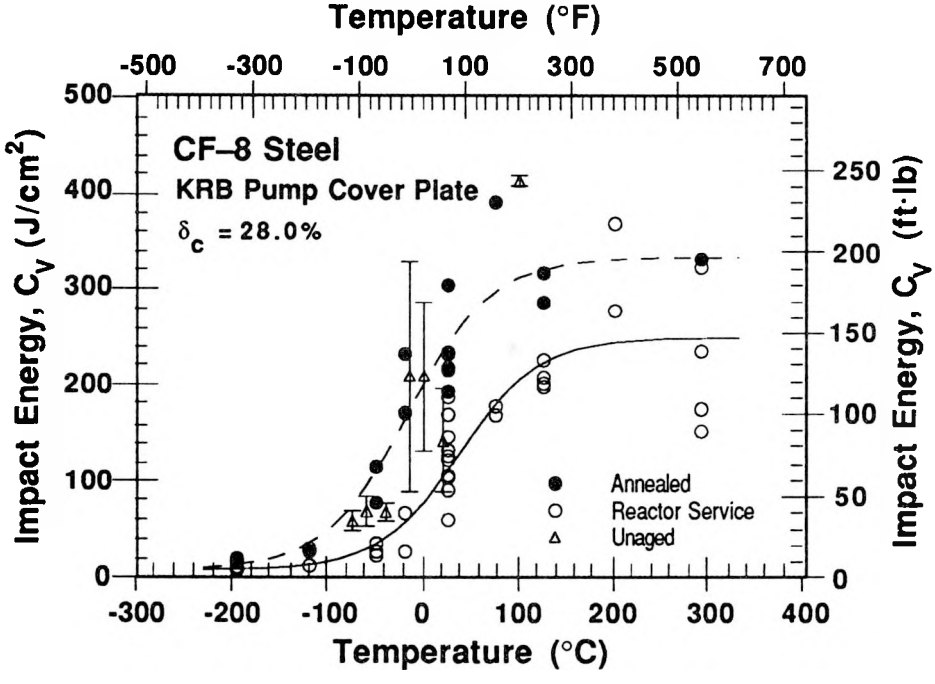

Figure 42. (Contd.)

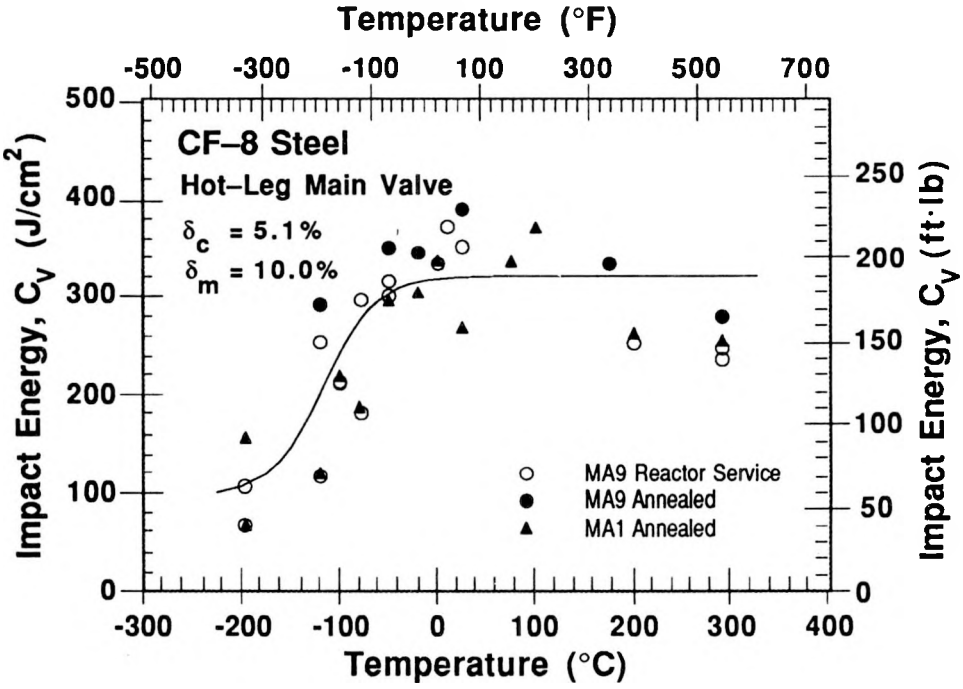

Figure 43. Effect of annealing on Charpy transition curve for cast material from the hot–leg main shutoff valve. Material MA9 is from a cooler region of the valve.

7.2.2 Charpy–Impact Energy

Charpy impact data for the various cast materials from the Shippingport reactor are given in Tables 5 and 6 and the Charpy transition curves are shown in Figs. 44–46. The results for MA9 and recovery–annealed MA1 materials are shown as the baseline Charpy transition curve for MA1 in Fig. 44. The baseline transition curves for CA4 and PV are represented by the results for recovery–annealed materials. The Charpy data were fitted with the hyperbolic tangent expression given in Eq. 48; the values of the constants for the various materials are given in Table 7. The results indicate that the room–temperature impact energy of the materials is relatively high and the mid–shelf CTT, i.e., constant C in Eq. 48, is very low. The check valve materials CA4 and CB7 are weaker than MA1 and PV, e.g., the mid–shelf CTT is ≈100°C higher for CA4 and CB7. The higher CTTs are due to the presence of phase–boundary carbides in the check valve materials (Fig. 40). The carbides weaken the phase boundaries and thus provide an easy path for fracture.

The decrease in impact strength from ≈13–y service at reactor temperatures is minimal for the materials. The room–temperature impact energy of PV, MA1, and CA4 materials is decreased by ≈90, 70, and 40 J/cm^2, respectively. The large difference in USE for the unaged and service–aged materials from row 1 of MA1 (Fig. 44), is not due to thermal aging. The inner 15–mm region of the MA1 valve body contains a high density of inclusions/flaws and is inherently weak. The inner surface of all the valves contained repair welds. There is no significant difference in the chemical composition or ferrite content of the material across the thickness of the valve body.

Table 5. Charpy-impact test results for cast stainless steel materials from the Shippingport reactor

Specimen ID	Material ID[a]	Temp. (°C)	Impact Energy (J/cm²)	Impact Energy (ft·lb)[b]	Yield Load (kN)	Yield Load (kip)	Maximum Load (kN)	Maximum Load (kip)
			Reactor Service[c]					
CA43-01	CA4	-197	31.1	18.3	13.192	2.966	15.213	3.420
CA41-01	CA4	-100	28.1	16.6	12.391	2.786	12.391	2.786
CA43-03	CA4	-78	33.8	19.9	10.995	2.472	12.420	2.792
CA42-02	CA4	-50	114.1	67.3	11.522	2.590	17.332	3.896
CA42-01	CA4	-20	126.8	74.8	10.946	2.461	16.854	3.789
CA44-01	CA4	0	84.3	49.7	10.145	2.281	14.051	3.159
CA41-02	CA4	25	162.1	95.6	9.354	2.103	15.535	3.492
CA44-02	CA4	25	128.5	75.8	9.589	2.156	14.881	3.345
CA43-04	CA4	50	138.2	81.5	8.427	1.894	13.211	2.970
CA43-02	CA4	75	202.8	119.7	7.948	1.787	13.582	3.053
CA41-03	CA4	125	281.4	166.0	7.118	1.600	13.123	2.950
CA44-03	CA4	200	183.3	108.1	6.142	1.381	11.473	2.579
CA42-03	CA4	290	179.0	105.6	5.546	1.247	9.891	2.224
CA43-05	CA4	290	178.9	105.6	5.390	1.212	10.419	2.342
CB72-01	CB7	-197	73.6	43.4	12.430	2.794	18.601	4.182
CB71-01	CB7	-100	83.8	49.4	11.717	2.634	16.531	3.716
CB72-02	CB7	-50	107.0	63.1	10.956	2.463	15.369	3.455
CB71-02	CB7	-20	142.4	84.0	10.262	2.307	16.922	3.804
CB73-01	CB7	0	211.2	124.6	8.983	2.019	15.428	3.468
CB71-03	CB7	25	162.4	95.8	9.022	2.028	14.012	3.150
CB73-02	CB7	25	203.7	120.2	8.700	1.956	14.666	3.297
CB73-03	CB7	50	269.4	158.9	7.733	1.738	13.592	3.056
CB73-03	CB7	75	295.9	174.6	7.489	1.684	13.592	3.056
CB73-04	CB7	100	304.6	179.7	6.454	1.451	11.317	2.544
CB71-04	CB7	125	241.5	142.5	6.874	1.545	12.313	2.768
CB72-05	CB7	200	339.3	200.2	5.458	1.227	11.464	2.577
CB71-05	CB7	290	292.1	172.3	5.097	1.146	10.712	2.408
CB72-04	CB7	290	256.1	151.1	5.488	1.234	10.302	2.316
CC43-02	CC4	-197	26.5	15.6	12.850	2.878	12.850	2.889
CC44-01	CC4	-120	39.1	23.1	14.022	3.152	14.022	3.152
CC44-03	CC4	0	104.2	61.5	10.458	2.351	14.041	3.157
CC43-03	CC4	25	121.7	71.8	9.686	2.177	14.198	3.192
CC44-02	CC4	125	216.3	127.6	7.079	1.591	12.186	2.740
CC43-01	CC4	290	306.3	180.7	5.605	1.260	11.239	2.527
MA11-05	MA1	-197	49.4	29.1	13.924	3.130	15.115	3.398
MA11-01	MA1	-100	190.6	112.5	13.026	2.928	21.902	4.924
MA11-02	MA1	-20	228.8	135.0	9.764	2.195	16.580	3.727
MA11-03	MA1	25	144.5	85.3	10.106	2.272	14.207	3.194
MA11-06	MA1	25	210.0	123.9	8.524	1.916	14.325	3.220
MA11-04	MA1	125	167.0	98.5	8.671	1.949	12.889	2.898
MA12-01	MA1	-197	96.9	57.2	12.001	2.698	19.148	4.305
MA12-05	MA1	-120	149.3	88.1	11.649	2.619	18.631	4.188
MA13-04	MA1	-100	318.6	188.0	11.561	2.599	22.185	4.987
MA12-02	MA1	-50	281.1	165.8	10.887	2.447	18.025	4.052
MA13-01	MA1	0	293.7	173.3	10.399	2.338	16.346	3.675
MA12-06	MA1	25	279.2	164.7	8.817	1.982	14.959	3.363
MA13-02	MA1	25	337.6	199.2	9.237	2.077	15.877	3.569
MA13-05	MA1	25	280.7	165.6	9.032	2.030	15.174	3.411
MA12-03	MA1	75	249.0	146.9	7.577	1.703	13.143	2.955
MA13-06	MA1	125	269.3	158.9	6.532	1.468	12.284	2.762
MA12-07	MA1	200	227.8	134.4	5.468	1.229	11.063	2.487

Table 5. (Contd.)

Specimen ID	Material ID[a]	Temp. (°C)	Impact Energy (J/cm²)	Impact Energy (ft·lb)[b]	Yield Load (kN)	Yield Load (kip)	Maximum Load (kN)	Maximum Load (kip)
MA13-07	MA1	200	231.7	136.7	6.786	1.526	11.551	2.597
MA12-04	MA1	290	197.6	116.6	6.318	1.420	10.594	2.382
MA13-08	MA1	290	175.2	103.4	5.156	1.159	9.940	2.235
MA91-01	MA9	-197	66.8	39.4	14.412	3.240	17.361	3.903
MA93-01	MA9	-197	106.2	62.7	12.625	2.838	19.617	4.410
MA92-01	MA9	-120	252.4	148.9	12.938	2.909	20.720	4.658
MA94-01	MA9	-120	116.2	68.6	11.766	2.645	16.746	3.765
MA91-02	MA9	-100	212.3	125.3	12.069	2.713	19.724	4.434
MA93-02	MA9	-100	210.7	124.3	11.317	2.544	19.168	4.309
MA92-02	MA9	-78	295.5	174.3	11.249	2.529	19.226	4.322
MA94-02	MA9	-78	181.2	106.9	10.184	2.289	18.562	4.173
MA91-03	MA9	-50	299.7	176.8	9.940	2.235	17.322	3.894
MA93-03	MA9	-50	314.7	185.7	10.878	2.445	18.006	4.048
MA92-03	MA9	-20	439.1	259.1	9.208	2.070	16.658	3.745
MA94-03	MA9	-20	411.6	242.8	9.872	2.219	16.805	3.778
MA92-04	MA9	0	332.7	196.3	8.661	1.947	14.910	3.352
MA94-04	MA9	10	370.2	218.4	8.915	2.004	14.852	3.339
MA91-04	MA9	25	350.2	206.6	8.515	1.914	15.233	3.425
MA93-04	MA9	25	408.6	241.1	8.993	2.022	15.223	3.422
MA92-05	MA9	75	316.7	186.9	7.401	1.664	13.465	3.027
MA94-05	MA9	75	312.1	184.1	7.226	1.624	13.270	2.983
MA91-05	MA9	125	338.5	199.7	7.011	1.576	13.192	2.966
MA92-06	MA9	125	259.8	153.3	6.718	1.510	11.971	2.691
MA93-05	MA9	125	314.2	185.4	6.601	1.484	11.522	2.590
MA94-06	MA9	200	251.3	148.3	5.497	1.236	11.444	2.573
MA91-06	MA9	290	246.4	145.4	5.927	1.332	9.852	2.215
MA93-06	MA9	290	235.3	138.8	5.380	1.209	9.901	2.226
PV1-01	PV	-197	96.5	56.9	11.766	2.645	18.748	4.215
PV2-01	PV	-197	136.0	80.2	10.790	2.426	20.730	4.660
PV3-01	PV	-120	192.5	113.6	11.454	2.575	20.544	4.618
PV1-02	PV	-100	256.4	151.3	11.522	2.590	19.841	4.460
PV2-02	PV	-100	295.8	174.5	11.210	2.520	21.023	4.726
PV3-02	PV	-50	277.4	163.7	10.311	2.318	19.099	4.294
PV1-03	PV	-20	338.2	199.5	10.917	2.454	18.025	4.052
PV2-03	PV	-20	374.2	220.8	9.970	2.241	17.781	3.997
PV1-04	PV	25	311.0	183.5	8.856	1.991	15.115	3.398
PV2-04	PV	25	316.9	187.0	8.817	1.982	15.106	3.396
PV3-03	PV	25	337.3	199.0	8.212	1.846	14.666	3.297
PV3-04	PV	75	411.4	242.7	7.851	1.765	14.159	3.183
PV1-05	PV	175	357.6	211.0	5.859	1.317	12.362	2.779
PV2-05	PV	175	342.1	201.8	6.240	1.403	11.229	2.524
PV3-05	PV	200	317.1	187.1	5.654	1.271	11.112	2.498
PV1-06	PV	290	193.5	114.2	5.468	1.229	10.360	2.329
PV2-06	PV	290	282.8	166.9	5.341	1.201	9.345	2.101
PV3-06	PV	290	275.6	162.6	5.322	1.196	9.550	2.147
PV6-01	PV	-197	74.6	44.0	11.317	2.544	16.277	3.659
PV6-02	PV	-100	192.5	113.6	11.454	2.575	20.544	4.618
PV6-03	PV	-20	255.2	150.6	10.936	2.459	16.541	3.719
PV6-04	PV	25	262.4	154.8	9.335	2.099	15.496	3.484
PV6-05	PV	175	235.6	139.0	7.021	1.578	12.284	2.762
PV6-06	PV	290	278.6	164.4	6.327	1.422	10.507	2.362

Table 5. (Contd.)

Specimen ID	Material ID[a]	Temp. (°C)	Impact Energy (J/cm²)	Impact Energy (ft·lb)[b]	Yield Load (kN)	Yield Load (kip)	Maximum Load (kN)	Maximum Load (kip)
			Annealed[d]					
CA42-10	CA4	-197	38.4	22.7	12.235	2.751	14.637	3.291
CA41-12	CA4	-120	72.7	42.9	12.293	2.764	17.478	3.929
CA44-08	CA4	-100	61.2	36.1	12.010	2.700	15.115	3.398
CA42-11	CA4	-50	93.1	54.9	10.770	2.421	16.443	3.697
CA43-11	CA4	-20	144.2	85.1	10.760	2.419	16.385	3.683
CA41-10	CA4	25	196.1	115.7	8.593	1.932	14.373	3.231
CA42-12	CA4	25	179.8	106.1	9.149	2.057	14.705	3.306
CA44-09	CA4	75	191.7	113.1	8.095	1.820	13.397	3.012
CA43-10	CA4	175	216.9	128.0	6.484	1.458	11.551	2.597
CA41-11	CA4	290	225.3	132.9	5.331	1.198	10.321	2.320
MA11-12	MA1	-196	66.9	39.5	12.167	2.735	14.598	3.282
MA11-11	MA1	-120	119.6	70.6	10.966	2.465	14.793	3.326
MA11-10	MA1	-80	186.7	110.2	10.760	2.419	17.752	3.991
MA11-09	MA1	-20	303.2	178.9	9.804	2.204	15.194	3.416
MA11-08	MA1	25	62.2	36.7	10.194	2.292	11.522	2.590
MA12-12	MA1	-196	156.3	92.2	12.235	2.751	21.540	4.842
MA12-11	MA1	-100	218.3	128.8	11.786	2.650	19.431	4.368
MA12-10	MA1	-50	294.7	173.9	10.243	2.303	16.736	3.762
MA13-12	MA1	0	336.1	198.3	9.003	2.024	15.526	3.490
MA12-09	MA1	25	267.1	157.6	8.476	1.905	13.768	3.095
MA13-11	MA1	75	334.9	197.6	8.026	1.804	13.133	2.952
MA12-09	MA1	100	369.3	217.9	6.923	1.556	12.645	2.843
MA13-10	MA1	200	261.6	154.3	6.376	1.433	11.922	2.680
MA13-09	MA1	290	254.0	149.9	4.492	1.010	9.638	2.167
MA91-15	MA9	-197	233.0	137.5	12.645	2.843	24.753	5.565
MA92-15	MA9	-120	290.7	171.5	10.741	2.415	19.695	4.428
MA94-16	MA9	-50	348.9	205.9	10.643	2.393	16.922	3.804
MA95-02	MA9	-20	344.1	203.0	10.956	2.463	16.824	3.782
MA95-01	MA9	25	388.1	229.0	9.286	2.088	14.276	3.209
MA94-17	MA9	175	332.9	196.4	5.976	1.343	12.030	2.704
MA95-12	MA9	290	278.5	164.3	5.781	1.300	9.774	2.197
PV1-09	PV	-197	228.2	134.6	11.356	2.553	22.742	5.113
PV2-09	PV	-197	233.4	137.7	10.995	2.472	22.107	4.970
PV1-10	PV	-120	368.6	217.5	11.298	2.540	21.511	4.836
PV3-09	PV	-120	270.7	159.7	10.887	2.447	18.797	4.226
PV1-11	PV	-100	270.8	159.8	12.508	2.812	22.185	4.987
PV2-10	PV	-100	160.3	94.6	11.063	2.487	16.902	3.800
PV2-11	PV	-80	301.2	177.7	10.555	2.373	19.168	4.309
PV3-10	PV	-80	269.3	158.9	10.262	2.307	18.416	4.140
PV3-11	PV	-50	415.5	245.1	10.331	2.323	19.236	4.324
PV3-12	PV	-20	322.4	190.2	9.999	2.248	15.526	3.490
PV2-12	PV	0	436.7	257.7	8.769	1.971	15.106	3.396
PV1-12	PV	25	404.6	238.7	9.032	2.030	13.885	3.121
PV2-13	PV	25	442.9	261.3	8.827	1.984	15.018	3.376
PV3-13	PV	75	375.9	221.8	7.597	1.708	13.368	3.005
PV1-13	PV	125	353.7	208.7	6.669	1.499	12.128	2.726
PV3-14	PV	290	309.1	182.4	5.576	1.254	11.444	2.573

Table 5. (Contd.)

Specimen ID	Material ID[a]	Temp. (°C)	Impact Energy (J/cm²)	Impact Energy (ft·lb)[b]	Yield Load (kN)	Yield Load (kip)	Maximum Load (kN)	Maximum Load (kip)
			Spare Volute[c]					
VR1-02	VR	-197	63.3	37.3	12.500	2.805	16.766	3.769
VR2-02	VR	-120	133.3	78.6	13.534	3.043	21.091	4.741
VR2-04	VR	-80	205.5	121.2	11.659	2.621	19.558	4.397
VR3-02	VR	-50	240.8	142.1	13.172	2.961	20.349	4.575
VR1-03	VR	0	232.3	137.1	11.620	2.612	17.078	3.839
VR1-01	VR	25	200.0	118.0	12.479	2.805	16.766	3.769
VR3-01	VR	25	274.2	161.8	10.839	2.437	16.395	3.686
VR2-03	VR	75	194.2	114.6	9.374	2.107	13.006	2.924
VR2-01	VR	125	197.5	116.5	8.222	1.848	12.831	2.885
VR3-03	VR	125	341.3	201.4	7.851	1.765	13.504	3.036
VR3-04	VR	200	189.9	112.0	6.503	1.462	10.780	2.423
VR1-04	VR	290	263.5	155.5	6.200	1.394	10.341	2.325

[a] The first digit represents the type of component, C = cold leg check valve, M = hot leg main shut-off valve, V = spare pump volute.
[b] Impact energy in ft·lb for a standard Charpy impact specimen. To convert J/cm² to ft·lb multiply by 0.8 and divide by 1.355818.
[c] The components were at the operating temperature of 281°C for hot leg and 264°C for cold leg for ≈13 y (113,900 h).
[d] Annealed at 550°C for 1 h and water quenched.
[e] In service only during the initial core loading and thus is essentially unaged.

Table 6. Room temperature Charpy-impact data for Shippingport cast stainless steels aged further in the laboratory

Specimen ID[a]	Material ID[b]	Aging Condition Temp. (°C)	Aging Condition Time (h)	Impact Energy (J/cm²)	Impact Energy (ft·lb)[c]	Yield Load (kN)	Yield Load (kip)	Maximum Load (kN)	Maximum Load (kip)
CA41-10	CA4	Reannealed	-	196.1	115.7	8.593	1.932	14.373	3.231
CA42-12	CA4	Reannealed	-	179.8	106.1	9.149	2.057	14.705	3.306
CA41-02	CA4	Reactor Aged	-	162.1	95.6	9.354	2.103	15.535	3.492
CA44-02	CA4	Reactor Aged	-	128.5	75.8	9.589	2.156	14.881	3.345
CA41-04	CA4	350	986	114.8	67.7	9.891	2.224	15.067	3.387
CA44-06	CA4	350	986	166.4	98.2	10.253	2.305	15.379	3.457
CA41-07	CA4	350	3000	96.2	56.8	9.618	2.162	14.285	3.211
CA42-07	CA4	350	3000	120.8	71.3	9.227	2.074	14.188	3.190
CA41-09	CA4	400	312	114.1	67.3	9.227	2.074	14.647	3.293
CA44-07	CA4	400	312	102.3	60.4	8.876	1.995	13.905	3.126
CA41-06	CA4	400	986	84.0	49.6	9.852	2.215	13.280	2.985
CA42-06	CA4	400	986	128.1	75.6	9.833	2.211	15.223	3.422
CA41-05	CA4	400	3000	61.9	36.5	10.302	2.316	12.840	2.887
CA42-05	CA4	400	3000	103.2	60.9	9.755	2.193	14.481	3.255
CB71-03	CB7	Reactor Aged	-	162.4	95.8	9.022	2.028	14.012	3.150
CB73-02	CB7	Reactor Aged	-	203.7	120.2	8.700	1.956	14.666	3.297
CB71-07	CB7	400	312	163.8	96.6	9.657	2.171	14.940	3.359
CB73-09	CB7	400	312	263.9	155.7	8.798	1.978	14.988	3.369
CB71-08	CB7	400	986	158.4	93.5	9.120	2.050	13.875	3.119
CB72-08	CB7	400	986	186.4	110.0	9.159	2.059	14.159	3.183
CB71-09	CA4	400	3000	189.1	111.6	9.628	2.164	13.963	3.139
CB72-09	CA4	400	3000	191.4	112.9	9.520	2.140	13.534	3.043

Table 6. (Contd.).

Specimen ID[a]	Material ID[b]	Aging Condition		Impact Energy		Yield Load		Maximum Load	
		Temp. (°C)	Time (h)	(J/cm^2)	(ft·lb)[c]	(kN)	(kip)	(kN)	(kip)
MA11-08	MA1	Annealed	-	62.2	36.7	10.194	2.292	11.522	2.590
MA11-06	MA1	Reactor Aged	-	210.0	123.9	8.524	1.916	14.325	3.220
MA11-04	MA1	Reactor Aged	-	144.5	85.3	10.106	2.272	14.207	3.194
MA11-18	MA1	350	1052	68.1	40.2	9.364	2.105	11.610	2.610
MA11-17	MA1	350	2987	159.2	93.9	9.403	2.114	14.256	3.205
MA11-19	MA1	400	379	56.3	33.2	9.589	2.156	11.092	2.494
MA11-15	MA1	400	1052	47.9	28.3	8.632	1.941	9.833	2.211
MA11-14	MA1	400	2987	96.3	56.8	10.428	2.344	13.885	3.121
MA11-20	MA1	400	2987	58.1	34.3	9.930	2.232	10.321	2.320
MA12-09	MA1	Annealed	-	267.1	157.6	8.476	1.905	13.768	3.095
MA12-06	MA1	Reactor Aged	-	279.2	164.7	8.817	1.982	14.959	3.363
MA13-02	MA1	Reactor Aged	-	337.6	199.2	9.237	2.077	15.877	3.569
MA13-05	MA1	Reactor Aged	-	280.7	165.6	9.032	2.030	15.174	3.411
MA12-18	MA1	350	1052	280.2	165.3	8.524	1.916	14.598	3.282
MA13-18	MA1	350	1052	253.3	149.4	8.612	1.936	14.715	3.308
MA12-17	MA1	350	2987	304.8	179.8	8.739	1.965	14.783	3.323
MA13-17	MA1	350	2987	234.7	138.5	9.794	2.202	15.203	3.418
MA12-19	MA1	400	379	263.4	155.4	8.437	1.897	14.852	3.339
MA12-15	MA1	400	1052	236.8	139.7	8.007	1.800	14.012	3.150
MA13-15	MA1	400	1052	236.4	139.5	8.417	1.892	14.998	3.372
MA12-14	MA1	400	2987	193.3	114.0	9.481	2.131	14.334	3.222
MA12-20	MA1	400	2987	230.3	135.9	10.253	2.305	15.545	3.495
MA13-14	MA1	400	2987	216.0	127.4	9.911	2.228	15.682	3.525
MA95-01	MA9	Annealed	-	388.1	229.0	9.286	2.088	14.276	3.209
MA91-04	MA9	Reactor Aged	-	350.2	206.6	8.515	1.914	15.233	3.425
MA93-04	MA9	Reactor Aged	-	408.6	241.1	8.993	2.022	15.223	3.422
MA91-14	MA9	320	2989	287.4	169.6	9.911	2.228	15.340	3.449
MA92-14	MA9	320	2989	262.5	154.9	8.817	1.982	14.325	3.220
MA93-18	MA9	350	311	334.1	197.1	8.788	1.976	14.403	3.238
MA94-18	MA9	350	311	307.9	181.7	8.749	1.967	14.666	3.297
MA95-14	MA9	350	311	416.7	245.9	8.993	2.022	15.028	3.378
MA91-18	MA9	350	986	286.9	169.3	9.882	2.222	14.608	3.284
MA92-18	MA9	350	986	319.0	188.2	8.954	2.013	13.953	3.137
MA91-13	MA9	350	2987	242.3	143.0	9.442	2.123	14.491	3.258
MA92-12	MA9	350	2987	258.3	152.4	9.003	2.024	14.139	3.179
MA92-13	MA9	350	2987	324.7	191.6	9.061	2.037	14.998	3.372
MA91-17	MA9	400	115	303.8	179.2	9.188	2.066	14.471	3.253
MA92-17	MA9	400	115	390.2	230.2	8.192	1.842	14.442	3.247
MA93-15	MA9	400	312	243.1	143.4	8.358	1.879	14.647	3.293
MA95-11	MA9	400	312	222.8	131.5	9.188	2.066	14.471	3.253
MA91-16	MA9	400	986	186.5	110.0	9.520	2.140	15.018	3.376
MA92-16	MA9	400	986	199.7	117.8	9.354	2.103	14.315	3.218
MA93-14	MA9	400	2987	205.4	121.2	9.423	2.118	14.832	3.334
MA94-14	MA9	400	2987	158.4	93.5	9.462	2.127	14.393	3.236
MA95-10	MA9	400	2987	159.8	94.3	10.458	2.351	14.080	3.165
VR1-01	VR	Unaged	-	200.0	118.0	12.479	2.805	16.766	3.769
VR3-01	VR	Unaged	-	274.2	161.8	10.839	2.437	16.395	3.686
VR1-13	VR	320	2989	223.9	132.1	11.434	2.570	15.916	3.578
VR2-13	VR	320	2989	271.9	160.4	10.477	2.355	16.746	3.765
VR1-19	VR	350	311	193.5	114.2	10.438	2.347	15.242	3.427
VR2-19	VR	350	311	204.7	120.8	9.081	2.041	15.125	3.400

Table 6. (Contd.).

Specimen	Material	Aging Condition		Impact Energy		Yield Load		Maximum Load	
ID[a]	ID[b]	Temp. (°C)	Time (h)	(J/cm^2)	(ft·lb)[c]	(kN)	(kip)	(kN)	(kip)
VR3-19	VR	350	311	242.5	143.1	9.061	2.037	15.194	3.416
VR1-20	VR	350	986	191.7	113.1	11.630	2.615	17.010	3.824
VR2-20	VR	350	986	184.7	109.0	10.887	2.447	16.629	3.738
VR1-14	VR	350	2987	118.9	70.2	11.063	2.487	14.813	3.330
VR2-14	VR	350	2987	124.9	73.7	10.516	2.364	14.481	3.255
VR3-14	VR	350	2987	114.6	67.6	10.214	2.296	14.783	3.323
VR1-16	VR	400	115	172.5	101.8	9.930	2.232	15.242	3.427
VR4-01	VR	400	115	182.0	107.4	10.233	2.300	16.209	3.644
VR1-17	VR	400	312	106.2	62.7	10.653	2.395	14.754	3.317
VR4-02	VR	400	312	85.3	50.3	10.858	2.441	14.276	3.209
VR1-18	VR	400	986	82.5	48.7	11.727	2.636	14.344	3.225
VR2-18	VR	400	986	104.9	61.9	10.966	2.465	15.145	3.405
VR4-05	VR	400	986	81.2	47.9	11.483	2.581	16.229	3.648
VR1-15	VR	400	2987	100.0	59.0	10.731	2.412	15.252	3.429
VR2-15	VR	400	2987	94.3	55.6	10.946	2.461	15.242	3.427
VR3-15	VR	400	2987	97.0	57.2	10.848	2.439	15.643	3.517

[a] The first digit represents the type of component, C = cold leg check valve,M = hot leg main shut-off valve, V = spare pump volute.

[b] Materials MA1 and MA9 are from the same valve except the latter is from a cooler region of the valve. Spare pump volute was in service only during the initial core loading and, thus, is essentially unaged.

[c] Impact energy in ft·lb for a standard Charpy-impact specimen. To convert J/cm^2 to ft·lb multiply by 0.8 and divide by 1.355818.

Table 7. Values of constants in Eq. 48 for Charpy transition curve of cast stainless steels from the Shippingport reactor

Material ID	Service Condition		Constants			
	Temp. (°C)	Time (y)	K_o (J/cm^2)	B (J/cm^2)	C (°C)	D (°C)
			Cold-Leg Check Valves			
CA4	Annealed	–	25	98.6	-37.0	97.9
CA4	264	13	25	79.2	-20.1	81.8
CB7	264	13	76	108.8	6.0	65.2
			Hot-Leg Main Shutoff Valve			
MA9[a]	Annealed	–	96	112.0	-116.3	54.1
MA9	<200	13	83	110.1	-110.7	48.3
MA1/23[a]	Annealed		96	112.0	-116.3	54.1
MA1/23[b]	281	13	73	87.6	-114.2	29.8
MA1/1[c]	281	13	69	63.7	-137.0	38.6
			Pump Volutes			
PV	Annealed	–	150	116.2	-151.9	109.7
PV	264	13	75	109.4	-141.9	49.5
VR	Unaged	–	61	88.1	-112.4	38.5
			Pump Cover Plate[d]			
KRB	Annealed	–	8	161.9	-16.5	87.2
KRB	284	8	8	119.7	36.8	83.2

[a] Determined from combined data for MA9 and annealed MA9 and MA1.

[b] Material from Rows 2 &3, which corresponds to 15- to 45-mm region of the wall.

[c] Material from Row 1, which corresponds to inner 15-mm region of the wall.

[d] Obtained from the KRB reactor in Gundremmingen, Germany.

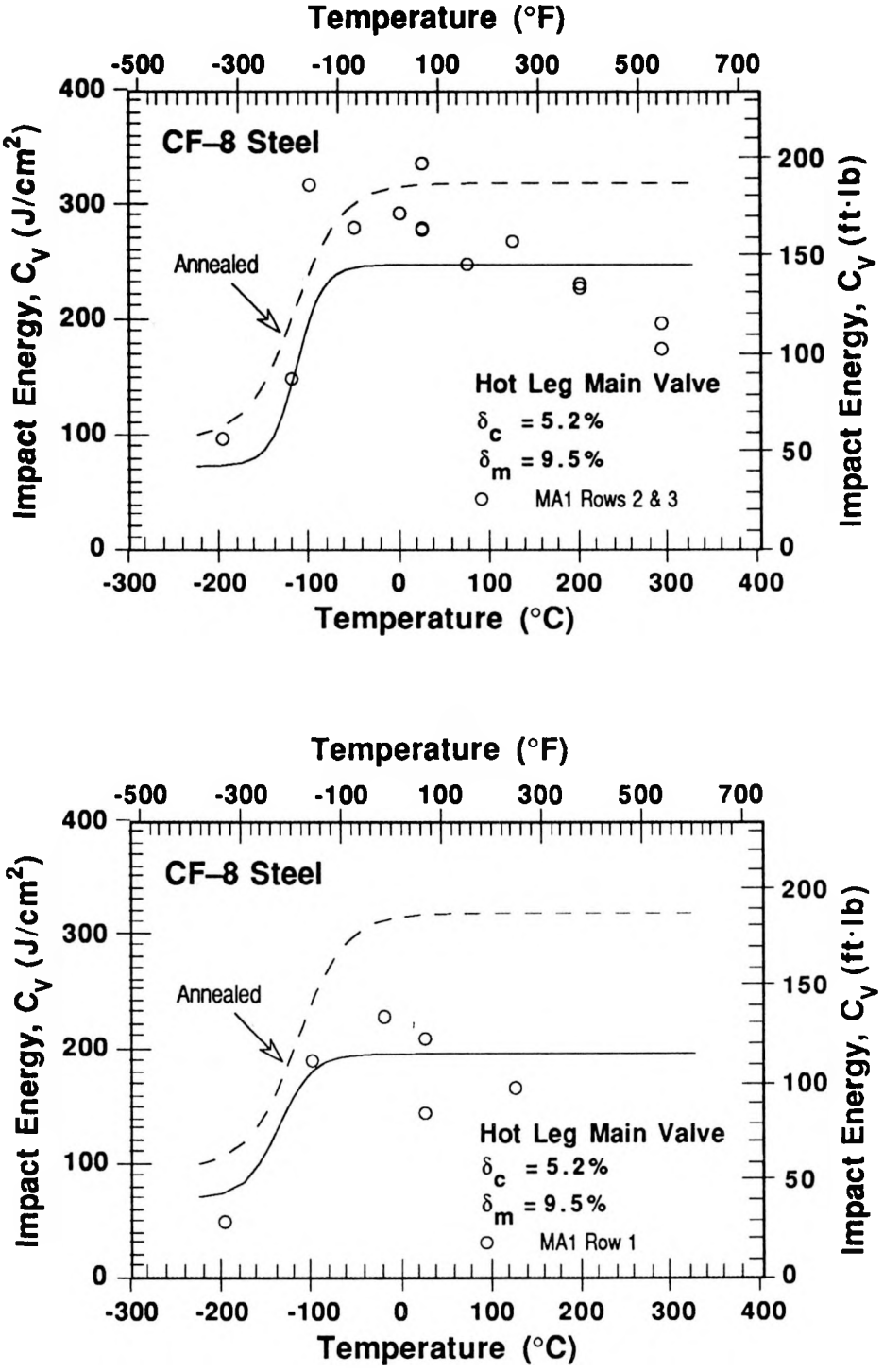

Figure 44. Charpy transition curves for hot-leg main shutoff valve after ≈13 y service at 281°C. Row 1 corresponds to inner 15-mm region and rows 2 and 3 represent 15- to 50-mm region of the valve body.

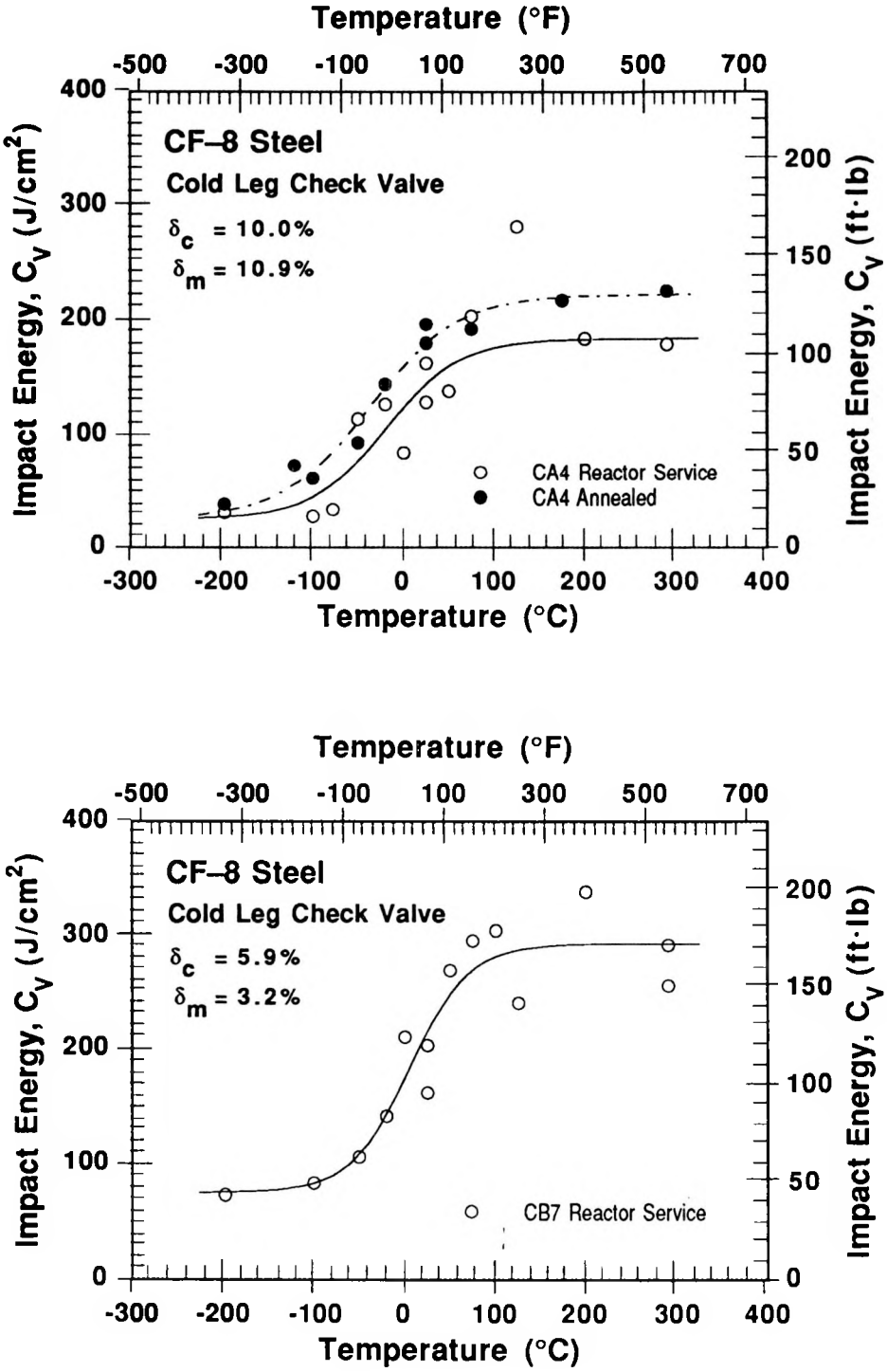

Figure 45. Charpy transition curves for cold-leg check valves from Loops A and B after ≈13 y service at 264°C

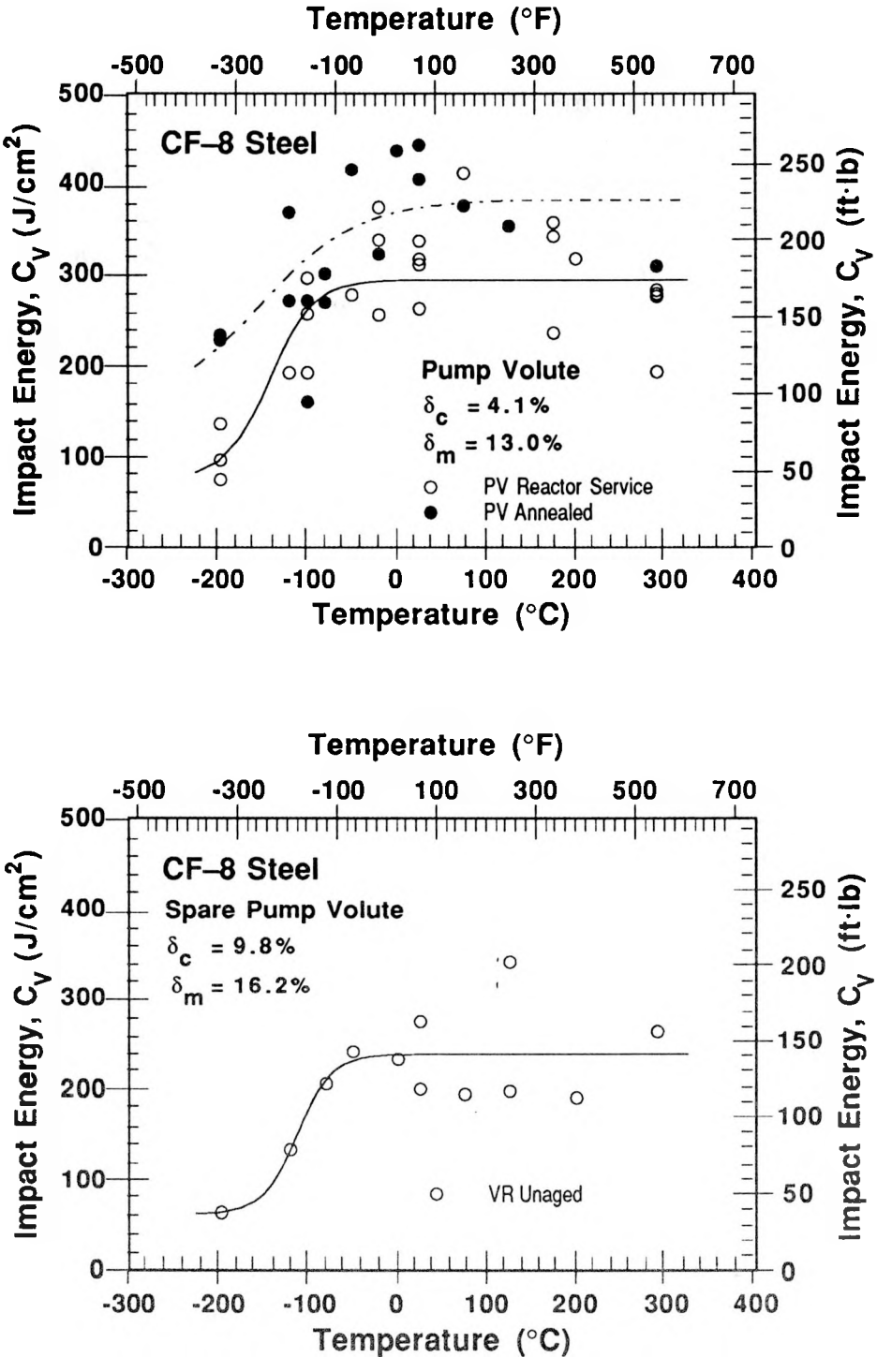

Figure 46. Charpy transition curves for service-aged (≈13 y service at 264°C) and spare pump volutes

Table 8. Tensile test results for cast stainless steel materials from the Shippingport reactor

Specimen ID[a]	Test Temp. (°C)	Engineering Stress 0.2% Yield (MPa)	Engineering Stress 0.2% Yield (ksi)	Engineering Stress Ultimate (MPa)	Engineering Stress Ultimate (ksi)	True Fracture Stress (MPa)	True Fracture Stress (ksi)	Elongation (%)	Red. in Area (%)
				Cold Leg Check Valves[b]					
CA41-T01	25	237.1	34.39	528.3	76.62	1268.7	184.0	63.5	66.0
CA41-T02	25	226.8	32.89	519.3	75.32	1404.0	203.6	57.9	73.7
CA42-T01	25	218.7	31.72	532.6	77.25	1466.0	212.6	60.3	68.6
CA41-T03	290	123.2	17.87	378.6	54.91	704.9	102.2	44.1	57.8
CA42-T02	290	132.2	19.17	370.2	53.69	–	–	32.7	35.5
CA42-T03	290	169.9	24.64	396.3	57.48	731.3	106.1	35.9	54.0
				Hot Leg Main Shutoff Valves[c]					
MA11-T01	25	226.8	32.89	490.9	71.20	1659.4	240.7	40.2	82.0
MA11-T02	25	252.3	36.59	429.6	62.31	–	–	22.8	30.9
MA12-T01	25	212.6	30.84	486.0	70.49	1374.7	199.4	27.4	73.6
MA11-T03	290	–	29.40	275.9	40.02	–	–	10.2	13.3
MA12-T02	290	129.6	18.80	330.9	47.99	520.0	75.4	32.6	47.6
MA12-T03	290	134.6	19.52	353.0	51.20	701.4	101.7	31.2	64.3

[a] First three digits represent the material identification number.
[b] In service for ≈13 y at 264°C.
[c] In service for ≈13 y at 281°C.

7.2.3 Tensile Properties

Tensile tests were conducted at room temperature and at 290°C on CA4 and MA1 materials; results are given in Table 8. The yield stresses of the two materials are comparable, whereas the ultimate stress of CA4 is higher than that of MA1. Tensile properties were also estimated from the instrumented Charpy-impact test data. For a Charpy specimen, yield stress is given by

$$\sigma_y = 1.50 P_y B / W b^2, \tag{41}$$

and ultimate stress by

$$\sigma_u = 2.28 P_m B / W b^2, \tag{42}$$

where P_y and P_m are the yield and maximum loads obtained from the load-time traces of the Charpy test, W is the specimen width, B is the specimen thickness, and b is the uncracked ligament. The estimated values of yield and ultimate stress, along with the values obtained from tensile tests, are shown in Fig. 47.

The estimated tensile properties are in good agreement with the measured values. However, specimens MA11-T02 and -T03, which were tested at room temperature and 290°C, respectively, show low ultimate strength and poor ductility. These specimens were obtained from the inner-15-mm region of the valve body. The poor tensile properties are caused by inclusions in the material. As discussed above, the room-temperature impact energy of Row 1 specimens is also low, e.g., ≈177 ±33 J/cm^2, compared to ≈299 ±33 J/cm^2

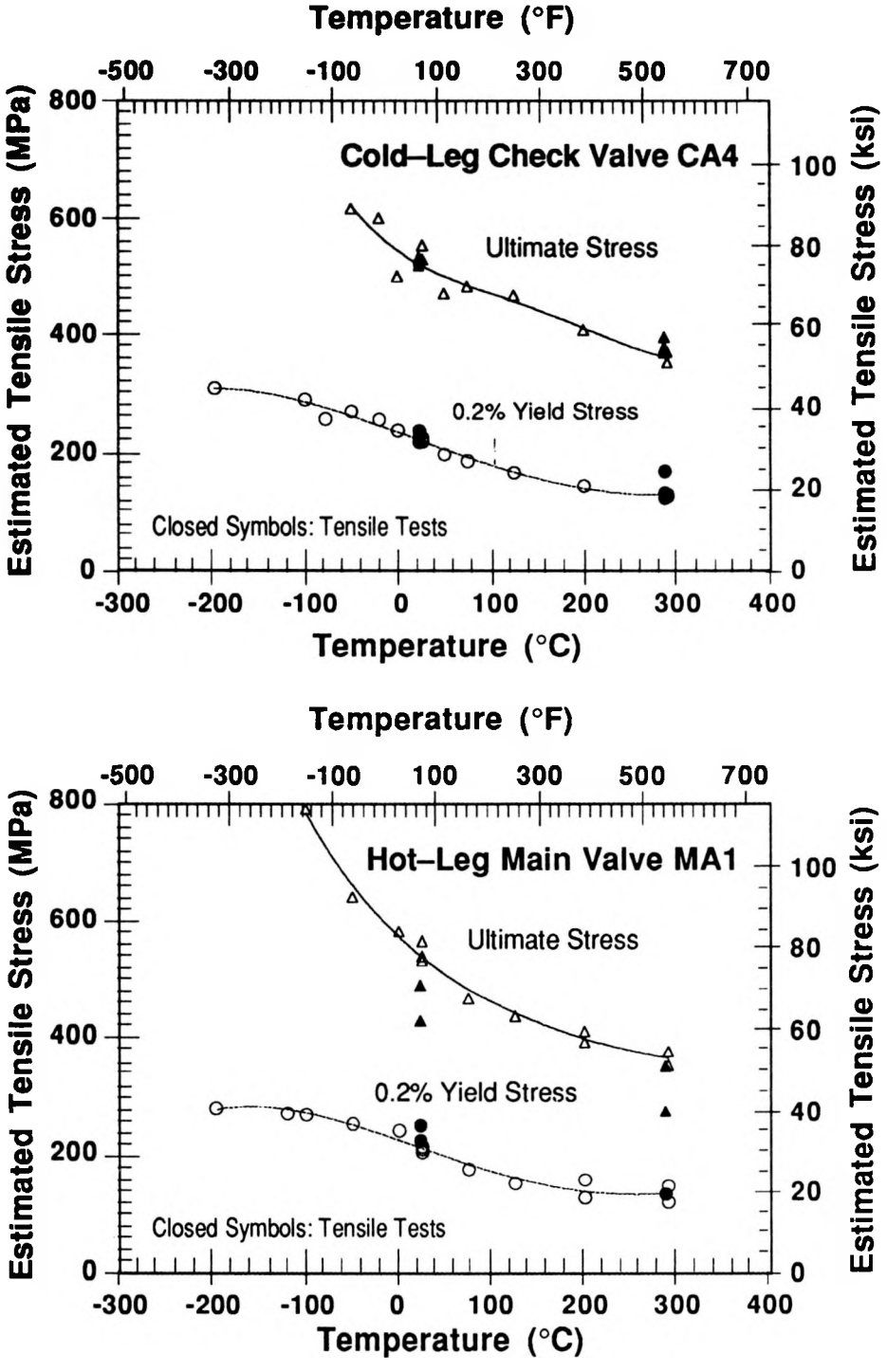

Figure 47. Yield and ultimate stress estimated from Charpy-impact data for CA4 and MA1 materials

for specimens from other regions of the valve body. Tensile tests are being conducted on recovery-annealed materials to establish the effect of aging. Tests are also in progress on material from the service-aged pump volute PV.

7.3 Estimation of Impact Energy

The procedure for estimating Charpy-impact energy and fracture toughness J-R curves of aged cast stainless steels from their chemical composition has been described in Section 6. For convenience, the correlations are repeated here. The extent of thermal embrittlement at saturation is described in terms of a material parameter Φ, which for CF-3 and CF-8 steels is expressed as

$$\Phi = \delta_c(Cr + Si)(C + 0.4N), \tag{43}$$

where the ferrite content δ_c is in % and chemical composition of the steel is in wt.%. The ferrite content is calculated from Hull's equivalent factors (Eqs. 1-3); the values for the various cast materials are given in Table 4. The saturation room-temperature impact energy C_{Vsat} (J/cm^2) is given by

$$\log_{10}C_{Vsat} = 1.15 + 1.374\exp(-0.0365\Phi). \tag{44}$$

The room-temperature impact energy as a function of time and temperature of aging is estimated from the kinetics of thermal embrittlement. The decrease in impact energy C_V (J/cm^2) with time is expressed as

$$\log_{10}C_V = \log_{10}C_{Vsat} + \beta\{1 - \tanh[(P - \theta)/\alpha]\}, \tag{45}$$

where C_{Vsat} (J/cm^2) is the saturation impact energy, β is half the maximum change in $\log C_V$, θ is the log of the time at 400°C (752°F) to achieve β reduction in impact energy at 400°C, and α is a shape factor. The aging parameter P is the log of the aging time for a specific degree of thermal embrittlement and is defined by

$$P = \log_{10}t - \frac{1000Q}{19.143}\left(\frac{1}{T_s + 273} - \frac{1}{673}\right), \tag{46}$$

where Q is the activation energy (kJ/mole) and t and T_s are the time (h) and temperature (°C) of aging. The activation energy for thermal embrittlement is also determined from the chemical composition of the steel. Thus, for CF-3 and CF-8 steels

$$Q = 10\,(74.06 - 7.66\theta - 4.35Si + 1.38Mo - 1.67Cr - 2.22Mn + 108.8N), \tag{47}$$

where Q is in kJ/mole and θ is defined in Eq. 45. The constants β and α are determined from the initial impact energy of the material C_{Vint} and the saturation impact energy C_{Vsat}. Thus,

$$\beta = (\log_{10}C_{Vint} - \log_{10}C_{Vsat})/2, \tag{48}$$

and

$$\alpha = -0.821 + 0.947\log_{10}C_{Vsat}. \quad (49)$$

For a specific cast stainless steel, the values of room-temperature impact energy as a function of time and temperature of reactor service and the minimum saturation impact energy that would be achieved for the material can be estimated from Eqs. 43–49. The information required for the estimations include the chemical composition, initial impact energy of the unaged material, and the constant θ. Values of θ are not available for cast components in the field, and can only be obtained by aging archive material for 5,000 to 10,000 h at 400°C. However, parametric studies indicate that the aging response at reactor temperatures, i.e., 280–320°C (536–308°F), is relatively insensitive to the value of θ. Varying θ between 2.3 and 3.3 results in aging behavior almost identical with that observed at 300°C (572°F). The differences in aging behavior at 280 or 320°C for values of θ in the range of interest are minimal.

Room-temperature impact energy was estimated for the cast materials from the Shippingport reactor. The initial impact energy of the unaged materials was determined from the data for recovery-annealed material or material from a cooler region of the casting. A value of 2.9 was assumed for the constant θ. Some materials were aged further in the laboratory at 400, 350, and 320°C (752, 662, and 608°F) to obtain an accurate value of θ and to validate the estimations of the saturation impact energy C_{Vsat} and activation energy for thermal embrittlement of the materials. The estimated values are given in Table 9. Estimations for the KRB reactor pump cover plate material are also included in the table. The estimated impact energies (Column 3 in Table 9) show good agreement with the measured values and are within the experimental scatter band.

The change in estimated Charpy-impact energy with aging time at temperatures between 400°C and reactor service temperature is shown in Figs. 48 and 49 for KRB, CA4,

Table 9. Measured and estimated Charpy-impact properties of cast stainless steel materials from the Shippingport reactor

Material ID	RT Impact Energy: Measured [J/cm² (ft·lb)]	RT Impact Energy: Estimated [J/cm² (ft·lb)]	θ[a]	C_{Vint}[b] [J/cm² (ft·lb)]	Estimated Embrittlement: C_{Vsat} [J/cm² (ft·lb)]	Estimated Embrittlement: Q [kJ/mole (kcal/mole)]	β	α	P
				Hot Leg					
CA4	145 (86)	156 (92)	2.65	188 (111)	76 (45)	156 (37)	0.196	0.962	1.993
CB7	183 (108)	–	2.90	–	139 (82)	174 (42)	–	1.209	1.632
CC4	122 (72)	–	2.90	–	132 (78)	169 (40)	–	1.187	1.726
PV	322 (190)	347 (205)	2.90	424 (250)	113 (67)	159 (38)	0.287	1.125	1.940
				Cold Leg					
MA1/23	299 (176)	289 (171)	3.20	320 (189)	94 (55)	180 (43)	0.160	1.248	2.052
MB2	–	–	2.90	–	223 (132)	233 (56)	–	1.403	1.177
				Unaged					
MA9	356 (210)	–	2.53	356 (210)	87 (51)	232 (55)	0.184	1.249	
VR	237 (140)	–	2.20	237 (140)	93 (55)	218 (52)	0.202	1.045	
				KRB Pump Cover Plate[c]					
KRB	131 (77)	157 (93)	2.30	217 (128)	24 (14)	183 (44)	0.481	0.480	1.875

[a] Determined from material that was aged further at 400°C or that was assumed to be 2.9.
[b] Determined from material from cooler region of the component or recovery-annealed material.
[c] Material obtained from KRB reactor in Gundremmingen, West Germany, which was in service at 284°C for ≈8 y.

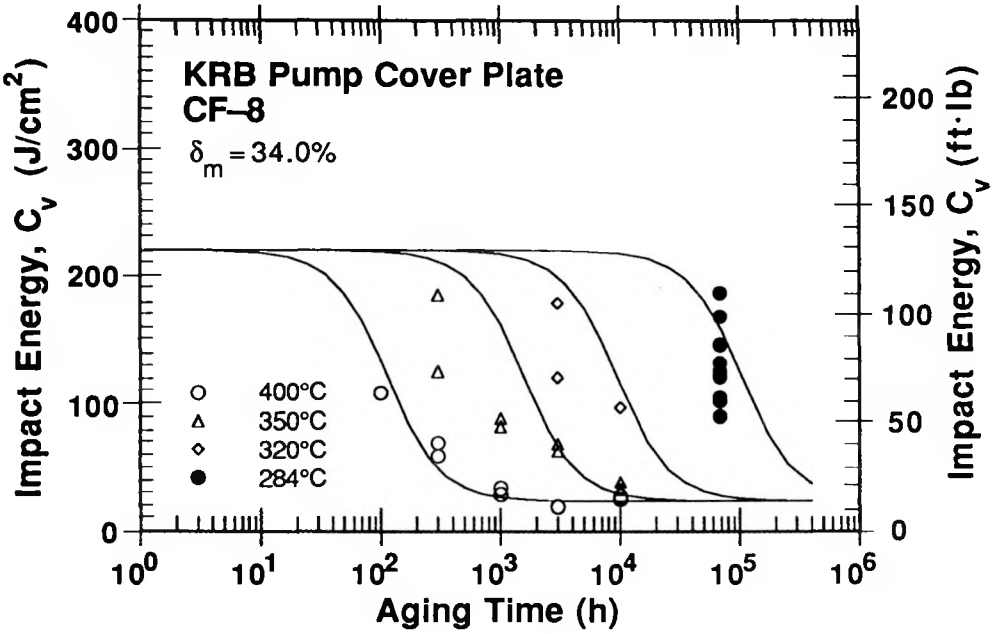

Figure 48. Estimated room-temperature Charpy-impact energy for KRB pump cover plate at 400, 350, 320, and 284°C

and MA1 materials. Estimated and measured impact energies for essentially unaged VR and MA9 materials aged at 400, 350, and 320°C (752, 662, and 608°F) are shown in Fig. 50. The high-temperature aging data for CA4 and MA1 materials represent service-aged material that was aged further in the laboratory at 350 and 400°C. Aging times were adjusted to include the effect of thermal aging at reactor temperature. For example, service of ≈13 y at a cold-leg temperature of 264°C corresponds to 234 h at 400°C for the CA4 material, and service of ≈13 y at a hot-leg temperature of 281°C corresponds to 113 h at 400°C for MA1 material. The high-temperature aging data for the KRB pump cover plate were obtained on recovery-annealed material. The estimated values are in good agreement with the measured impact energies, particularly at reactor operating temperatures.

The predicted minimum saturation Charpy impact energies also are in very good agreement with the experimental data. The measured impact energies for VR, MA9, and KRB materials aged at 400°C achieve saturation at the predicted values. The materials are being aged up to 30,000 h at 400, 350, and 320°C to validate the estimated extent and kinetics of thermal embrittlement.

7.4 Estimation of Fracture Toughness

The fracture toughness J-R curve for a specific cast stainless steel can be estimated from its room-temperature impact energy. The J-R curve is expressed by power-law relation $J_d = C\Delta a^n$, where J_d is deformation J (kJ/m^2) per ASTM Specifications E 813-85 and E 1152-87, Δa is the crack extension (mm), and C and n are constants. For CF-3 and CF-8 steels, the J-R curve at room temperature is given by

$$J_d = 49[C_V]^{0.52}[\Delta a]^n; \quad (50)$$

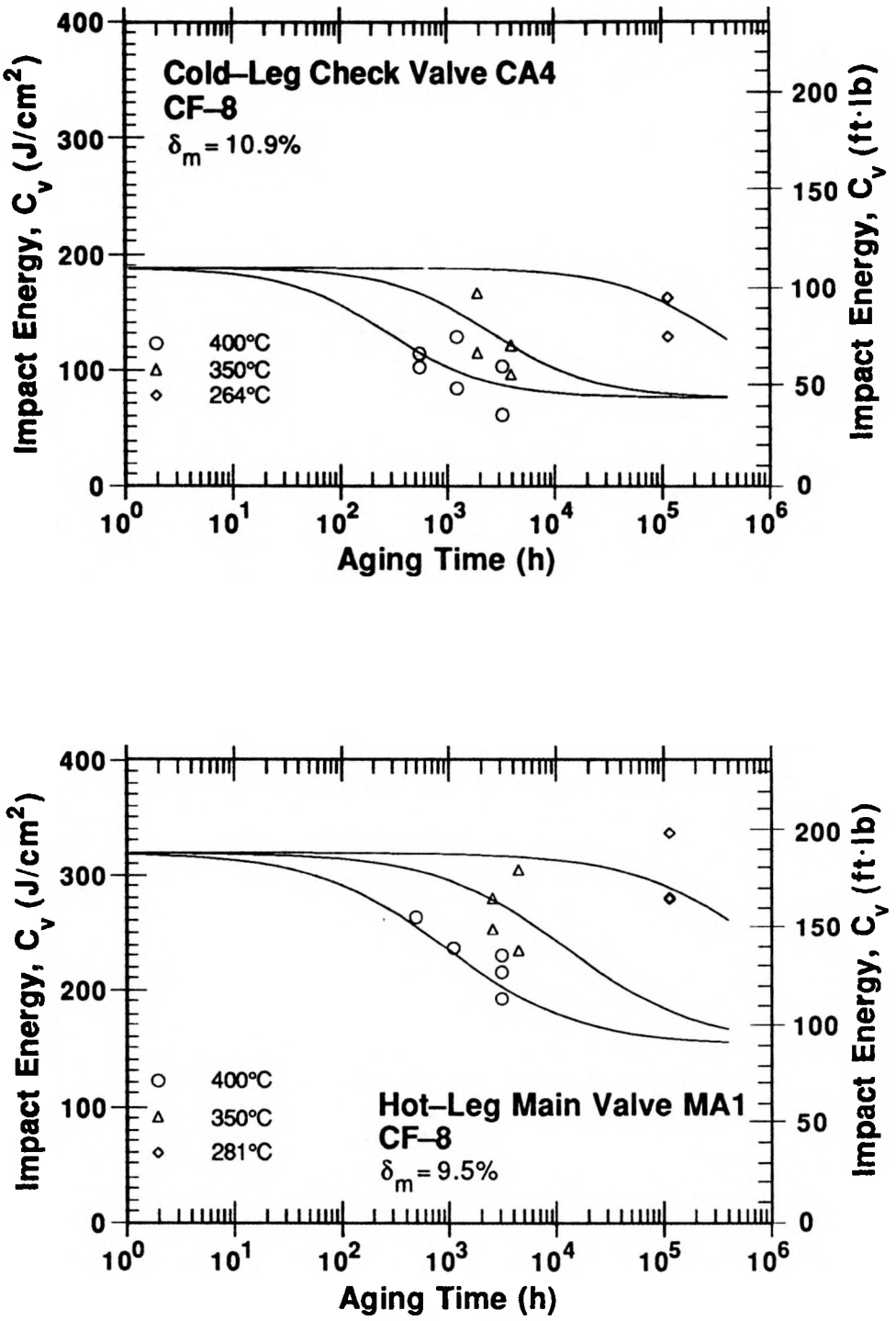

Figure 49. Estimated room-temperature Charpy-impact energy for cold-leg check valve CA4 and hot-leg main valve MA1 at 400 and 350°C and reactor service temperature

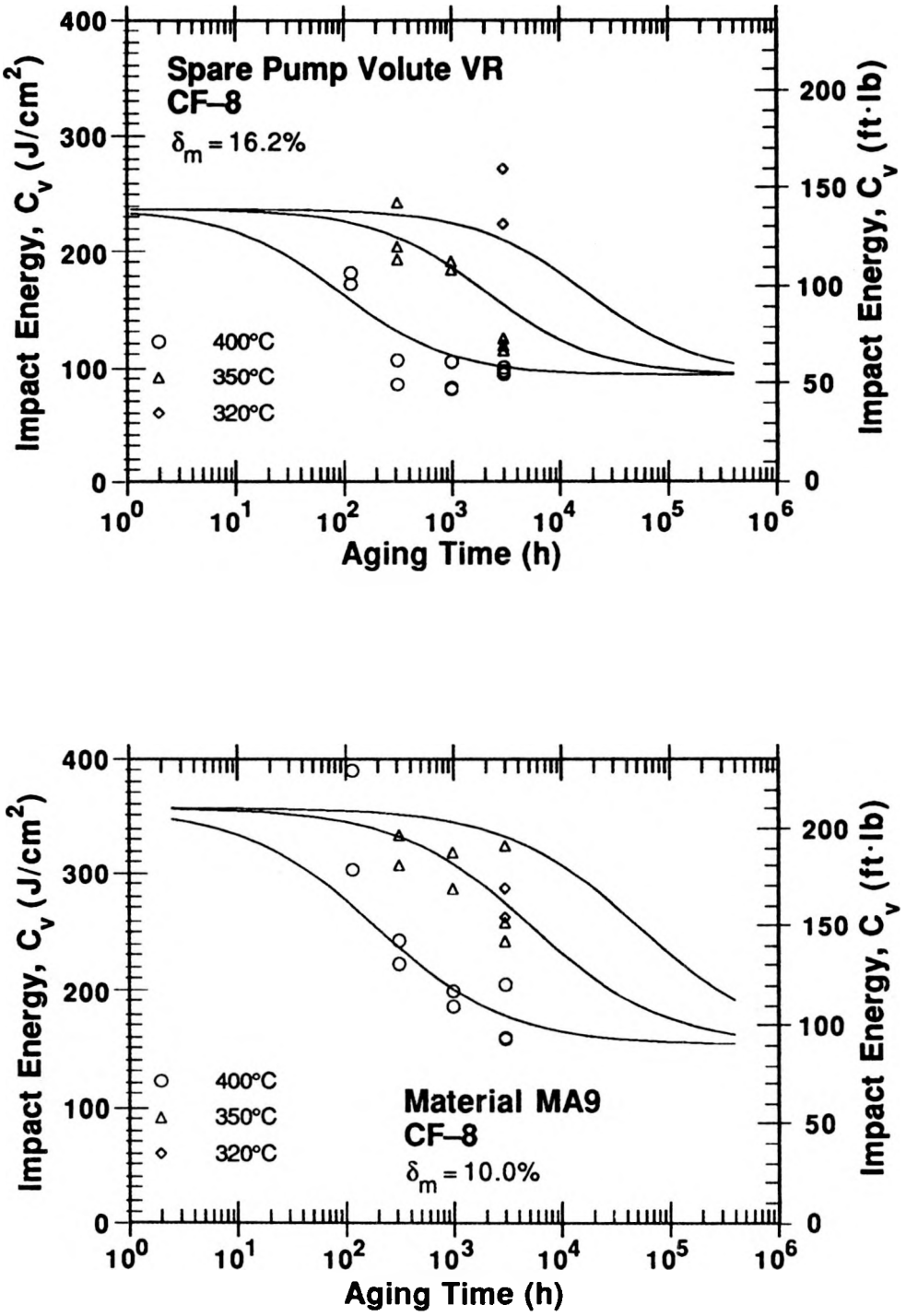

Figure 50. Estimated room-temperature Charpy-impact energy for spare pump volute and material MA9 at 400, 350, and 320°C

at temperatures between 290–320°C (554–608°F), it is given by

$$J_d = 82[C_V]^{0.34}[\Delta a]^n, \quad (51)$$

where the impact energy C_V is in J/cm^2. At room temperature, the exponent n for CF–3 and CF–8 steels is given by

$$n = 0.32 + 0.0131[C_{Vsat}]^{0.52}; \quad (52)$$

at temperatures between 290–320°C (554–608°F), it is given by

$$n = 0.25 + 0.0293[C_{Vsat}]^{0.34}. \quad (53)$$

Experimental data and estimated fracture toughness J–R curves at room temperature and at 290°C (554°F) for the CA4, MA1, PV, and KRB materials are shown in Figs. 51–53. The estimated J–R curves very show good agreement with the experimental results. All materials exhibit relatively high fracture toughness. The fracture toughness J_{IC} for the materials is estimated to be >300 kJ/m^2 at room temperature and >350 kJ/m^2 at 290°C. Tests are in progress on recovery–annealed materials to determine the fracture toughness J–R curves of the unaged material, and also on fully–aged materials (i.e., aged for ≈10,000 h at 400°C) to obtain the saturation fracture toughness.

8 Conclusions

A procedure and correlations are presented for predicting fracture toughness J–R curves and impact strength of aged cast stainless steels from known material information. Fracture toughness of a specific cast stainless steel is estimated from the extent and kinetics of thermal embrittlement. Embrittlement of cast stainless steels is characterized in terms of room–temperature Charpy–impact energy. The extent or degree of thermal embrittlement at "saturation," i.e., the minimum impact energy that can ever be achieved by the material after long–term aging, is described in terms of a material parameter Φ that is determined from chemical composition and ferrite morphology. Room–temperature impact energy as a function of time and temperature of reactor service is estimated from the kinetics of thermal embrittlement, which are also determined from the chemical composition. The fracture toughness J–R curve for the material is then obtained from correlations between room–temperature Charpy–impact energy and fracture toughness parameters. A common "lower–bound" J–R curve for cast stainless steels with unknown chemical composition is also defined. Examples for estimating impact strength and fracture toughness of cast stainless steel components during reactor service are described. Estimated fracture toughness J–R curves show good agreement with experimental results for most of the cast materials and are conservative for some materials, e.g., centrifugally cast stainless steels.

Charpy–impact and tensile properties of several cast stainless steel materials from the Shippingport reactor have been characterized. Baseline mechanical properties for as–cast material were determined from tests on either recovery–annealed material, i.e., annealed for 1 h at 550°C and then water quenched, or material from the cooler region of the component. The materials exhibit a modest decrease in impact energy. The room–temperature impact energy is relatively high, >120 J/cm^2 (>70 ft·lb). The check–valve

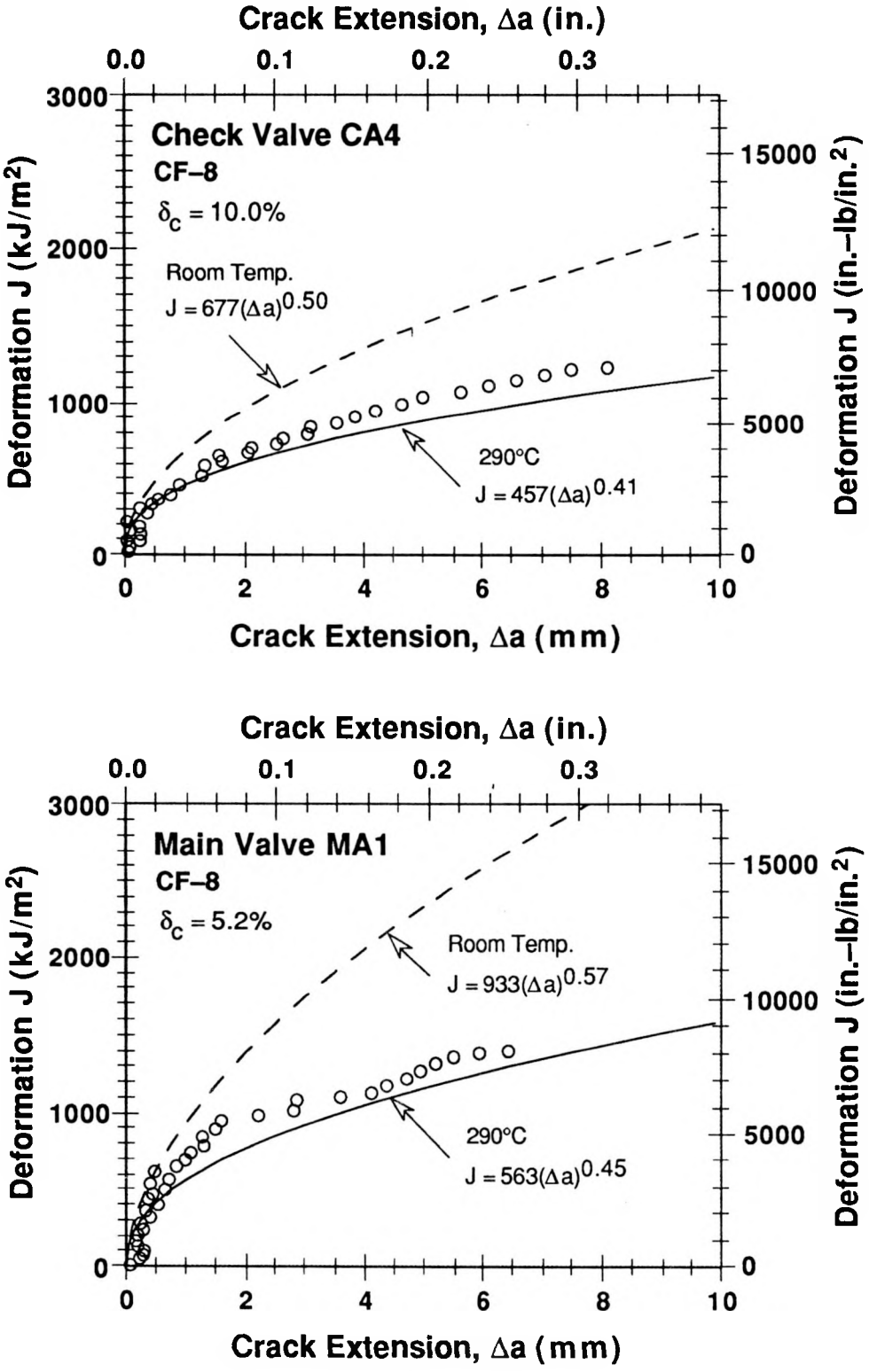

Figure 51. Experimental data and estimated fracture toughness J–R curve at room temperature and at 290°C for cold–leg check valve CA4 and hot–leg main valve MA1

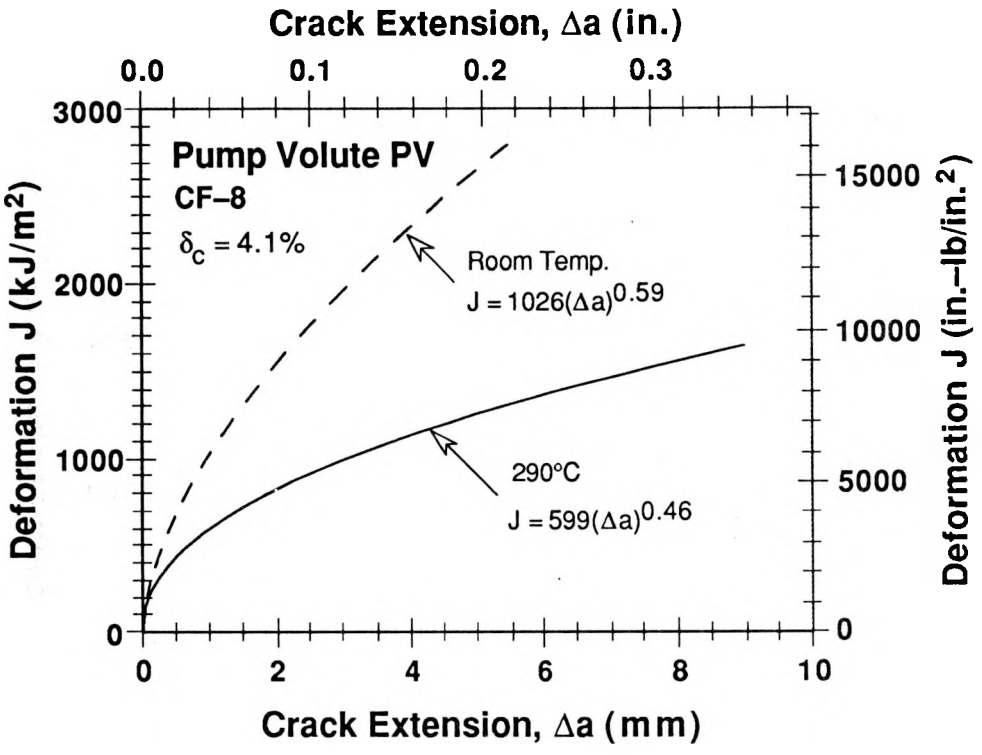

Figure 52. Estimated fracture toughness J–R curve at room temperature and at 290°C for pump volute PV

are weaker than the main-valve materials because of the presence of phase-boundary carbides. The results show good agreement with estimations based on accelerated laboratory-aging studies. The correlations for estimating thermal aging degradation of cast stainless steels indicate that the degree of thermal embrittlement of the Shippingport materials is low. After long-term aging of the materials, the minimum room-temperature impact energy that would be achieved is estimated to be >75 J/cm^2; and fracture toughness J_{IC}, >300 kJ/m^2. The estimated activation energies for thermal embrittlement range from 150 to 230 kJ/mole.

Mechanical-property tests are being conducted on long-term-aged materials as well as on reactor-aged components to validate the correlations. This additional data will be used to modify the correlations and account for the casting process and macrostructure of the steel. The correlations for estimating the flow stress of aged steels will be used to predict the J_{IC} value and tearing modulus of cast stainless steel components during reactor service.

Acknowledgments

This work was supported by the Office of the Nuclear Regulatory Research in the U. S. Nuclear Regulatory Commission. The authors are grateful to A. Sather, L. Y. Bush, T. M. Galvin, G. M. Dragel, and W. F. Burke for their contribution to the experimental effort. The authors also thank J. Muscara, W. J. Shack, and T. F. Kassner for their helpful discussions.

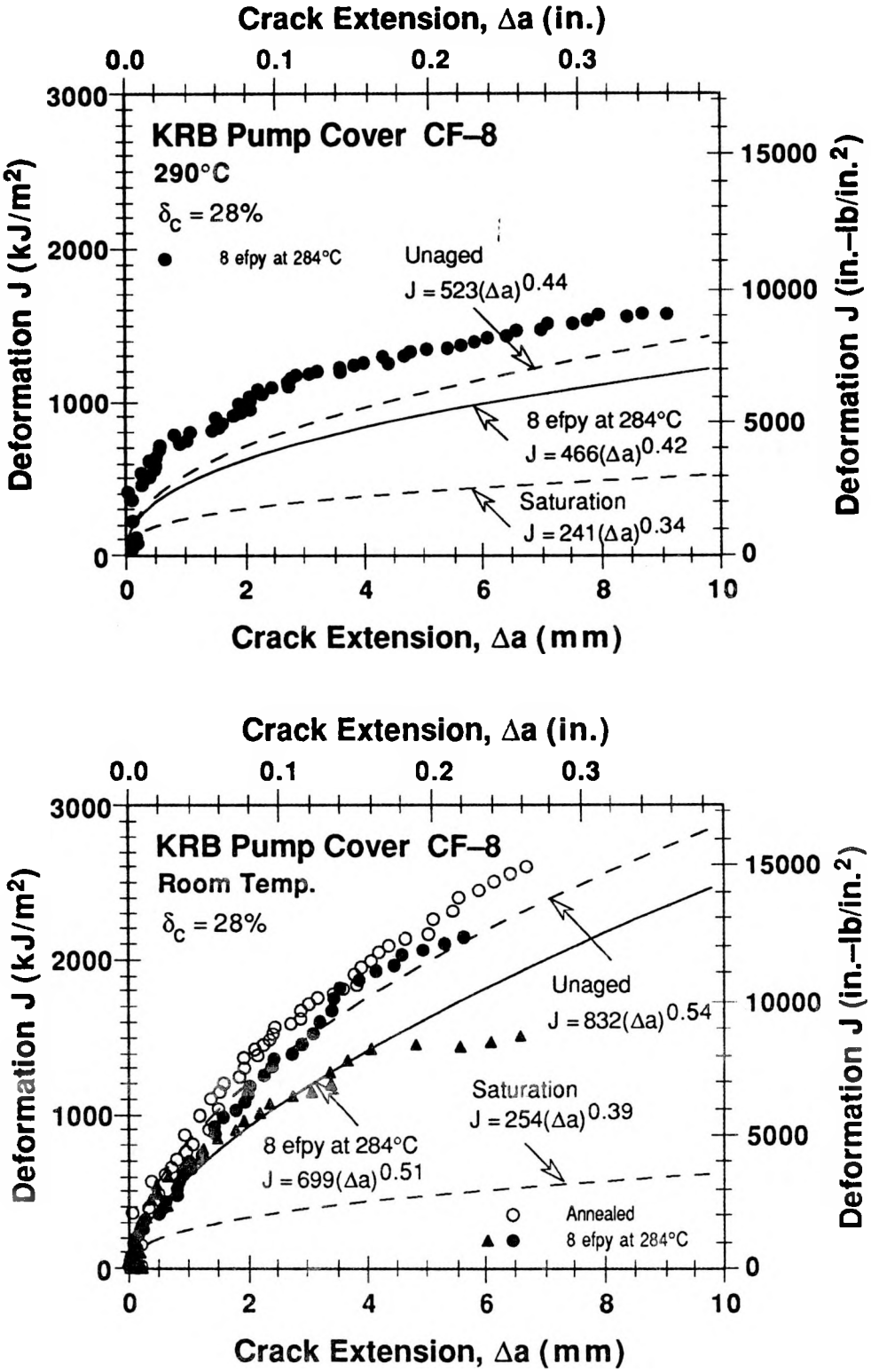

Figure 53. Experimental data and estimated fracture toughness J–R curve at room temperature and at 290°C for KRB pump cover plate

References

1. A Trautwein and W. Gysel, "Influence of Long Time Aging of CF-8 and CF-8M Cast Steel at Temperatures Between 300 and 500°C on the Impact Toughness and the Structure Properties," in Spectrum, Technische Mitteilungen aus dem+GF+Konzern, No. 5 (May 1981); also in *Stainless Steel Castings*, V. G. Behal and A. S. Melilli, eds., ASTM STP 756, pp. 165–189 (1982).

2. O. K. Chopra and H. M. Chung, *Long-Term Embrittlement of Cast Duplex Stainless Steels in LWR Systems: Annual Report, October 1983–September 1984*, NUREG/CR-4204, ANL-85-20 (March 1985); *Nucl. Eng. Des.* **89**, 305 (1985).

3. O. K. Chopra and H. M. Chung, *Long-Term Embrittlement of Cast Duplex Stainless Steels in LWR Systems: Annual Report, October 1984–September 1985*, NUREG/CR-4503, ANL-86-3 (January 1986).

4. O. K. Chopra and H. M. Chung, *Long-Term Embrittlement of Cast Duplex Stainless Steels in LWR Systems: Semiannual Report, October 1985–March 1986*, NUREG/CR-4744 Vol. I, No. 1, ANL-86-54 (January 1987).

5. O. K. Chopra and G. Ayrault, in *Materials Science and Technology Division Light-Water-Reactor Safety Research Program: Quarterly Progress Report, October-December 1983*, NUREG/CR-3689 Vol. IV, ANL-83-85 Vol. IV, pp. 129–151 (August 1984).

6. O. K. Chopra and H. M. Chung, in *Materials Science and Technology Division Light-Water-Reactor Safety Materials Engineering Research Programs: Quarterly Progress Report, January-March 1984*, NUREG/CR-3998 Vol. I, ANL-84-60 Vol. I, p. 52 (September 1984).

7. O. K. Chopra and H. M. Chung, "Aging Degradation of Cast Stainless Steels: Effects on Mechanical Properties," in *Environmental Degradation of Materials in Nuclear Power Systems-Water Reactors*, G. J. Theus and J. R. Weeks, eds., The Metallurgical Society, Warrendale, PA., pp. 737–748 (1988).

8. O. K. Chopra and H. M. Chung, "Effect of Low-Temperature Aging on the Mechanical Properties of Cast Stainless Steels," in *Properties of Stainless Steels in Elevated Temperature Service*, M. Prager, ed., MPC-Vol. 26, PVP-Vol. 132, ASME, New York, pp. 79–105 (1988).

9. O. K. Chopra and H. M. Chung, *Long-Term Embrittlement of Cast Duplex Stainless Steels in LWR Systems: Semiannual Report, April-September 1987*, NUREG/CR-4744 Vol. 2, No. 2, ANL-89/6 (August 1989).

10. O. K. Chopra and H. M. Chung, *Long-Term Embrittlement of Cast Duplex Stainless Steels in LWR Systems: Semiannual Report, October 1987–March 1988*, NUREG/CR-4744 Vol. 3, No. 1, ANL-89/22 (February 1990).

11. O. K. Chopra and H. M. Chung, *Long-Term Embrittlement of Cast Duplex Stainless Steels in LWR Systems: Semiannual Report, April-September 1988*, NUREG/CR-4744 Vol. 3, No. 2, ANL-90/5 (August 1990).

12. O. K. Chopra and A. Sather, "*Initial Assessment of the Mechanisms and Significance of Low-Temperature Embrittlement of Cast Stainless Steels in LWR Systems*," NUREG/CR-5385, ANL-89/17 (August 1990).

13. O. K. Chopra, "Thermal Aging of Cast Stainless Steels: Mechanisms and Predictions," in *Fatigue, Degradation, and Fracture - 1990*, W. H. Bamford, C. Becht, S. Bhandari, J. D. Gilman, L. A. James, and M. Prager, eds., MPC Vol. 30, PVP Vol. 195, ASME, New York, pp. 193-214 (1990).

14. O. K. Chopra and H. M. Chung, *Long-Term Embrittlement of Cast Duplex Stainless Steels in LWR Systems: Semiannual Report October 1988-March 1989*, NUREG/CR-4744, Vol. 4, No. 1, ANL-90/44 (May 1991).

15. O. K. Chopra and H. M. Chung, *Long-Term Embrittlement of Cast Duplex Stainless Steels in LWR Systems: Semiannual Report April-September 1989*, NUREG/CR-4744, Vol. 4, No. 2, ANL-90/49 (June 1991).

16. O. K. Chopra and H. M. Chung, *Long-Term Embrittlement of Cast Duplex Stainless Steels in LWR Systems: Semiannual Report October 1989-March 1990*, NUREG/CR-4744, Vol. 5, No. 1, ANL-91/7 (July 1991).

17. O. K. Chopra, "Estimation of Fracture Toughness of Cast Stainless Steels in LWR Systems," in *Proc. 18th Water Reactor Safety Information Meeting*, U.S. Nuclear Regulatory Commission, NUREG/CP-0114 Vol. 3, p. 195 (April 1991).

18. H. M. Chung and O. K. Chopra, "Kinetics and Mechanism of Thermal Aging Embrittlement of Duplex Stainless Steels," in *Environmental Degradation of Materials in Nuclear Power Systems-Water Reactors*, G. J. Theus and J. R. Weeks, eds., The Metallurgical Society, Warrendale, PA, pp. 359-370 (1988).

19. H. M. Chung and O. K. Chopra, "Long-Term Aging Embrittlement of Cast Austenitic Stainless Steels - Mechanism and Kinetics," in *Properties of Stainless Steels in Elevated Temperature Service*, M. Prager, ed., MPC-Vol. 26, PVP-Vol. 132, ASME, New York, pp. 17-34 (1988).

20. H. M. Chung, "Thermal Aging of Decommissioned Reactor Cast Stainless Steel Components and Methodology for Life Prediction," in *Life Assessment and Life Extension of Power Plant Components*, T. V. Narayanan, C. B. Bond, J. Sinnappan, A. E. Meligi, M. Prager, T. R. Mager, J. D. Parker, and K. Means, eds., PVP Vol. 171, ASME, New York, pp. 111-125 (1989).

21. H. M. Chung and T. R. Leax, "Embrittlement of Laboratory and Reactor Aged CF3, CF8, and CF8M Duplex Stainless Steels," *Mater. Sci. and Technol.* **6**, 249-262 (1990).

22. A. L. Hiser, *Tensile and J-R Curve Characterization of Thermally Aged Cast Stainless Steels*, NUREG/CR-5024, MEA-2229, Materials Engineering Associates, Inc., (September 1988).

23. E. I. Landerman and W. H. Bamford, "Fracture Toughness and Fatigue Characteristics of Centrifugally Cast Type 316 Stainless Steel Pipe after Simulated Thermal Service Conditions," in *Ductility and Toughness Considerations in Elevated Temperature Service*, MPC 8, ASME, New York, pp. 99-127 (1978).

24. S. Bonnet, J. Bourgoin, J. Champredonde, D. Guttmann, and M. Guttmann, "Relationship between Evolution of Mechanical Properties of Various Cast Duplex Stainless Steels and Metallurgical and Aging Parameters: An Outline of Current EDF Programmes," *Mater. Sci. and Technol.*, **6**, 221-229 (1990).

25. P. H. Pumphrey and K. N. Akhurst, "Aging Kinetics of CF3 Cast Stainless Steel in Temperature Range 300-400°C," *Mater. Sci. and Technol.*, **6**, 211-219 (1990).

26. G. Slama, P. Petrequin, and T. Mager, "Effect of Aging on Mechanical Properties of Austenitic Stainless Steel Castings and Welds," presented at *SMIRT Post-Conference Seminar 6, Assuring Structural Integrity of Steel Reactor Pressure Boundary Components*, August 29-30, 1983, Monterey, CA.

27. Y. Meyzaud, P. Ould, P. Balladon, M. Bethmont, and P. Soulat, "Tearing Resistance of Aged Cast Austenitic Stainless Steel," presented at *Intl. Conf. on Thermal Reactor Safety (NUCSAFE 88)*, October 1988, Avignon, France.

28. P. McConnell and J. W. Sheckherd, *Fracture Toughness Characterization of Thermally Embrittled Cast Duplex Stainless Steel*, Report NP-5439, Electric Power Research Institute, Palo Alto, CA (September 1987).

29. L. S. Aubrey, P. F. Wieser, W. J. Pollard, and E. A. Schoefer, "Ferrite Measurement and Control in Cast Duplex Stainless Steel," in *Stainless Steel Castings*, V. G. Behal and A. S. Melilli, eds., ASTM STP 756, pp. 126-164 (1982).

30. O. K. Chopra, "Studies of Aged Cast Stainless Steel from the Shippingport Reactor," in *Proc. 18th Water Reactor Safety Information Meeting*, U.S. Nuclear Regulatory Commission, NUREG/CP-0114 Vol. 3, p. 369 (April 1991).

31. A. L. Hiser, *Fracture Toughness Characterization of Nuclear Piping Steels*, NUREG/CR-5188, MEA-2325, Materials Engineering Associates, Inc. (Novenber 1989).

32. G. M. Wilkowski, et. al., *Degraded Piping Program - Phase II*, Semiannual Report, NUREG/CR-4082, Vol. 2 (June 1985).

33. W. J. Mills, "Heat-to-Heat Variations in the Fracture Toughness of Austenitic Stainless Steels," *Eng. Fracture Mech.*, ***30***, 469-492 (1988).

34. M. G. Vassilaros, R. A. Hays, and J. P. Gudas, "Investigation of the Ductile Fracture Properties of Type 304 Stainless Steel Plate, Welds, and 4-Inch Pipe," in *Proc. 12th*

Water Reactor Safety Information Meeting, U.S. Nuclear Regulatory Commission, NUREG/CP-0058 Vol. 4, p. 176 (January 1985).

35. P. Balladon, J. Heritier, and P. Rabbe, "Influence of Microstructure on the Ductile Rupture Mechanisms of a 316L Steel at Room and Elevated Temperatures," in *Fracture Mechanics: Fourteenth Symposium*, ASTM STP **791**, II496–II513 (1983).

36. W. H. Bamford and A. J. Bush, "Fracture Behavior of Stainless Steel," *Elastic–Plastic Fracture*, ASTM STP **668**, 553–577 (1979).

37. W. H. Shack, O. K. Chopra, and H. M. Chung, "Aging Studies on Materials from the Shippingport Reactor," in *Compilation of Contract Research for the Materials Engineering Branch, Division of Engineering: Annual Report for FY 1988*, NUREG–0975, Vol. 7, p. 218 (May 1989).

Distribution for NUREG/CR-4744 Vol. 5, No. 2 (ANL-91/10)

Internal:

O. K. Chopra (25)
H. M. Chung
C. Malefyt (2)
W. J. Shack
C. E. Till
R. W. Weeks
T. F. Kassner
TIS Files (3)
ANL Patent File
ANL Contract File

External:

NRC, for distribution per R5
ANL Libraries (2)
Manager, Chicago Operations Office, DOE
Materials and Components Technology Division Review Committee
H. Berger, Industrial Quality, Inc., Gaithersburg, MD
M. S. Dresselhaus, Massachusetts Institute of Technology, Cambridge, MA
S. J. Green, Electric Power Research Institute, Palo Alto, CA
R. A. Greenkorn, Purdue U., West Lafayette, IN
C.-Y. Li, Cornell U., Ithaca, NY
P. G. Shewmon, Ohio State U., Columbus
R. E. Smith, Electric Power Research Institute, NDE Ctr., Charlotte, NC
D. Atteridge, Battelle Pacific Northwest Laboratory
W. H. Bamford, Westinghouse Electric Corp., Pittsburgh
N. G. Cofie, Nutech, San Jose, CA
A. Cowan, Risley Nuclear Power Development Labs., Risley, Warrington, UK
E. L. Creamer, Shell Oil Co., Houston
W. H. Cullen, Materials Engineering Associates, Inc., Lanham, MD
B. J. L. Darlaston, Berkeley Nuclear Laboratories, Berkeley, Gloucestershire, UK
H. Domian, Alliance Research Center, Babcock & Wilcox Co., Alliance, OH
J. Gilman, Electric Power Research Inst., Palo Alto, CA
M. Guttmann, Electricité de France, Les Renardieres Roule de Sens, France
W. Gysel, Georg Fischer, Ltd., Schaffhausen, Switzerland
G. E. Hale, The Welding Institute, Abington, Cambridge, UK
P. Hedgecock, APTECH Engineering Services, Inc., Palo Alto, CA
B. Hemsworth, HM Nuclear Installations Inspectorate, London
C. G. Interrante, Center for Materials Science, National Institute of Standards and Technology, Gaithersburg, MD
J. Jansky, Buro für Technische Beratung, Leonberg, Germany
C. E. Jaske, CC Technologies, Cortest, Columbus, OH
C. Kim, Westinghouse Electric Corp., Pittsburgh
P. M. Lang, Office of Converter Reactor Deployment, U.S. Dept. of Energy, Washington, DC
G. J. Licina, Structural Integrity Associates, San Jose, CA
T. R. Mager, Westinghouse Electric Corp., Pittsburgh
Y. Meyzaud, Framatome, Paris
M. Prager, Materials Properties Council, Inc., New York

P. H. Pumphrey, National Power, Technology and Environment Center, Leatherhead, Surrey, UK
V. N. Shah, EG&G Idaho, Inc., P. O. Box 1625, Idaho Falls, Idaho
V. K. Sikka, Oak Ridge National Laboratory
A. Singh, Unical Science & Technology Division, Brea, CA
G. Slama, Framatome, Paris La Defense, France
G. D. W. Smith, Oxford University, Oxford, UK
H. D. Solomon, General Electric Co., Schenectady, NY
D. M. Stevens, Lynchburg Research Center, Babcock & Wilcox Co., Lynchburg, VA
L. Taylor, Nuclear Electric plc., Chelsford Rd., Knutsford, Cheshire, UK
J. M. Vitek, Oak Ridge National Laboratory
J. Wilks, AMOCO, Naperville, IL

NRC FORM 335 (2–89) NRCM 1102, 3201, 3202

U. S. NUCLEAR REGULATORY COMMISSION

BIBLIOGRAPHIC DATA SHEET

(See instructions on the reverse)

1. REPORT NUMBER *(Assigned by NRC. Add Vol., Supp., Rev., and Addendum Numbers, if any.)*

NUREG/CR–4744
Vol. 5, No. 2
ANL–91/10

2. TITLE AND SUBTITLE

Long–Term Embrittlement of Cast Duplex Stainless Steels in LWR Systems

Semiannual Report
April–September 1990

3. DATE REPORT PUBLISHED

MONTH	YEAR
July	1991

4. FIN OR GRANT NUMBER

A2243, A2256

5. AUTHOR(S)

O. K. Chopra

6. TYPE OF REPORT

Technical; Semiannual

7. PERIOD COVERED *(Inclusive Dates)*

April–September 1990

8. PERFORMING ORGANIZATION – NAME AND ADDRESS *(If NRC, provide Division, Office or Region, U.S. Nuclear Regulatory Commission, and mailing address; if contractor, provide name and mailing address.)*

Argonne National Laboratory
9700 South Cass Avenue
Argonne, IL 60439

9. SPONSORING ORGANIZATION – NAME AND ADDRESS *(If NRC, type "Same as above": if contractor, provide NRC Division, Office or Region, U.S. Nuclear Regulatory Commission, and mailing address.)*

Division of Engineering
Office of Nuclear Regulatory Research
U. S. Nuclear Regulatory Commission
Washington, DC 20555

10. SUPPLEMENTARY NOTES

11. ABSTRACT (200 words or less)

This progress report summarizes work performed by Argonne National Laboratory on long–term embrittlement of cast duplex stainless steels in LWR systems during the six months from April–September 1990. A procedure and correlations are presented for predicting fracture toughness J–R curves and impact strength of aged cast stainless steels from known material information. Fracture toughness of a specific cast stainless steel is estimated from the extent and kinetics of embrittlement. The extent of embrittlement is characterized by the room–temperature Charpy–impact energy. A correlation for the extent of embrittlement at saturation is given in terms of a material parameter, Φ, which is determined from the ferrite morphology and/or chemical composition. Charpy–impact energy as a function of time and temperature of reactor service is estimated from the kinetics of embrittlement, which are determined from chemical composition. The fracture toughness J–R curve for the material is then obtained from correlations between room–temperature Charpy–impact energy and fracture toughness parameters. A "lower–bound" J–R curve for cast stainless steels with unknown chemical composition is also defined for a given material specification and temperature. Mechanical–property degradation suffered by cast stainless steel components from the decommissioned Shippingport reactor has been characterized. The results are used to validate the correlations and benchmark the laboratory studies. Charpy–impact, tensile, and fracture toughness data for materials from the hot–leg shutoff valve and cold–leg check valves and pump volute are presented. The results indicate a modest degree of embrittlement.

12. KEY WORDS/DESCRIPTORS *(List words or phrases that will assist researchers in locating this report.)*

Cast duplex stainless steel
Thermal aging
Embrittlement
Fracture toughness
Impact strength
Activation Energy

13. AVAILABILITY STATEMENT

Unlimited

14. SECURITY CLASSIFICATION

(This Page)

Unclassified

(This Report)

Unclassified

15. NUMBER OF PAGES

16. PRICE

NRC FORM 335 (2–89)